

TELLURIUM SPECIATION USING HYDRIDE GENERATION ATOMIC ABSORPTION
SPECTROMETRY AND *in-situ* GRAPHITE CUVETTE TRAPPING

A THESIS SUBMITTED TO
THE GRADUATE SCHOOL OF NATURAL AND APPLIED SCIENCES
OF
MIDDLE EAST TECHNICAL UNIVERSITY

BY

EMRAH YILDIRIM

IN PARTIAL FULFILLMENT OF THE REQUIREMENTS
FOR
THE DEGREE OF MASTER OF SCIENCE
IN
CHEMISTRY

SEPTEMBER 2009

Approval of the Thesis;

**TELLURIUM SPECIATION USING HYDRIDE GENERATION ATOMIC ABSORPTION
SPECTROMETRY AND *in-situ* GRAPHITE CUVETTE TRAPPING**

Submitted by **EMRAH YILDIRIM** in a partial fulfillment of the requirements for
the degree of **Master of Science in Chemistry Department, Middle East
Technical University** by

Prof. Dr. Canan Özgen
Dean, Graduate School of **Natural and Applied Sciences** _____

Prof. Dr. Ahmet M. Önal
Head of Department, **Chemistry** _____

Prof Dr. O. Yavuz Ataman
Supervisor, **Chemistry Department, METU** _____

Examining Committee Members:

Prof. Dr. E. Hale Göktürk
Chemistry Department, METU _____

Prof. Dr. O. Yavuz Ataman
Chemistry Department, METU _____

Prof. Dr. Orhan Acar
Atatürk Vocational High School, Gazi University _____

Prof. Dr. Mürvet Volkan
Chemistry Department, METU _____

Assoc. Prof. Dr. Hasan Basan
Faculty of Pharmacy, Gazi University _____

Date: 11.09.2009

I hereby declare that all information in this document has been obtained and presented in accordance with academic rules and ethical conduct. I also declare that, as required by these rules and conduct, I have fully cited and referenced all material and results that are not original to this work.

Name, Last name: Emrah Yıldırım

Signature

ABSTRACT

TELLURIUM SPECIATION USING HYDRIDE GENERATION ATOMIC ABSORPTION SPECTROMETRY AND *in-situ* GRAPHITE CUVETTE TRAPPING

Yıldırım, Emrah

M.S., Department of Chemistry

Supervisor: Prof. Dr. O. Yavuz Ataman

September 2009, 127 pages

In recent years speciation analysis is becoming more important as it is known that each chemical form of an element behaves differently in biological and environmental media. Since abundance of tellurium in earth crust is extremely low, very sensitive and accurate methods are needed to determine the concentration of tellurium. Hydride generation atomic absorption is a sensitive, fast and economical technique applied for the determination of tellurium. Speciation of tellurium can be achieved by making use of different kinetic behaviors of Te(IV) and Te(VI) upon its reaction with sodiumborohydride.

A continuous flow hydride generation system was developed and parameters that affect the analytical signal were optimized. Sample solutions were prepared in 4.0 mol/L HCl; as reductant 0.5 % (w/v) sodiumborohydride in 0.5 % (w/v) NaOH was used.

Quantitative reduction of Te(VI) was achieved through application of a microwave assisted prereduction of Te(VI) in 6.0 mol/L HCl solution.

Sensitivity of the system was further enhanced by *in-situ* trapping of the formed H₂Te species in a previously heated graphite furnace whose surface was modified using Pd or Ru.

Overall efficiency of pyrolytic coated graphite surface was found to be 15% when hydrides are trapped for 60 seconds at 300 °C. LOD and LOQ values were calculated as 86 pg/mL and 287 pg/mL according to peak height values. Efficiency was increased by 46% and 36% when Pd and Ru modifiers were used, respectively. With Ru modified graphite tube 173 fold enhancement was obtained over 180 seconds trapping period with respect to direct ETAAS. LOD values were 6.4 and 2.2 pg/mL for Pd and Ru treated systems, respectively, for 180 s collection of 9.6 mL sample solution.

Keywords: Tellurium, speciation, graphite cuvette, *in-situ* trapping, hydride generation, preconcentration, atomic absorption spectrometry

ÖZ

HİDRÜR OLUŞTURMA VE *in-situ* GRAFİT KÜVET İÇİNDE TUZAKLAYARAK ATOMİK ABSORPSİYON SPEKTROMETRİYLE TELLÜR TÜRLENDİRMESİ

Yıldırım, Emrah

Yüksek Lisans, Kimya Bölümü

Tez Yöneticisi: Prof. Dr. O. Yavuz Ataman

Eylül 2009, 127 sayfa

Çevresel ve biyolojik örneklerde farklı davranışlar göstermelerinden ötürü günümüzde elementlerin farklı kimyasal türlerinin tayin edilmesi giderek önem kazanmaktadır. Tellür elementi doğada eser derişimlerde bulunduğu için tayininde çok hassas ve doğru yöntemlerin kullanılması gerekmektedir. Hidrür oluşturmali atomik absorpsiyon spektrometri kolay, duyarlı ve ekonomik bir yöntem olduğu için tellür tayininde sıkılıkla kullanılmaktadır. Tellür türlendirmesinde Te(IV) ve Te(VI) bileşiklerinin sodyum bor hidrür ile reaksiyonlarındaki farklı kinetik kullanılmaktadır.

Öncelikle sürekli hidrür oluşturmali bir sistem geliştirilmiş ve analitik sinyali etkileyen parametreler optimize edilmiştir. 4.0 mol/L HCl içerisinde hazırlanmış örnek çözelti ve %0.5 (g/v) NaOH içerisinde stabilize edilmiş %0.5 (g/v) sodyumbor hidrür çözeltileri en uygun çalışma şartları olarak bulunmuştur.

Te(VI) formunun Te(IV) formuna indirgenmesi 6.0 mol/L HCl çözeltisinde mikrodalga yardımıyla gerçekleştirılmıştır.

Sistemin duyarlılığı oluşan H₂Te gazının önceden ısıtılmış ve yüzeyi Pd ve Ru ile değiştirilmiş grafit küvet içerisinde *in-situ* olarak toplanması ile artırılmıştır.

Grafit yüzeyin toplam verimliliği hidrür türleri 300 °C'de ve 60 saniye süreyle toplandığında % 15 olarak bulunmuştur. Gözlenebilme ve tayin sınırları sinyal yüksekliğine göre sırasıyla 86 pg/mL ve 287 pg/mL olarak hesaplanmıştır. Grafit yüzey Pd ve Ru ile değiştirildiğinde verimliliğin sırasıyla % 46 ve % 36 arttığı gözlemlenmiştir. Oluşan türler Ru ile modifiye edilmiş grafit tüpte 180 saniye süreyle toplandığında ETAAS tekniğine göre 173 kat duyarlılık artış elde edilmiştir. Pd ve Ru ile işleme sokulmuş sistemlerde, 9.6 mL örnek çözeltisi 180 s süreyle toplandığında LOD değerleri sırasıyla 6.4 ve 2.2 pg/mL olarak bulunmuştur.

Anahtar Kelimeler: Tellür, türlendirme, grafit küvet, *in-situ* tuzaklama, hidrür oluşturma, önzenginleştirme, atomik absorpsiyon spektrometri

To My Family

ACKNOWLEDGEMENTS

I would like to express my sincere thanks to my supervisor Prof. Dr. O. Yavuz Ataman not only for his guidance, support, encouragement, patience and for teaching us how to become a good scientist but also for listening and helping us in many ways.

I would like to thank to Sezgin Bakırdere and Yasin Arslan for their ideas, constructive comments, moral support and their endless helps. I learned a lot from them.

I am deeply grateful to Pınar Akay, İlknur Demirtaş, Kamil Coşkun and Selin Bora for their help, support and friendship. Whenever I need something, they are always there.

I would like to thank to Necati Koç for his help about technical issues.

I should also thank to my C-49 and C-50 lab mates for their friendship and moral support.

Finally, my special thanks to my family and Sezen Keser for their trust, patience, support and love. I always know that they are with me and never leave me alone.

I would like to thank to TÜBİTAK for supplying financial support during my master work.

TABLE OF CONTENT

| | |
|--|------|
| ABSTRACT | iv |
| ÖZ..... | vi |
| ACKNOWLEDGEMENTS | ix |
| TABLE OF CONTENT | x |
| LIST OF TABLES..... | xiv |
| LIST OF FIGURES..... | xvi |
| LIST OF ABRREVIATIONS..... | xxiv |
| CHAPTERS | 1 |
| 1. INTRODUCTION..... | 1 |
| 1.1 Tellurium | 1 |
| 1.1.1 Occurrence and Production | 2 |
| 1.1.2 Industrial Usage..... | 4 |
| 1.1.3 Tellurium and Metabolism..... | 4 |
| 1.1.4 Determination of Tellurium | 6 |
| 1.1.4.1 Inorganic Speciation of Tellurium | 7 |
| 1.2 Atomic Absorption Spectrometry (AAS) | 8 |
| 1.2.1 Flame AAS (FAAS) | 10 |
| 1.2.2 Electrothermal AAS (ETAAS)..... | 11 |
| 1.3 Vapor Generation AAS (VGAAS)..... | 12 |
| 1.3.1 Hydride Generation AAS (HGAAS) | 13 |
| 1.3.1.1 Chemical Hydride Generation (CHG) | 15 |
| 1.3.1.2 Electrochemical Hydride Generation (ECHG) | 16 |
| 1.3.1.3 Advantages and Drawbacks of Hydride Generation Atomic Absorption Spectrometry | 17 |
| 1.3.2 Hydride Atomization | 18 |
| 1.3.2.1 Flame in Tube Atomizers (FITA)..... | 19 |
| 1.3.2.2 Conventional Externally Heated Quartz Tube Atomizer (CEHQTA) | 21 |
| 1.3.2.3 Multiple Microflame Quartz Tube Atomizer (MMQTA)..... | 22 |
| 1.4 Trapping Systems | 24 |

| | | |
|---------|--|----|
| 1.4.1 | Molecular Traps..... | 24 |
| 1.4.1.1 | Absorbing Medium..... | 24 |
| 1.4.1.2 | Pressure Collection | 25 |
| 1.4.1.3 | Cryogenic Traps..... | 25 |
| 1.4.2 | Atom Traps | 26 |
| 1.4.2.1 | Graphite Furnace Trap | 26 |
| 1.4.2.2 | Quartz Trap | 27 |
| 1.4.2.3 | Metal Traps..... | 28 |
| 1.5 | Chemical Vapour Generation of Transition and Noble Metals..... | 29 |
| 1.6 | Interferences..... | 30 |
| 2 | EXPERIMENTAL | 32 |
| 2.1 | Chemicals and Reagents | 32 |
| 2.2 | Spectrometer | 33 |
| 2.3 | Hydride Generation System..... | 34 |
| 2.4 | Atomization Units..... | 36 |
| 2.4.1 | Continuous Flow Atomization Unit | 36 |
| 2.4.2 | Graphite Furnace Atomization Unit | 37 |
| 2.5 | Procedures | 38 |
| 2.5.1 | Electrothermal Atomic Absorption System | 38 |
| 2.5.2 | Continuous Flow Hydride Generation System | 39 |
| 2.5.3 | Microwave Assisted Te(VI) Reduction System..... | 40 |
| 2.5.4 | Graphite Trapping System..... | 40 |
| 2.5.5 | Coating Procedure | 42 |
| 2.6 | Accuracy Check..... | 43 |
| 3 | RESULTS AND DISCUSSION | 45 |
| 3.1 | Direct ETAAS Study..... | 46 |
| 3.1.1 | Pyrolysis Temperature | 47 |
| 3.1.2 | Atomization Temperature..... | 48 |
| 3.1.3 | Calibration Graphs and Analytical Signals..... | 49 |
| 3.1.4 | Analytical Figures of Merit | 54 |
| 3.2 | Continuous Flow Hydride Generation System..... | 56 |
| 3.2.1 | NaBH ₄ and HCl Concentrations | 56 |
| 3.2.2 | Sample Solution and NaBH ₄ Flow Rates | 57 |

| | | |
|-------|---|-----|
| 3.2.3 | Length of Reaction Coil | 59 |
| 3.2.4 | Length of Stripping Coil..... | 60 |
| 3.2.5 | NaOH Concentration..... | 61 |
| 3.2.6 | Stripping Ar Flow Rate | 62 |
| 3.2.7 | Linear Range and Calibration Plot for Te(IV)..... | 63 |
| 3.2.8 | Speciation Strategy | 66 |
| 3.2.9 | Reduction Studies | 66 |
| 3.3 | Trapping of H ₂ Te on Pyrolytic Coated Graphite Tube | 73 |
| 3.3.1 | Stripping Ar Flow Rate | 75 |
| 3.3.2 | Sample Flow Rate | 76 |
| 3.3.3 | Trapping Temperature..... | 78 |
| 3.3.4 | Atomization Temperature..... | 80 |
| 3.3.5 | Collection Period | 81 |
| 3.3.6 | Calibration Plot and Linear Range | 81 |
| 3.3.7 | Analytical Figures of Merit | 83 |
| 3.4 | Trapping of H ₂ Te on Pd Modified Graphite Tube | 85 |
| 3.4.1 | Stripping Ar Flow Rate | 85 |
| 3.4.2 | Flow Rates of Sample and Reductant Solutions..... | 87 |
| 3.4.3 | Trapping Temperature..... | 88 |
| 3.4.4 | Atomization Temperature..... | 89 |
| 3.4.5 | Pyrolysis Temperature | 90 |
| 3.4.6 | Amount of Pd Modifier | 91 |
| 3.4.7 | Collection Period | 93 |
| 3.4.8 | Calibration Plot and Linear Range | 94 |
| 3.4.9 | Analytical Figures of Merit and Method Validation | 97 |
| 3.5 | Trapping of H ₂ Te on Ru Modified Graphite Tube | 99 |
| 3.5.1 | Stripping Ar Flow Rate | 100 |
| 3.5.2 | Sample Flow Rate | 101 |
| 3.5.3 | Trapping Temperature..... | 101 |
| 3.5.4 | Atomization Temperature..... | 103 |
| 3.5.5 | Collection Period | 103 |
| 3.5.6 | Calibration Plot and Linear Range | 104 |
| 3.5.7 | Analytical Figures of Merit and Method Validation | 107 |

| | | |
|-----|--|-----|
| 3.6 | Evaluation of System Performance | 109 |
| 3.7 | Interference Study..... | 111 |
| 3.8 | Analysis of Samples and Recovery Studies | 117 |
| 4 | CONCLUSIONS..... | 119 |
| | REFERENCES | 122 |

LIST OF TABLES

Tables

| | |
|---|----|
| Table 1 Yearly production of Te for world leading Te producer countries..... | 3 |
| Table 2 World yearly Te Production Rate | 3 |
| Table 3 Limiting concentrations of tellurium and its compounds (Merian, Anke, Ihnat, & Stoepller, 2004)..... | 5 |
| Table 4 Physical properties and generic names of some hydrides (Dedina & Tsalev, 1995)..... | 14 |
| Table 5 Operating conditions of AA spectrometer..... | 34 |
| Table 6 Temperature program used for the ETAAS system..... | 39 |
| Table 7 Temperature program for the microwave assisted reduction of Te(VI) .. | 40 |
| Table 8 Temperature program applied for the <i>in-situ</i> trapping of H ₂ Te in pyrolytic coated and Ru modified graphite tubes | 41 |
| Table 9 Temperature program applied for the <i>in-situ</i> trapping of H ₂ Te in Pd modified graphite tube | 42 |
| Table 10 Temperature program applied for the permanent coating of graphite tube | 43 |
| Table 11 Certified Values for NIST 1643e “Trace elements in Water” SRM | 44 |
| Table 12 Optimized parameters for pyrolytic coated, Pd modified and Ru modified graphite tubes..... | 53 |
| Table 13 Analytical parameters of pyrolytic coated, Pd modified and Ru modified graphite tubes..... | 55 |
| Table 14 Analytical figures of merit for continuous flow HGAAS system..... | 65 |

| | |
|--|-----|
| Table 15 Optimized parameters for continuous flow hydride generation system | 65 |
| Table 16 Final Te(IV) and Te(VI) concentrations in mixtures prepared for the reduction system. | 69 |
| Table 17 Analytical figures of merit for reduced Te(VI) species using HGAAS. | 73 |
| Table 18 Analytical figures of merit for Te determination by HG-ETAAS using pyrolytic coated graphite tube. | 84 |
| Table 19 Analytical figures of merit for trapping of H ₂ Te in Pd modified graphite tube. | 98 |
| Table 20 Results of accuracy check for trapping of H ₂ Te on Pd modified graphite tube using NIST 1643e “Trace elements in water” SRM..... | 99 |
| Table 21 Analytical figures of merit for trapping of H ₂ Te on Ru modified graphite tube. | 108 |
| Table 22 Results of accuracy check for trapping of H ₂ Te on Ru modified graphite tube using HG-ETAAS and NIST 1643e “Trace elements in water” SRM..... | 109 |
| Table 23 Comparison of the performance of developed methods..... | 110 |
| Table 24 Results of spike recovery test for some water samples (N=3)..... | 118 |

LIST OF FIGURES

Figures

| | |
|---|----|
| Figure 1 One of the first AAS instrument designed by Walsh (L'vov, 2005)..... | 9 |
| Figure 2 Schematic representation of T-shape FITA (Dedina & Tsalev, 1995)..... | 21 |
| Figure 3 Schematic representation of EHQTA..... | 22 |
| Figure 4 Schematic representation of MMQTA (Dedina & Matousek, 2000)..... | 23 |
| Figure 5 Schematic representation of cylindirical type GLS..... | 35 |
| Figure 6 Schematic representation of hydride generation system..... | 36 |
| Figure 7 Schematic Representation of externally heated quartz tube atomizer.. | 37 |
| Figure 8 Schematic representation of graphite furnace atom trapping system... | 38 |
| Figure 9 Effect of pyrolysis temperature on the analytical signal of 20 μ L 50.0 ng/mL Te solution in 0.5 mol/L HNO ₃ . 2000 $^{\circ}$ C atomization temperature was used for pyrolytic coated and Ru modified graphite tubes. 2300 $^{\circ}$ C atomization temperature was used for Pd modified graphite tube. Each point represents mean value of three replicate measurements..... | 47 |
| Figure 10 Effect of atomization temperature on analytical signal of 20 μ L 50.0 ng/mL Te solution prepared in 0.5 mol/L HNO ₃ . 500 $^{\circ}$ C pyrolysis temperature was used for pyrolytic coated graphite tube and 1000 $^{\circ}$ C pyrolysis temperature was used for Pd modified and Ru modified graphite tubes. Each point represents mean value of three replicate measurements..... | 48 |
| Figure 11 Calibration plot for 20 μ L injection volumes for pyrolytic coated, Pd modified and Ru modified graphite tubes. 500 $^{\circ}$ C pyrolysis temperature and 2000 $^{\circ}$ C atomization temperatures were used for pyrolytic coated graphite. 1000 $^{\circ}$ C pyrolysis temperature and 2300 $^{\circ}$ C atomization temperatures were used for Pd modified graphite tube. 1000 $^{\circ}$ C pyrolysis temperature and 2000 $^{\circ}$ C atomization temperatures were used for Ru modified graphite tube. | 49 |

| | |
|--|----|
| Figure 12 Linear portion of the calibration plot and best line equation for pyrolytic coated graphite tube. 500 $^{\circ}\text{C}$ pyrolysis temperature and 2000 $^{\circ}\text{C}$ were used..... | 50 |
| Figure 13 Linear portion of calibration plot and best line equation for Pd modified graphite tube. 1000 $^{\circ}\text{C}$ pyrolysis temperature and 2300 $^{\circ}\text{C}$ atomization temperature was used. | 51 |
| Figure 14 Linear portion of the calibration plot and best line equation for Ru modified graphite tube. 1000 $^{\circ}\text{C}$ pyrolysis temperature and 2000 $^{\circ}\text{C}$ atomization temperature were used. | 51 |
| Figure 15 Analytical signals in duplicate for 20 μL of 40 ng/mL Te solutions for A- Pyrolytic coated graphite tube, B- Pd modified graphite tube, C- Ru modified graphite tube. Temperature changes are indicated by the straight lines. | 53 |
| Figure 16 Variation of HGAAS signal with NaBH_4 and HCl concentration for 20 ng/mL Te(IV) sample solution. Sample and reductant flow rates were adjusted to 2.9 and 3.1 mL/min, respectively. | 57 |
| Figure 17 Effect of sample and NaBH_4 flow rates on the HGAAS signal of 20 ng/mL Te(IV) solution. Sample solution was prepared in 4.0 mol/L HCl and 0.5% (w/v) NaBH_4 solutions were used. | 58 |
| Figure 18 Effect of reaction coil length on the HGAAS signal of 20 ng/mL Te(IV) solution. Sample solution was prepared in 4.0 mol/L HCl solution and pumped at 6.5 mL/min flow rate. 0.5% (w/v) NaBH_4 was used at a flow rate of 1.5 mL/min. | 59 |
| Figure 19 Effect of stripping coil length on the HGAAS signal of 20 ng/mL Te(IV) solution. Sample solution was prepared in 4.0 mol/L HCl solution and pumped at 6.5 mL/min flow rate. 0.5% (w/v) NaBH_4 was used at a flow rate of 1.5 mL/min. | 60 |
| Figure 20 Effect of NaOH concentration in 0.5% (w/v) NaBH_4 solution on HGAAS signal for 20 ng/mL Te(IV) solution..... | 61 |
| Figure 21 Effect of stripping Ar flow rate on HGAAS signal of 20 ng/mL Te(IV) solution. Sample solution was prepared in 4.0 mol/L HCl solution and pumped at | |

| | |
|--|----|
| 6.5 mL/min flow rate. 0.5% (w/v) NaBH ₄ was used at a flow rate of 1.5 mL/min. | 62 |
| Figure 22 Effect of stripping Ar flow rate on shape of HGAAS signal of 20.0 ng/mL Te(IV) solution pumped at 6.5 mL/min flow rate..... | 63 |
| Figure 23 Calibration plot for continuous flow HGAAS system for Te(IV) solution. Sample solution was prepared in 4.0 mol/L HCl solution and pumped at 6.5 mL/min flow rate. 0.5% (w/v) NaBH ₄ was used at a flow rate of 1.5 mL/min. | 64 |
| Figure 24 Linear portion of calibration plot for Te(IV) continuous flow HGAAS system..... | 64 |
| Figure 25 Effect of HCl concentration on the reduction of 20 ng/mL Te(VI) species upon waiting for 2.5 hours at ambient conditions..... | 67 |
| Figure 26 Effect of HCl concentration on the reduction of 20 ng/mL Te(VI) to Te(IV) by using microwave assisted reduction system..... | 68 |
| Figure 27 Calibration plot obtained without a prereduction step using HGAAS.. | 70 |
| Figure 28 Absorbance values of mixtures after applying prereduction using HGAAS..... | 70 |
| Figure 29 Calibration plot of reduced Te(VI) using HGAAS..... | 71 |
| Figure 30 Calibration plot for reduced Te(VI) using HGAAS. Sample solution was prepared in 4.0 mol/L HCl solution and pumped at 6.5 mL/min flow rate. 0.5% (w/v) NaBH ₄ was used at a flow rate of 1.5 mL/min. | 72 |
| Figure 31 Linear portion of the calibration plot and best line equation for reduced Te(VI) using HGAAS..... | 73 |
| Figure 32 Effect of Ar flow rate on HG-ETAAS signal of 2.0 ng/mL Te(IV) solution trapped over 60 seconds. Sample flow rate was adjusted to 1.6 mL/min. Trapping temperature was 300 °C and atomization temperature was 1900 °C. | 75 |
| Figure 33 Effect of sample flow rate on HG-ETAAS signal of 800 µL 2.0 ng/mL Te solutions. Trapping temperature was 300 °C and atomization temperature was 1900 °C. The ratio of sample to NaBH ₄ flow rate was kept constant as 2.2 | 77 |

| | |
|---|----|
| Figure 34 Effect of sample flow rate on HG-ETAAS signal of 2.0 ng/mL Te solution at 60 seconds trapping time. Trapping temperature was 300 °C and atomization temperature was 1900 °C. The ratio of sample to NaBH ₄ flow rate was kept constant as 2.2..... | 78 |
| Figure 35 Effect of trapping temperature on HG-ETAAS signal of 2.0 ng/mL Te(IV) solution trapped over 60 second time period. Atomization temperature was kept at 1900 °C. | 79 |
| Figure 36 Effect of atomization temperature on HG-ETAAS signal of 2.0 ng/mL Te solution trapped over 60 seconds time period. Trapping temperature was kept at 300 °C. | 80 |
| Figure 37 Effect of trapping period on analytical signal of 2.0 ng/mL Te solution. Trapping temperature and atomization temperature was 300 °C and 1900 °C, respectively. | 81 |
| Figure 38 Calibration plot for trapping of H ₂ Te on pyrolytic coated graphite tube using HG-ETAAS. Trapping temperature and atomization temperatures were set to 300 and 1900 °C, respectively. Sample flow rate was adjusted to 1.6 mL/min. | 82 |
| Figure 39 Linear portion of the calibration plot and best line equation for Te determination by HG-ETAAS using pyrolytic coated graphite tube. | 83 |
| Figure 40 Effect of Ar flow rate on the HG-ETAAS signal of 0.5 ng/mL Te(IV) solution trapped over 60 seconds time period. Trapping temperature and atomization temperature were adjusted to 300 °C and 2300 °C, respectively. 10 µL 1000 mg/L Pd modifier was injected into the graphite tube before each measurement. | 86 |
| Figure 41 Sample flow rate on HG-ETAAS signal of 0.5 ng/mL Te(IV) solution trapped over 60 seconds time period. Trapping temperature and atomization temperature were adjusted to 300 °C and 2300 °C, respectively. 10 µL 1000 mg/L Pd modifier was injected into the graphite tube before each measurement. | 87 |

| | |
|---|----|
| Figure 42 Effect of trapping temperature on HG-ETAAS signal intensity for 60 seconds trapping of 0.5 ng/mL Te(IV) solution. Atomization temperature was 2300 °C. 10 µL 1000 mg/L Pd modifier was injected into the graphite tube before each measurement..... | 88 |
| Figure 43 Effect of atomization temperature on HG-ETAAS signal of 0.5 ng/mL Te(IV) solution trapped over 60 seconds time period. Trapping temperature was 300 °C. 10 µL 1000 mg/L Pd modifier was injected into the graphite tube before each measurement..... | 90 |
| Figure 44 Effect of pyrolysis temperature on HG-ETAAS signal of 0.5 ng/mL Te(IV) solution trapped over 60 seconds time period. Trapping temperature and atomization temperature was 300 °C and 2300 °C, respectively. 10 µL 1000 mg/L Pd modifier was injected into the graphite tube before each measurement..... | 91 |
| Figure 45 Effect of Pd amount injected on HG-ETAAS signal of 0.5 ng/mL Te(IV) solution trapped over 60 seconds. Trapping temperature and atomization temperature was 300 °C and 2300 °C, respectively. Pyrolysis temperature was adjusted to 800 °C. 10 µL Pd modifier was injected into the graphite tube before each measurement..... | 92 |
| Figure 46 Shapes and positions of analytical signal with changing Pd amount. Shapes and positions of HG-ETAAS signal with varying Pd amount. 0.5 ng/mL Te(IV) solution was trapped over 60 seconds. Trapping temperature and atomization temperature was 300 °C and 2300 °C, respectively. Pyrolysis temperature was adjusted to 800 °C. 10 µL Pd modifier was injected into the graphite tube before each measurement..... | 92 |
| Figure 47 Effect of collection period on HG-ETAAS signal of 0.5 ng/mL Te(IV) solution. Trapping temperature and atomization temperature was 300 °C and 2300 °C, respectively. Pyrolysis temperature was adjusted to 800 °C. 10 µL 1000 mg/L Pd modifier was injected into the graphite tube before each measurement. | |
| | 93 |

| | |
|---|-----|
| Figure 48 Calibration plot for Te using HG-ETAAS using Pd modified graphite tube over 60 seconds time period. Trapping temperature and atomization temperatures were set to 300 and 2300 °C, respectively. Pyrolysis temperature was adjusted to 800 °C. 10 µL 1000 mg/L Pd modifier was injected into the graphite tube before each measurement. Sample flow rate was adjusted to 3.2 mL/min..... | 94 |
| Figure 49 Linear portion of the HG-ETAAS calibration plot and best line equation for Te using Pd modified graphite tube and trapping for 60 seconds time period. Trapping temperature and atomization temperatures were set to 300 and 2300 °C, respectively. Pyrolysis temperature was adjusted to 800 °C. 10 µL 1000 mg/L Pd modifier was injected into the graphite tube before each measurement. Sample flow rate was adjusted to 3.2 mL/min..... | 95 |
| Figure 50 Calibration plot for Te using HG-ETAAS and Pd modified graphite tube over 180 seconds time period. Trapping temperature and atomization temperatures were set to 300 and 2300 °C, respectively. Pyrolysis temperature was adjusted to 800 °C. 10 µL 1000 mg/L Pd modifier was injected into the graphite tube before each measurement. Sample flow rate was adjusted to 3.2 mL/min..... | 96 |
| Figure 51 Linear portion of the calibration plot and best line equation for Te using HG-ETAAS and Pd modified graphite tube over 180 seconds time period. Trapping temperature and atomization temperatures were set to 300 and 2300 °C, respectively. Pyrolysis temperature was adjusted to 800 °C. 10 µL 1000 mg/L Pd modifier was injected into the graphite tube before each measurement. Sample flow rate was adjusted to 3.2 mL/min..... | 96 |
| Figure 52 Effect of stripping Ar flow rate on HG-ETAAS signal of 0.5 ng/mL Te(IV) solution trapped over 60 seconds time period. Sample solution was pumped at 3.2 mL/min. Trapping temperature and atomization temperatures were adjusted to 300 °C and 2000 °C, respectively..... | 100 |

| | |
|--|-----|
| Figure 53 Effect of sample flow rate on HG-ETAAS signal of 0.5 ng/mL Te(IV) solution trapped over 60 seconds on Ru modified graphite tube. Ar flow rate was set to 133 mL/min, trapping temperature and atomization temperatures were adjusted to 300 and 2000 °C, respectively..... | 101 |
| Figure 54 Effect of trapping temperature on HG-ETAAS signal of 0.5 ng/mL Te(IV) solution trapped over 60 seconds. Atomization temperature was set to 2000 °C and sample flow rate was 3.2 mL/min..... | 102 |
| Figure 55 Effect of atomization temperature on the HG-ETAAS signal of 0.5 ng/mL Te solution trapped over 60 seconds. 300 °C trapping temperature was used and sample flow rate was adjusted to 3.2 mL/min..... | 103 |
| Figure 56 Effect of collection period on HG-ETAAS signal of 0.5 ng/mL Te solution pumped at 3.2 mL/min flow rate. Collection and atomization temperatures were adjusted to 300 °C and 2000 °C, respectively. | 104 |
| Figure 57 Calibration plot for trapping of H ₂ Te on Ru modified graphite tube over 60 seconds using HG-ETAAS. Sample flow rate was adjusted to 3.2 mL/min. 300 °C and 2000 °C were selected as trapping temperature and atomization temperature, respectively..... | 105 |
| Figure 58 Calibration plot for trapping of H ₂ Te on Ru modified graphite tube trapped over 180 seconds using HG-ETAAS. Sample flow rate was adjusted to 3.2 mL/min. 300 °C and 2000 °C were used as trapping temperature and atomization temperature, respectively..... | 105 |
| Figure 59 Linear portion of the calibration plot and best line equations for 60 seconds trapping time using HG-ETAAS. Sample flow rate was adjusted to 3.2 mL/min. 300 °C and 2000 °C were used as trapping temperature and atomization temperature, respectively..... | 106 |
| Figure 60 Linear portion of the calibration plot and best line equations for 180 seconds trapping time using HG-ETAAS. Sample flow rate was adjusted to 3.2 mL/min. 300 °C and 2000 °C were used as trapping temperature and atomization temperature, respectively..... | 107 |

| | |
|---|-----|
| Figure 61 Effect of hydride forming elements on the analytical signal of 50.0 ng/mL Te solution by direct ETAAS analysis..... | 112 |
| Figure 62 Effect of hydride forming elements on the HG-ETAAS signal of 1.0 ng/mL Te(IV) solution trapped over 60 seconds..... | 112 |
| Figure 63 Effect of some transition metals on the analytical signal of 50.0 ng/mL Te solution by direct ETAAS analysis. | 113 |
| Figure 64 Effect of some transition metals on the HG-ETAAS signal of 1.0 ng/mL Te(IV) solution trapped over 60 seconds. | 114 |
| Figure 65 Effect of cold vapor forming element on the analytical signal of 50.0 ng/ml Te solution by direct ETAAS analysis. | 115 |
| Figure 66 Effect of cold vapor forming elements on the HG-ETAAS signal of 1.0 ng/mL Te(IV) solution trapped over 60 seconds. | 115 |
| Figure 67 Effect of some soil based elements on the analytical signal of 50.0 ng/mL Te solution by direct ETAAS analysis..... | 116 |
| Figure 68 Effect of some soil based elements the HG-ETAAS signal of 1.0 ng/mL Te(IV) solution trapped over 60 seconds. | 116 |
| Figure 69 Effect of Al on the shape of analytical signal on 50.0 ng/mL Te solution. The straight line denotes the furnace temperature..... | 117 |

LIST OF ABRREVIATIONS

| | |
|-------|---|
| AAS | Atomic Absorption Spectrometry |
| AFS | Atomic Fluorescence Spectrometry |
| C_0 | Characteristic Concentration |
| CHG | Chemical Hydride Generation |
| E | Enhancement Factor |
| ECHG | Electrochemical Hydride Generation |
| EHQTA | Externally Heated Quartz Tube Atomizer |
| E_t | Enhancement Factor in Unit Time |
| ETAAS | Electrothermal Atomic Absorption Spectrometry |
| E_v | Enhancement Factor in Unit Volume |
| FAAS | Flame Atomic Absorption Spectrometry |
| FITA | Flame in Tube Atomizer |
| GLS | Gas Liquid Separator |
| GTA | Graphite Tube Atomizer |
| HCL | Hollow Cathode Lamp |

| | |
|----------|--|
| HG | Hydride Generation |
| HGAAS | Hydride Generation Atomic Absorption Spectrometry |
| HGAFS | Hydride Generation Atomic Fluorescence Spectrometry |
| HG-ETAAS | Hydride Generation Electrothermal Atomic Absorption Spectrometry |
| ICPMS | Inductively Coupled Plasma Mass Spectrometry |
| ICPOES | Inductively Coupled Plasma Optical Emission Spectrometry |
| INAA | Instrumental Neutron Activation Analysis |
| id | Inner Diameter |
| LOD | Limit of Detection |
| LOQ | Limit of Quantification |
| m_a | Characteristic Mass for Peak Area |
| MMQTA | Multiple Microflame Quartz Tube Atomizer |
| m_p | Characteristic Mass for Peak Absorption |
| PSD | Programmable Sample Dispenser |
| PTFE | Polytetrafluoroethylene |
| QTA | Quartz Tube Atomizer |
| RSD | Relative Standard Deviation |
| SRM | Standard Reference Material |

VGAAS

Vapor Generation Atomic Absorption Spectrometry

CHAPTER 1

INTRODUCTION

1.1 Tellurium

Tellurium is a p-block semimetal with an atomic number of 52, atomic mass of 127.6 g/mol, melting point of 449.8 °C and a boiling point of 989.9 °C (**Merian, Anke, Ihnat, & Stoeppler, 2004**). It is one of the nine rarest elements on earth crust. Its relative abundance on earth crust is estimated to be at 0.001-0.005 µg/g level (**Tellurium: geological information, 2009**). It belongs to the same chemical family as oxygen, sulfur, selenium, and polonium.

Tellurium was discovered in 1782 by the Hungarian Franz-Joseph Müller von Reichenstein in Nagyszeben, Transylvania. The name Tellurium was originated from the Latin word tellus meaning “earth” and was given by Klaproth, who isolated it in 1798 (**Sindeeva, 1964**).

Crystalline tellurium has a silvery white appearance, and when pure it exhibits a metallic luster. It is also quite brittle and easily pulverized. Elemental tellurium is insoluble in water, benzene, and carbon disulfide. There exist eight naturally found Te isotopes. Among them ^{122}Te , ^{124}Te , ^{125}Te , ^{126}Te are stable while ^{120}Te ($t_{1/2}>10^{16}$ y), ^{123}Te ($t_{1/2}>10^{13}$ y), ^{128}Te ($t_{1/2}>10^{24}$ y), ^{130}Te ($t_{1/2}>10^{20}$ y) are radioactive but have very long half life (**Merian, Anke, Ihnat, & Stoeppler, 2004**).

Tellurium occurs at +6, +4, +2, 0 and -2 valance states. Compounds containing the TeO_4^{2-} and TeO_6^{6-} ions are known as tellurates and TeO_3^{2-} is known as tellurite (**Merian, Anke, Ihnat, & Stoeppler, 2004**).

1.1.1 Occurrence and Production

Although tellurium occurs at very low levels in earth crust, its cosmic abundance is much higher. It is suggested that Te abundance is the highest in the universe among the elements having the molecular mass greater than 40 (**Cohen, 1984**). Its unexpected low abundance in earth crust is explained by the formation stages of earth. During the formation stages of the earth, most of the O_2 was bonded to the crustal rocks as carbonates and the atmosphere was driven by H_2 gas. It is well known that Te forms volatile hydrides upon reduction. It was suggested that most of the Te was lost to the open space by formation of volatile hydrides (**Wikipedia, 2009**).

Tellurium is found mostly as bonded to other metals such as silver, gold (calaverite, krennerite, petzite and sylvanite) and bismuth. There are no ore deposits which could be mined for tellurium and it is, like selenium, a by-product of the electric copper-refining industry. Electric copper refining serves as the source for 80% of the world's supply of tellurium, and the remainder is recovered from slimes and slags of lead refining and sulfuric acid plants (**Merian, Anke, Ihnat, & Stoeppler, 2004**).

World's leading Te producing countries are Canada, Japan, Peru, Belgium, Philippines and USA. Yearly production of some countries are given in Table 1 and yearly production of Te from 1999 to 2006 is given in Table 2 (**George, 2003**).

Table 1 Yearly production of Te for world leading Te producer countries

| | Production (Tones) | | |
|--------|--------------------|------|------|
| | 2005 | 2006 | 2007 |
| Canada | 11 | 11 | 8 |
| Japan | 23 | 24 | - |
| Peru | 33 | 33 | 33 |

Table 2 World yearly Te Production Rate

| Year | World Production (tones) |
|------|--------------------------|
| 1999 | 116 |
| 2000 | 110 |
| 2001 | 109 |
| 2002 | 89 |
| 2003 | 95 |
| 2004 | 93 |
| 2005 | 130 |
| 2006 | 132 |

1.1.2 Industrial Usage

Tellurium is a p-type semiconductor and it is extensively used in semiconductor and electronics industry. Te-O-Pd phase change films are used in the construction of high density recording data storage discs such as rewritable new generation blue-ray discs (**Nishiuchi, Kitaura, Yamada, & Akahira, 1998**).

Tellurium is used in the construction of high efficiency cadmium telluride (CdTe) or CdZnTe solar panels and radiation detectors (**Bolotnikov, Camarda, Carini, Cui, Li, & James, 2007**).

Another use is in the medical industry for the cure of syphilis disease.

Tellurium is also used as an additive to improve physical properties of alloys. Addition of tellurium improves the strength of tin and the mechanical properties of lead. When added to stainless steel and copper it makes these metals more workable. It is alloyed into cast iron for chill control. Powdered tellurium is used as a secondary vulcanizing agent in various types of rubbers (natural rubber and styrene-butadiene rubbers) as it decreases the time of curing and endows the rubbers. Addition of Te also increases the resistance to heat and abrasion of rubber (**Merian, Anke, Ihnat, & Stoepller, 2004**).

1.1.3 Tellurium and Metabolism

Daily intake of Te in human body is estimated to be 100 µg/day level mainly from the food consumed. There is no information on the absorption of tellurium by humans but animal studies showed that elemental tellurium and tellurium dioxide were very poorly absorbed, whereas 25% of water soluble tellurium was absorbed and distributed in the body (**Hollins, 1969**). 90% of the absorbed tellurium is

bonded to erythrocytes and majority of the rest is bonded to plasma proteins. Very small amount of the adsorbed tellurium is exhaled as dimethyltelluride producing garlic like odor.

Most common tellurium toxicity signs are garlic like odor of breath, loss of appetite, dryness of the mouth, suppression of sweating and metallic taste in the mouth. Target organs of tellurium poisoning are kidney, nervous system, lungs and gastrointestinal tract. Intramuscular injection of tellurium dioxide in guinea pigs caused hemorrhage and necrosis of the kidneys, which became dark gray in color. Young rats exposed to a diet containing elemental tellurium presented with a segmental demyelination of the sciatic nerve and paralysis of the hind limbs. Inhalation of tellurium vapor or hydrides causes irritation of respiratory tract. Rat experiments also showed that exposure to tellurium hexafluoride caused pulmonary edema. Limiting concentrations of tellurium and its compounds are given in Table 3.

Table 3 Limiting concentrations of tellurium and its compounds (Merian, Anke, Ihnat, & Stoepller, 2004).

| | <i>ACGIH TLV</i> | <i>OSHA PEL</i> | <i>Federal Republic of Germany</i> |
|-----------------|-------------------------------|-------------------------------|------------------------------------|
| Elemental Te | TWA 0.1 mg m ⁻³ | TWA 0.1 mg m ⁻³ | — |
| Te dioxide | TWA 0.1 mg Te m ⁻³ | TWA 0.1 mg Te m ⁻³ | — |
| Te Dust or fume | — | TWA 100 µgm ⁻³ | 0.1 mgm ⁻³ |
| Te chloride | TWA 0.1 mgm ⁻³ | TWA 0.1 mgm ⁻³ | — |
| Te hexafluoride | TWA 0.02 ppm | TWA 0.2 mgm ⁻³ | 0.1 mgm ⁻³ |
| Bi telluride | TWA 10 mgm ⁻³ | TWA 0.1 mg Te m ⁻³ | — |

ACGIH TLV: American Conference of Governmental Industrial Hygienists,
Threshold Limit Values

OSHA PEL: Occupational Safety and Health Administration, Permissible
Exposure Limits

TWA: Total Weight Average

1.1.4 Determination of Tellurium

Since tellurium is present in samples at very low concentrations, accurate and sensitive methods are required for the determination of tellurium in environmental and biological samples. Due to low sensitivity, conventional flame atomic absorption spectrometry (FAAS) and inductively coupled plasma optical emission spectrometry (ICPOES) are not suitable for the determination of Te in real samples. Instead, electrothermal atomic absorption spectrometry(ETAAS), inductively coupled plasma mass spectrometry (ICPMS), instrumental neutron activation analysis (INAA), hydride generation atomic absorption spectrometry (HGAAS), hydride generation atomic fluorescence spectrometry (HGAFS) coupled to a preconcentration system is usually applied for the determination of Te.

One of the preconcentration techniques is the coprecipitation of Te species with metal hydroxides. Coprecipitation with La(OH)_3 , Fe(OH)_3 and Mg(OH)_2 was successfully applied in the literature (**D'Ulivo, 1997**). **Andreae (Andreae, 1984)** was able to separate and quantify Te(IV) and Te(VI) species from natural water and seawater samples by selective coprecipitation with Mg(OH)_2 followed by graphite furnace atomic absorption spectrometric determination. He achieved a LOD value of 0.5 pmol/L (63.8 pg/L).

Pedro et al. (**Pedro, Stripekis, Bonivardi, & Tudino, 2008**) developed two methods for the preconcentration of Te. First method used Dowex 1X8 resin and second method used coprecipitation with La(OH)_3 following a preconcentration with XAD resin. After the preconcentration step, Dowex 1X8 and XAD were eluted with acetic acid and nitric acid, respectively. Eluted solutions were sent to Ir pretreated graphite furnaces for the analytical determination. LOD values of the two methods were 7ng/L and 66 ng/L, respectively.

Liao and Haug (**Liao & Haug, 1997**) trapped H₂Te in graphite cuvettes that were pretreated with Zr, Nb, Ta, W, Ir, Ir/Mg and Pd/Ir permanent modifiers. Among the modifiers Ir and Ir/Mg provided the best analytical performance; it was possible to reach an absolute detection limits of 0.011 (Ir coated) and 0.014 ng (Ir/Mg coated) for Se and 0.007 ng for Te with both coatings, according to peak height measurements. They also investigated the long term stability of the Ir/Mg coating and found out that coating was stable over 400 cycles.

Matusiewicz and Krawczyk (**Matusiewicz & Krawczyk, 2007**) combined hydride generation with integrated atom trap flame AAS and reached an LOD value of 0.9 ng/mL. Precision of the method was estimated to be 7.0% RSD (N=6).

Chen and Jiang (**Chen & Jiang, 2000**) coupled flow injection hydride generation to inductively coupled plasma mass spectrometry for the determination of Te in nickel-based alloys. They used several masking agents to eliminate transition metal interferences; a mixture of 0.1% (w/v) L-cysteine and 0.5% (w/v) thiourea was found to be sufficient. Concentration of Te was determined by using isotope dilution and standard addition techniques. LOD value was estimated as 27 ng/g for nickel based alloys.

1.1.4.1 Inorganic Speciation of Tellurium

In addition to the total analyte determination, characterization and quantification of the elements with different oxidation states is also very important due to the unique behavior of these species in the surrounding environment. It is well known that Te(IV) is 10 times more toxic than Te(VI) species (**Karlson & Frankenberger, 1993**). Speciation of Te can be achieved by chromatographic separation followed by an element specific detection technique or applying a nonchromatographic

separation of species by making use of different chemical behavior of each species (**Kumar & Riyazuddin, 2007**).

Körez et al. (**Körez, Eroğlu, Volkan, & Ataman, 2000**) used a mercapto-modified silica microcolumn for selective separation and preconcentration of Te(IV) from water samples. Te(IV) was determined by direct preconcentration and elution of sample solution from the column following analysis by HGAAS. Total Te was determined by similar procedure after reduction of Te(VI) species to Te(IV) in 6.0 mol/L HCl solution. Te(VI) concentration was determined as the difference of total Te and Te(IV). No Te species were found in water samples studied and spike recovery values for several water samples varied between 84% and 110%. An LOD value of 0.037 ng/mL was achieved with a preconcentration factor of 50.

Cava-Montesinos et al. (**Cava-Montesinos, Guardia, Teutsch, Cervera, & Guardia, 2004**) developed a method for the speciation of Te in milk samples by hydride generation atomic fluorescence spectrometry. They used a simple procedure for the quantitative extraction of Te and Se species. Procedure involves sonication of 1.0 g of milk samples in 2.0 mL of aqua regia solution for about 10 minutes. Tetravalent forms of Te and Se were determined without application of a pre-reduction step and total Te and Se were determined after reduction by KBr.

1.2 Atomic Absorption Spectrometry (AAS)

History of optical spectroscopy is dated back to seventeenth century and was first observed by Sir Isaac Newton. He first discovered that sunlight can be splitted into colors using a prism. Later in the history many scientist performed numerous experiments to understand the nature of light. When the black lines in the spectrum of sun were detected by Wollaston in 1802, the scientists realized the close relation

between light and matter. Bunsen and Kirchhoff were the first scientists underlying the principle of absorption and solving the mechanism of formation of dark lines in sun's spectrum. They discovered that matter absorbs light at the same wavelength at which it emits light. This was the first basic principle of atomic absorption spectrometry (**Welz & Sperling, 1999**). Later in 1955, Walsh and a team of Australian researchers introduced the world with the modern form of AAS by publishing the article "*The application of atomic absorption spectra to chemical analysis*" (**Walsh, 1955**).

Walsh and his colleagues were first developed and used hollow cathode lamps (HCL) as radiation source (**L'vov, 2005**). One of the early designs developed by Walsh and his colleagues is given in Figure 1. Until then numerous papers making use of this concept and its applications have been published.



Figure 1 One of the first AAS instrument designed by Walsh (L'vov, 2005).

Theory of AAS is based on the fact that ground state gas phase atoms absorb electromagnetic radiation at specific wavelengths to be excited to a specific excited

electronic state. The energy difference between the two states determines the wavelength of radiation absorbed. Mainly an AAS instrument consists of a radiation source, a heated atomization unit, a wavelength selection unit, a detector and data processing system. AAS instruments can be classified on the basis of sample atomization units as flame AAS and electrothermal AAS.

1.2.1 Flame AAS (FAAS)

The technique of FAAS requires a liquid sample to be aspirated, aerosolized, and mixed with combustible gases. The mixture is then sent to a slot burner where it is ignited in a flame. Target species are atomized by the help of heat generated as a result of the combustion process. A light beam specific to target atom is passed over the flame. The amount of absorbed radiation is a quantitative measure for the concentration of the element to be analyzed (**Welz & Sperling, 1999**).

Temperature is a critical factor for the atomization, thus the performance of flame as well. Temperature of a flame is dependent on the type and flow rate of fuel and oxidant used. A typical FAAS instrument using air-acetylene flame has a temperature of around 2300°C and flow rate of acetylene is about 4.0 L/min.

Another critical point is the sample introduction unit. Most FAAS instruments are equipped with a pneumatic nebulizer that converts the sample solution into finely divided small droplets by the help of high pressure gas flow. Pneumatic nebulization has been commonly used in real analysis because of its simplicity, good stability and low memory effects, but these nebulizers have the disadvantages of low nebulization efficiency, mostly 3-10 %, and consumption of relatively large volume of sample solution (**Rademeyer, 1996**).

1.2.2 Electrothermal AAS (ETAAS)

When first flame AAS instruments were developed they had the sensitivity problem due to low transport efficiency of the sample solution to the flame and limited residence time of the atoms. To overcome these problems a Russian physicist and also a chemist, B. V. L'vov, searched for a more efficient way of introduction of sample to the AAS system and came up with the idea of ETAAS. His idea was quite simple; instead of aspirating the solution in a flame he placed a small amount of sample solution, about micro liter level, directly in a graphite tube located on the optical path of an AAS system. After some drying and ashing processes he was able to atomize the analyte at an elevated temperature by applying a high potential across the graphite tube. He published his ideas in 1959 (**L'vov, 2005**); but there was very little interest among the analytical chemists at that time. Later in 1960s H. Massman from the Institute of Spectrochemistry and Applied Spectroscopy in Dortmund, Germany worked on the ideas of L'vov. He simplified the design and analytical procedure applied and ETAAS become more and more popular through the world of analytical chemistry.

Modern ETAAS systems mostly use graphite cuvettes as the sample holder and atomization unit. An inert gas is supplied through the system to isolate the graphite from the surrounding atmosphere. A low voltage corresponding to a low temperature (100-200 $^{\circ}\text{C}$) is applied to the sample cuvette for the drying of solvents present in the sample matrix. Following this step, an ashing process is applied to remove the organic and low boiling point components of the matrix. Selection of the ashing temperature is quite critical; it should be high enough to destroy the matrix components and other interferences but also it should not cause the loss of analyte atoms by volatilization. This step is necessary for samples that contain considerable amount of matrix components that, otherwise, cause spectral and

nonspectral interferences affecting the analytical signal. Atomization takes place at an elevated temperature and flow of inert gas is stopped to increase the residence time of analyte atoms. After this point a cleaning step with a little higher temperature is usually applied to remove any residue left in the system (**Fuller, 1977**).

Despite the advantages of ETAAS over FAAS, there are also pronounced disadvantages of the method. One problem related with the ETAAS is the interferences faced in the graphite cuvette especially if the analyte is present in a heavy matrix. Another disadvantage is the inhomogeneous atomization of the analyte atoms due to inhomogeneous temperature profile of the graphite. Frech and Baxter (**Frech & Baxter, 1995**) showed that inhomogeneous heating of graphite tube results in nonuniform distribution of non-atomic species over the tube cross-section. Distorted or splitted peaks are observed when analyte atoms present more than one form in the sample matrix.

1.3 Vapor Generation AAS (VGAAS)

As mentioned above conventional FAAS instruments using pneumatic nebulizers suffer from the low transport efficiency of sample solution (3-10%) to the atomization unit. One alternative sample introduction technique is the vapor generation (VG). A definition VG is given below (**Sturgeon, Guo, & Mester, 2005**):

"A process wherein volatile or semi-volatile analyte species are generated from nonvolatile precursors (usually ionic, metallic or organometallic) to permit their subsequent transfer from a condensed phase to the gas phase for enhanced detection capability."

According to this technique, target atoms are converted to volatile species by chemical or electrochemical means (**Nakahara, 1991**). These volatile species are then transported to a heated atomizer by the help of a carrier gas. Volatilization of species can be performed by hydride formation (**González, Llorens, Cervera, Armenta, & Guardia, 2009**), cold vapor formation (**Liva, Muñoz-Olivas, & Camara, 2000**), chelate formation (**Leskela, Niinistö, Nykanen, Soininen, & Titta, 1991**), alkyl formation (**Chau, Wrong, & Bengert, 1982**), carbonyl formation (**Johansson, Snell, Frech, & Hansson, 1998**), oxide formation (**Gregorie, 1990**) and halide formation (**Skogerboe, Dick, Pavlica, & Lichte, 1975**). Among these, hydride generation is the most frequently applied method for the determination of As, Bi, Ge, Pb, Sb, Se, Sn, and Te.

1.3.1 Hydride Generation AAS (HGAAS)

Hydride generation technique relies on the conversion of analyte atoms to volatile hydrides by chemical or electrochemical means. Hydride generation was first used for arsenic determination, known as Marsh reaction. Adaptation of hydride generation to AAS was first proposed and successfully applied by Holak in 1969 (**Holak, 1969**). Later in the history tremendous effort has been put into action in the literature. Among the elements As, Bi, Ge, Pb, Sb, Sn, Se and Te are known to form stable hydrides upon reduction with a suitable means. Molecular formulas and some physical properties of those hydrides are given in Table 4. HGAAS can be applied in a variety of fields including food, environment, metallurgy, waste management and geology (**Dedina & Tsalev, 1995**).

Table 4 Physical properties and generic names of some hydrides (Dedina & Tsalev, 1995)

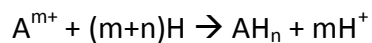
| Element | Name | Formula | Melting Point, °C | Boiling Point, °C | Solubility in Water (μg/mL) |
|---------|-------------------|-------------------|-------------------|-------------------|-----------------------------|
| As | Arsine | AsH ₃ | -116.3 | -62.4 | 696 |
| Bi | Bismuthine | BiH ₃ | -67 | 16.8 | - |
| Ge | Germane | GeH ₄ | -164.8 | -88.4 | Insoluble |
| Pb | Plumbane | PbH ₄ | -135 | -13 | - |
| Sb | Stibine | SbH ₃ | -88 | -18.4 | 4100 |
| Se | Hydrogen Selenide | H ₂ Se | -65.7 | -41.3 | 37700-68000 |
| Sn | Stannane | SnH ₄ | -146 | -52.5 | - |
| Te | Tellurium Hydride | H ₂ Te | -51 | -4 | Very Soluble |

Hydride generation can be classified as chemical hydride generation (CHG) and electrochemical hydride generation (ECHG).

1.3.1.1 Chemical Hydride Generation (CHG)

A chemical reaction between a reducing agent and acidified sample solution is utilized in CHG. As a result of the chemical reaction volatile hydride species are formed.

First method for chemical hydride generation is through nascent hydrogen formation. In early times researchers made use of Marsh reaction, which is based on the reaction of a metal with acid. Zn-HCl pair is used for most of the cases due to their high reactivity. As the next step, it is assumed that formed nascent hydrogen reacts with analyte ions and forms hydride species.



Other metals and reducing agents, such as Mg, Al and TiCl₃ were also used in the literature (**Dedina & Tsalev, 1995**).

Second and the most popular method involves the reaction of either NaBH₄ or KBH₄ with acidified sample. Use of borohydride for hydride generation was first proposed by Braman et al. (**Braman, Justen, & Foreback, 1972**) for the determination of nanogram levels of arsenic and antimony. First applications used the pellet or solid forms but later granular borohydride dissolved in basic aqueous medium became popular. Usually NaOH or KOH is added to decrease the rate of hydrolysis of borohydride in water.

In first studies, it was believed that reaction of NaBH_4 with acid result in nascent hydrogen formation and consecutive hydride formation via nascent hydrogen mechanism. However, D'Ulivo et al. (**D'Ulivo, Mester, & Sturgeon, 2005**) studied the mechanism of hydride formation by use of GC-MS system and deuterium labeled species and found out that the mechanism of hydride formation is much more complicated than it was thought. They proved that formation of bismuthine involves direct transfer of hydrogen originally bonded to boron. Nascent hydrogen theory fails with this result since if the hydride generation was achieved through the nascent hydrogen formation; then hydrogens of the bismuthine should be oriented both from HCl and borohydride. This result implies the formation of an intermediate boron-bismuth complex and consecutive decomposition of this complex. On the other hand, hydrogen of GeH_4 and SnH_4 are originated from both acid and NaBH_4 . Same group also investigated the hydrogen exchange possibility of formed hydrides and found that hydrogen exchange could take place between formed hydrides with the surrounding water or acids at certain pH ranges (**D'Ulivo A. , Mester, Meija, & Sturgeon, 2006**).

1.3.1.2 Electrochemical Hydride Generation (ECHG)

ECHG was first proposed and successfully applied by Rigin (**Rigin, 1978**). Basic principle of the system is a redox reaction taking place in an electrochemical cell. A catholyte solution containing the analyte and anolyte solutions are pumped through the cell and reaction products are sent to a gas liquid separator where formed gaseous species are separated from the liquid phase.

ECHG offers some advantages compared to CHG. Firstly, there is no need for the use of NaBH_4 which is expensive and difficult to handle and store due to low stability. It is also the main source of blank signal, whereas ECHG uses only acids for

production of volatile compound. Purification of acids is much simpler. As a result, this method offers lower blanks and thus lower detection limits. Additionally, it does not depend on the oxidation state of the analyte when using cathode materials with high hydrogen overvoltage like Pb or amalgamated Ag. Speciation analysis can be done by careful selection of the catholyte solution (**Menemenlioğlu, Korkmaz, & Ataman, 2007**).

In addition to its advantages there are disadvantages of the ECHG technique. Firstly, daily conditioning of the cathode and anode surfaces is needed to get reproducible signals. Interfering atoms may deposit on the surface of electrodes which may alter the electrode potentials, hence hydride formation (**Denkhaus, Gollock, Guo, & Huang, 2001**).

1.3.1.3 Advantages and Drawbacks of Hydride Generation Atomic Absorption Spectrometry

HGAAS offers many advantages over conventional systems as high analyte transport efficiency, partial separation from sample matrix, high sensitivity with a relatively low cost, flexibility, adoptability to online and offline preconcentration systems and easy operation (**Welz & Sperling, 1999**).

Despite the advantages, HGAAS has certain disadvantages that worth mentioning. Since the method involves reaction of an acidified sample with a powerful reducing agent, usually NaBH_4 , a vigorous reaction with a rather complex reaction mechanism is involved. This complexity makes the optimization of reaction conditions difficult. Reaction yields and kinetics are also strongly affected from oxidation state and form of the analyte elements. It is well known that inorganic trivalent arsenic forms hydride with high yield as compared to its pentavalent form. Thus, usually a prereaction step is needed when total As concentration is to be

determined. Additional prereduction steps mean extra workload and possible contamination from chemicals and reagents used (**Tsalev, 2000**). Another disadvantage is regarding the transport of hydride species to atomization unit. Willie et al. (1986) (**Willie, Sturgeon, & Berman, 1986**) showed that significant amount of volatile Se species can be lost over the walls of transport line. Usually a silanization process is needed to prevent adsorption losses on glass surfaces. It is also known that presence of water droplets on surfaces can cause adsorption losses. Chemical interference is another serious problem regarding HG. This influence is more severe for analytes of low hydride generation efficiency (**Ding & Sturgeon, 1997**). Additionally, specific optimum experimental conditions are needed for individual elements and multielement determination capability is very limited.

1.3.2 Hydride Atomization

Atomization is the last and probably the most important step of a HGAAS system. This step includes the conversion of analyte into free atoms. According to Dedina (**Dedina, 2007**) an ideal atomizer should fulfill some requirements as;

1. Atomizer should completely convert the analyte atoms to free atoms,
2. Atomizer should prevent atomization interference hence loss of analyte atoms in observed volume,
3. Atomizer should provide a long residence time for analyte atoms on the optical path,
4. Atomizer should minimize measurement noise,
5. Atomizer should be adaptable to preconcentration systems,
6. Atomizer should be operated with minimum effort and minimum cost.

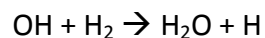
It should be noted that no single real world atomizer meets these requirements, only some reaches individual criteria to some extent. Choice of atomizer is highly dependent on the type of analysis applied.

In the literature by far the most popular online atomizer is the heated quartz tube atomizers (QTA). There are many different design of QTA present in the literature. Basically the design consist of an inlet arm where formed hydrides and other necessary gasses are introduced to a tube placed on the optical path of the AAS spectrometer. QTA systems can be subdivided into two as flame in tube atomizers (FITA) and conventional externally heated QTA (conventional EHQTA).

1.3.2.1 Flame in Tube Atomizers (FITA)

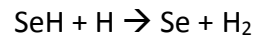
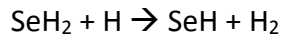
This kind of atomizers makes use of a highly fuel rich hydrogen-oxygen microflame formed inside a quartz tube. As a result of combustion of hydrogen a high temperature (about 2800 °C) is obtained in a very restricted area. These atomizers do not need an external heating system but carrier gas should contain enough hydrogen and oxygen to sustain a microflame. Siemer et al. (**Siemer & Hageman, 1975**) first described FITA for Se determination. Schematic representation of this design is shown in Figure 2. Outlet of the GLS is connected to the horizontal arm of T tube. An external hydrogen-inert gas mixture is used for the stripping of volatile species and as carrier. Oxygen is supplied from the bottom of the junction point via a capillary as an oxidant. At the tip of the capillary a hydrogen diffusion flame is sustained where atomization takes place. Although, the system essentially can be operated without any external heat source, heat is usually applied (around 150 °C) to prevent formation of water droplets on the cooler parts of the atomizer. Dedina and Rubeška (**Dedina & Rubeska, 1980**) found out that atomization of SeH_2 is much more efficient in a hydrogen flame where there are a lot of hydrogen radicals

produced. They proposed the following mechanism for the formation of hydrogen radicals.



Amount of radicals formed is very much dependent on O_2/H_2 ratio. For an efficient radical formation excess of H_2 is needed and amount gets lower as the ratio approaches 0.5 which is the stoichiometric ratio.

Formed hydrogen radicals further react and deprotonate the SeH_2 via the following proposed mechanism. It is believed that atomization process is more or less similar for other hydrides.



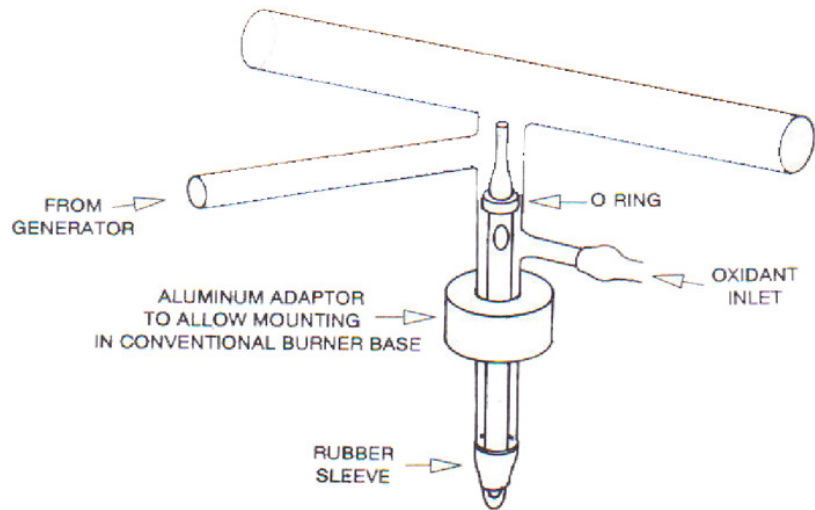


Figure 2 Schematic representation of T-shape FITA (Dedina & Tsalev, 1995).

As the concentration of radicals in the atomization zone increases, rate of deprotonation of the analyte increases since the system is ruled kinetically rather than thermodynamically. From this perspective FITA has better atomization performance and less atomization interference compared to externally heated atomizers (Dedina & Tsalev, 1995).

1.3.2.2 Conventional Externally Heated Quartz Tube Atomizer (EHQTA)

Design of EHQTA is similar to those of FITA with the exception that there is no hydrogen flame suspended. This design is the most widely used atomizer design due to easy operation and applicability to ordinary AA systems with little modification. An external air-acetylene flame or electrical heating using resistive wires located inside a furnace system is applied to sustain a temperature of about 700 to 1100 °C inside the atomizer. Atomizer is most often in T-shape design where hydrides and carrier gas are supplied to the inlet arm connected to the horizontal part on the

optical path. Horizontal part is usually about 10-15 cm long and has an id of 2-5 cm as shown in Figure 3. Other L-shaped and concentric atomizers are also applied in the literature (**Thompson & Thomerson, 1974; Rezacova & Dedina, 2009**).

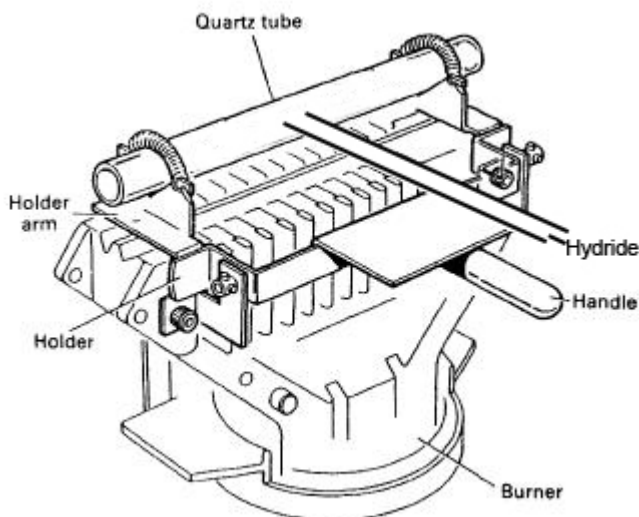


Figure 3 Schematic representation of EHQTA.

It has been shown that hydrides cannot be atomized without hydrogen (**Dedina & Tsalev, 1995**). Hydrogen is usually supplied as a result of the decomposition of tetrahydroborate.

1.3.2.3 Multiple Microflame Quartz Tube Atomizer (MMQTA)

FITA has the disadvantage of low residence time resulting in low sensitivity but superior to EHQTA from atomization point of view since analyte atoms are in contact with H radicals. On the other hand EHQTA have high sensitivity due to relatively long residence time in the optical path. Dedina and Matousek (**Dedina &**

Matousek, 2000) designed a new atomizer, which they call multiple microflame quartz tube atomizer (MMQTA) to combine the advantages of both designs.

Design consists of two concentric quartz tubes. Light beam passes through the inner tube which contains small holes distributed throughout its body. Air or oxygen is supplied into the area between tubes at a flow rate of 25-30 mL/min and hydrides are introduced to the system by the help of an arm just like the EHQTA. A schematic view of the MMQTA is shown in Figure 4. Upon heating microflames are formed at the tip of the holes throughout the atomizer. By this way a high H radical density is sustained in a large area. This result in more efficient atomization and hence elimination of curvature in the calibration plot and one to two orders of magnitude better resistance to interferences (**Dedina, 2007**).

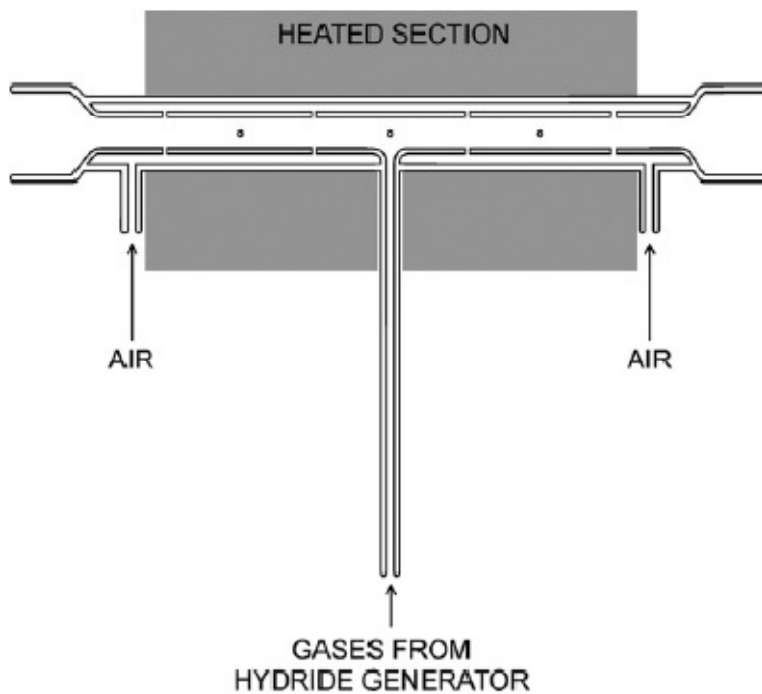


Figure 4 Schematic representation of MMQTA (Dedina & Matousek, 2000).

1.4 Trapping Systems

In order to increase the sensitivity, vapor generation systems can be coupled to trapping units. These trapping units can be classified as molecular traps and atom traps.

1.4.1 Molecular Traps

This technique traps analyte atoms in molecular form. Molecular traps can be divided into three as adsorbent medium trapping, pressure trapping and cryogenic trapping.

1.4.1.1 Absorbing Medium

This technique uses either an absorbing solutions or solid absorption media. Madsen (**Madsen, 1971**) first used 0.01 mol/L AgNO_3 solution to collect arsine generated in a batch reactor system. There are several advantages of this approach. This technique is suitable for cases where formed hydrides have to be stored for some time before analysis, i.e. it suits for offline analysis. Moreover, no special atomizer is needed and conventional systems can be used for atomization. Disadvantage of the technique is that it is time consuming and a rather high contamination risk is involved (**Dedina & Tsalev, 1995**).

1.4.1.2 Pressure Collection

This technique involves the use of a closed container where the formed hydrides are kept under high pressure. After a certain collection period, formed species are sent to atomization unit at once and usually a transient signal is obtained. Narasaki (**Narasaki, 1988**) used the interior volume of a gas liquid separator as the collection vessel for determination of As and Se in water samples and achieved LOD values of 0.01 and 0.005 ng for arsenic (III) and selenium (IV), respectively.

Although the system was popular in early 1970s nowadays its use is rather limited due to development of more sensitive techniques that are relatively easy to operate. Another drawback is that some of the hydrides, namely plumbane, tellurium hydride and stannane, are not stable enough for collection as gaseous phase (**Dedina & Tsalev, 1995**).

1.4.1.3 Cryogenic Traps

This technique involves the use of a U-tube that is immersed in liquid nitrogen. Outlet of gas-liquid separator (GLS) is connected to this U-tube where hydrogen gas evolved passes freely and formed hydrides are trapped on the cold surfaces of the tube. After the collection step tube is heated externally and trapped hydrides are evaporated and sent to atomization unit. Howard and Salou (**Howard & Salou, 1998**) were able to perform speciation analysis of arsenic by using the differences in boiling points of formed As hydride species. Sensitivity of system can be further increased by placing an adsorbent material inside U-tube collector. An advantage of the system over other collection methods is that trapping can be applied to large volume of samples. Only limitation is the capacity of the trap. Disadvantages are that precise control of experimental variables, especially temperature, is needed to get reproducible signals. Another disadvantage is that during revolatilization step

losses can be observed for unstable hydrides. Lee (**Lee, 1982**) showed that 80 % of the bismuthine was decomposed during revolatilization step.

1.4.2 Atom Traps

1.4.2.1 Graphite Furnace Trap

In situ collection of volatile species on heated graphite tube surface was first introduced by Drasch et al. (**Drasch, Meyer, & Kauert, 1980**) for determination of As. They used a commercially available graphite tube for the collection of volatile As species. For this method formed hydrides were introduced to a heated graphite tube sample port via a glass, quartz or polytetrafluoroethylene (PTFE) tubing. This step is called as collection or trapping. At this stage hydrides are decomposed and deposited on the heated walls of graphite tube and tube assembly. Lee (**Lee, 1982**) studied the deposition of bismuthine and found out that 61% of the generated bismuthine was captured in the graphite interface, 11% in the atomizer tube and the rest is lost. After the collection step trapped atoms are reatomized by the application of temperature usually above 2000 °C to assure complete atomization. Trapping temperature and position of tip are crucial and should be optimized to minimize losses.

Surface of the graphite tubes are mostly treated with high boiling point and carbide forming elements such as Zr, Ir, Pd, Rh or combination of those elements (**Furdíková & Dočekal, 2009; Laborda, Medrano, Cortés, Mir, & Castillo, 1999**) to increase the lifetime of graphite tube. Applied metals may also increase trapping efficiency of the surface for certain elements. Another advantage of metal modifiers is that they increase appearance temperature in atomization step.

Popularity of the method comes from the relatively easy operation, high sensitivity, stable signal and lack of need for an external hydrogen supply. Despite the advantages there are certain disadvantages to bear in mind. Due to their small sizes trapping efficiency and linear range of graphite tubes are relatively lower than quartz tube atomizers. In addition, presence of hydrogen gas coming from the reaction of NaBH_4 and acid reduces the lifetime of tube by reacting with graphite (**Krivan & Petrick, 1990**). In the same manner transfer of water as aerosol decreases the lifetime of tube and lead to high background readings. Furthermore, application of high atomization temperature result in decreasing the signal height (**Dedina & Tsalev, 1995**)

1.4.2.2 Quartz Trap

This technique uses an externally heated quartz surface as trapping media. Usually inlet arm of a T-tube atomizer can be used directly or crushed quartz particles may be placed inside the arm to increase the surface area (**Korkmaz, Ertaş, & Ataman, 2002**). Working principle of quartz trap is similar to that of graphite furnace with some exceptions. Quartz surface is heated externally to an optimized temperature at the trapping stage. After this stage temperature is further increased to a higher value for revolatilization. Usually hydrogen gas is introduced to the system to create a reducing environment and help revolatilization of the trapped species. Main difference between a quartz trap and graphite furnace is that the former is used as a trap and later is used as both trap and atomizer. In addition, using the quartz trap, more economical analysis is provided since there is no need for a graphite furnace; a simple flame AA spectrometer and a laboratory-made HG system is sufficient. Distance between the quartz trap and atomizer is an important parameter to be optimized for individual element since each element forms different volatile species with a distinct lifetime. Species should be stable enough to travel between the trap

and the atomizer. Other important parameters that affect signal are trapping and revolatilization temperature and carrier gas composition at both stages (**Ataman, 2008**).

Kratzer and Dedina (**Kratzer & Dedina, 2008**) used the inlet arm of a multiple microflame atomizer to trap stibine and bismuthine. In addition to external heating they used a hydrogen microflame created by the reaction between hydrogen gas formed during hydride generation and external oxygen supplied via a glass capillary at the trapping stage. Subsequent revolatilization was achieved by application of higher temperature and extinguishing the microflame flame by closing the oxygen supply and hence creating a reducing atmosphere rich in hydrogen gas. Mechanism of trapping and revolatilization are not fully understood but it definitely involves oxidation-reduction of species.

Korkmaz et al. (**Korkmaz, Ertaş, & Ataman, 2002**) used an externally heated quartz trap for determination of Pb and reached a LOD value of 19 ng/L.

The heating rate of quartz is relatively slow, about 60 s to reach steady state temperature; therefore, volatilization step requires some time which may lead losses of trapped atoms and thus broad peaks may be observed.

1.4.2.3 Metal Traps

An alternative trapping technique is the use of resistively heated metal traps. Most popular metal trap is W coil atom trap since it has a high heating rate and easily and economically obtained mostly from a commercial light bulb. First application of W coil as trapping surface for hydride generation were reported by two different groups about the same time (**Cankur, Ertaş, & Ataman, 2002; Barbosa, Souza, & Krug, 2002**). Tungsten coil is placed in the inlet arm of a T-tube atomizer and

connected to a variable power supply. Temperature of the coil is set by adjusting the potential over the W coil. At the trapping step formed hydrides are sent to the surface of resistively heated coil. Hopefully the hydrides are decomposed and deposits on the hot surface. Trapping step is followed by the revolatilization at which a high voltage is applied which result in high temperature. Barbosa et al. (**Barbosa, Souza, & Krug, 2002**) used the W coil as atomizer whereas Cankur et al. (**Cankur, Ertas, & Ataman, 2002**) used it for volatilization of the sample only; there is no need for an atomizer for the former design whereas latter needs an atomizer.

Obviously O₂ enters the system from the connection points, from Ar gas and from the sample itself and cause oxidation of W surface. These formed W-oxides cause increase of the background absorption by forming small particles that scatter incident radiation. For both collection and revolatilization steps an external H₂ supply is needed to prevent the oxidation of W coil. Oxidation of the surface can readily be monitored by naked eye by the formation of brown, blue and blue colored surfaces corresponding to formation of WO₂, W₂O₅ and W₄O₁₁, respectively (**Cankur O., 2004**). Although there is H₂ evolution from the reaction between acid and reductant, this is usually not enough to protect the W coil surface from oxidation.

Kula et al. (**Kula, Arslan, Bakirdere, & Ataman, 2008**) were able to achieve 20.1 times enhancement over conventional hydride formation system for selenium determination by using a resistively heated tungsten coil atom trap.

1.5 Chemical Vapor Generation of Transition and Noble Metals

HG offers a convenient way for the introduction of an analyte to an atomic detection system. One of the pronounced drawbacks of HG is that it is limited to a

group of elements, such as As, Sb, Se, Sn, Ge, Bi, Pb and Te, that are capable of forming stable hydrides upon the reaction with a reductant solution. In the last decade several researches extended the scope of HG to transition metals and noble metals due to pronounced advantages of the method (Section 1.3). Formation of volatile species of Ag, Cd, Co, Cu, Ni and Zn was investigated by Villanueva-Alonso et al. (**Villanueva-Alonso, Peña-Vázquez, & Bermejo-Barrera, 2009**) and it was shown that in the presence of an enhancement reagent, cobalt and 8-hydroxyquinoline, vapor generation efficiency of those metals increases. Role of these enhancement reagents are still unknown but it is believed that enhancement reagents may form metastable complexes with NaBH₄ and reaction proceeds through those intermediates (**Sun & Suo, 2004**). Feng et al. reported that Ag, Au, Cu, Pd, Ag, Pt, Au, Co, Ni, Rh, Ti, Mn, Zn, Fe and Ir are, to some extent, capable of forming volatile species (**Feng, Sturgeon, & Lam, 2003**). Nature of these formed volatile species and formation mechanism is yet unknown but it was observed that species are relatively unstable and decay rapidly.

1.6 Interferences

In spectroscopy, interferences can be divided into two as spectral interferences and nonspectral interferences.

Spectral interferences are the result of absorption or scattering of radiation by species other than analyte atoms (**Dedina & Tsalev, 1995**). In hydride generation, probability of line overlapping is very low due to partial separation of matrix from analyte atoms. Spectral interferences mostly occur due to band absorption caused by transported molecular species. Molecular transport is significant as concentration of acid and reductant increase. This increase is due to harsh reaction conditions which produce large amount of aerosol.

Another reason of background absorption at low wavelengths is due to presence of oxygen since oxygen molecules have structured absorbance in that field. Droessler and Holcombe (**Droessler & Holcombe, 1986**) showed that observed absorbance increase with increasing temperature in graphite furnaces.

Nonspectral interference is due mainly to matrix-induced signal enhancement or suppression. In hydride generation nonspectral interferences can further be classified as liquid phase and gaseous phase interferences.

Liquid phase interferences are due to change in the rate of hydride release from liquid phase and/or due to decreased efficiency of hydride release. This may happen through several possible mechanisms but can be categorized as compound interferences and matrix interferences. Compound interference happens when the analyte in the sample is present in different forms. This mostly happens when analyte atoms are bonded to organic groups that decrease generation efficiency. Elements like Sb and As have different valencies and each of these species has a different hydride forming efficiency. Matusiewicz and Krawczyk (**Matusiewicz & Krawczyk, 2008**) investigated the hydride formation efficiency of Sb and use different kinetics for ultratrace speciation analysis.

CHAPTER 2

EXPERIMENTAL

2.1 Chemicals and Reagents

All reagents used throughout this study were of analytical grade or higher purity. A 1000 mg/L Te(IV) stock solution was prepared by dissolving appropriate amount of TeO₂ (Fisher Laboratory Chemical, U.S.A.) in 10% (v/v) HCl solution by the help of an Elma S40 H ultrasonic water bath (Germany). A 1000 mg/L CertiPUR Te (VI) solution prepared from H₆TeO₆ in 0.5 mol/L HNO₃ was obtained from Merck (Darmstadt, Germany). Working solutions of Te (IV) and Te (VI) were prepared daily by successive dilutions. Dilutions were made using 18 MΩ·cm deionized water obtained from a Millipore (Molsheim, France) Milli-Q water purification system which was fed using the water produced by Millipore Elix 5 electro deionization system. Working standard solutions were acidified with proanalysis grade HCl (Merck, Darmstadt, Germany). Purity of the acid used was controlled routinely by comparing the blank values of stock and distilled acid obtained by using a PTFE subboiled acid distillation system (Berghof, Eningen, Germany). Since no blank was observed, acids were used directly without further purification. High purity Ar (99.999 %) was used throughout the study.

Working solutions were prepared in 4.0 mol/L HCl solution. Prepared solutions were transported and stored in polypropylene boxes. All glassware and plastics used

throughout the study were immersed in 10% (v/v) HNO₃ at least 24 hours and rinsed with deionized water before use.

Reductant solution was prepared daily or more frequently by dissolving appropriate amount of powdered proanalysis grade NaBH₄ (Merck, Darmstadt, Germany) in 0.5% NaOH (Riedel, Germany). Solution was used directly without filtration.

A 1000 mg/L Pd stock solution was prepared by dissolving solid K₂(PdCl₆) in 1.0 mol/L HNO₃. 100 mg/L Ru solution was prepared by dissolving appropriate amount of solid Ru(Cl)₃. 3H₂O (Aldrich) in 5.0 mL aqua regia and successive dilution to final volume.

2.2 Spectrometer

For continuous flow hydride generation studies a Varian AA140 (Victoria, Australia) atomic absorption spectrometer equipped with a deuterium arc background correction system and 10.0 cm burner head was used. Instrument was controlled and data were processed by the help of SpectrAA software (version 5.1). A Photron (Australia) uncoded Te hollow cathode lamp was used as the radiation source. Summary of the instrumental parameters are given in Table 5.

Table 5 Operating conditions of AA spectrometer

| Parameter | Value |
|----------------------------|------------------------------|
| Measurement Wavelength, nm | 214.3 |
| Spectral bandpass, nm | 0.2 |
| Lamp Current, mA | 10 |
| Flame Type | Stoichiometric Air/Acetylene |
| Read Time, s | 10 |
| Measurement mode | Integration |

Graphite furnace studies were performed by replacing the flame assembly with Varian GTA 120 graphite tube atomizer apparatus. Measurements were performed by the help of Varian PSD 120 programmable sample dispenser. Longitudinally heated pyrolytic coated graphite tubes were used throughout the study.

2.3 Hydride Generation System

Experiments were performed in continuous mode. Sample solution and NaBH₄ solutions were pumped through the system by Gilson Minipuls 3 (Villers Le Bell,

France) 4-channel peristaltic pumps and yellow-blue color coded 1.27 mm id Tygon® peristaltic pump tubings were used. Waste solution was removed from the system by the help of a Gilson Minipuls 3 4-channel peristaltic pump. 3 way T-shaped PTFE connectors (Cole Palmer, Illinois, USA) were used in junction points of solutions and gasses. PTFE connection tubings (Cole Palmer) with 0.56 mm id were used throughout the construction of system.

For stripping of the formed hydrides from sample solution high purity gasses were introduced to the system by the help of PTFE rotameters (Cole Palmer). Rotameters were calibrated regularly by a laboratory made soap bubble flowmeter.

A laboratory made borosilicate GLS was placed after stripping coil. Dimensions and schematic diagrams of the GLS used is given in Figure 5.

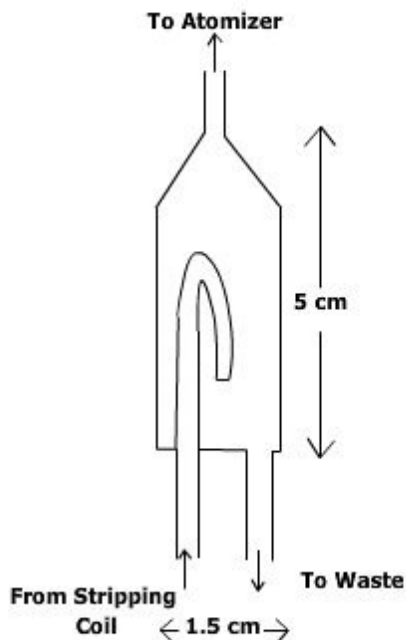


Figure 5 Schematic representation of cylindirical type GLS.

Formed volatile species were transported to the atomization cell by the help of 20.0 cm length 0.056 mm id PTFE tubing. A schematic representation of the hydride generation system is given in Figure 6.

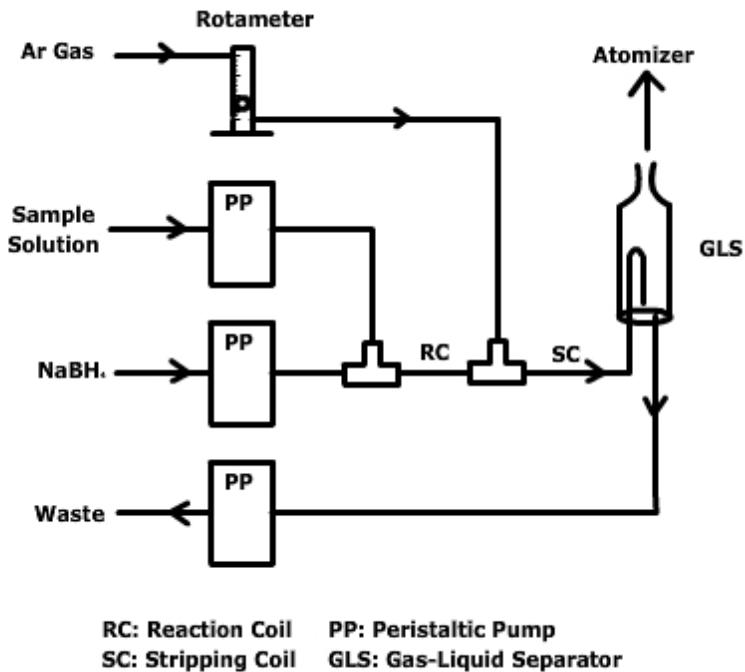


Figure 6 Schematic representation of hydride generation system.

2.4 Atomization Units

2.4.1 Continuous Flow Atomization Unit

An externally heated T-shaped QTA (Çalışkan Cam, Ankara, Turkey) was used throughout the study. QTA dimensions are given in Figure 7. QTA was placed 3.0 mm above the burner head by the help of QTA holding apparatus. When a new T-tube was used, it was conditioned by using 50 mL of 1.0 mg/L Te(IV) solution with

the optimized hydride generation conditions. This conditioning was necessary to saturate the quartz surface, otherwise signal fluctuations were observed.

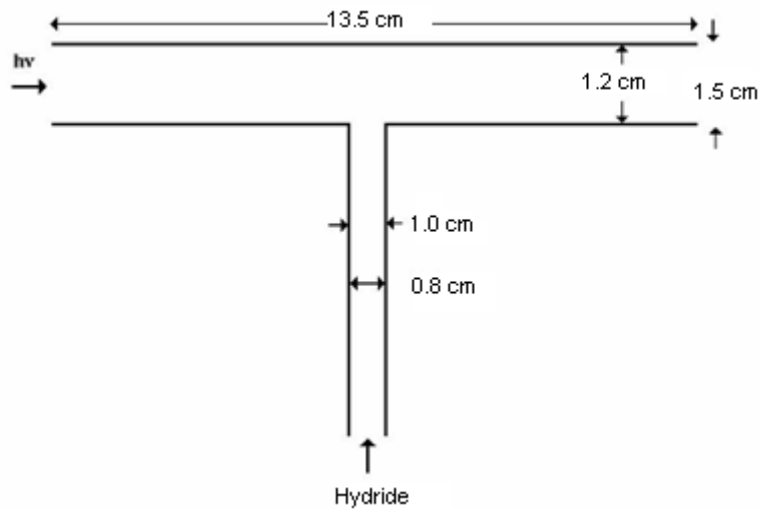


Figure 7 Schematic Representation of externally heated quartz tube atomizer

2.4.2 Graphite Furnace Atomization Unit

For graphite furnace trapping system, outlet of GLS was connected to the graphite furnace autosampler arm by the help of 0.056 mm id PTFE tubing. A quartz capillary with a 0.5 mm id was placed at the tip of the autosampler arm. Sampler arm was adjusted such that at the collection step, quartz capillary was aligned at the center of the graphite tube. Varian furnace camera apparatus was used to align quartz capillary. Schematic diagram of the system is given in Figure 8.

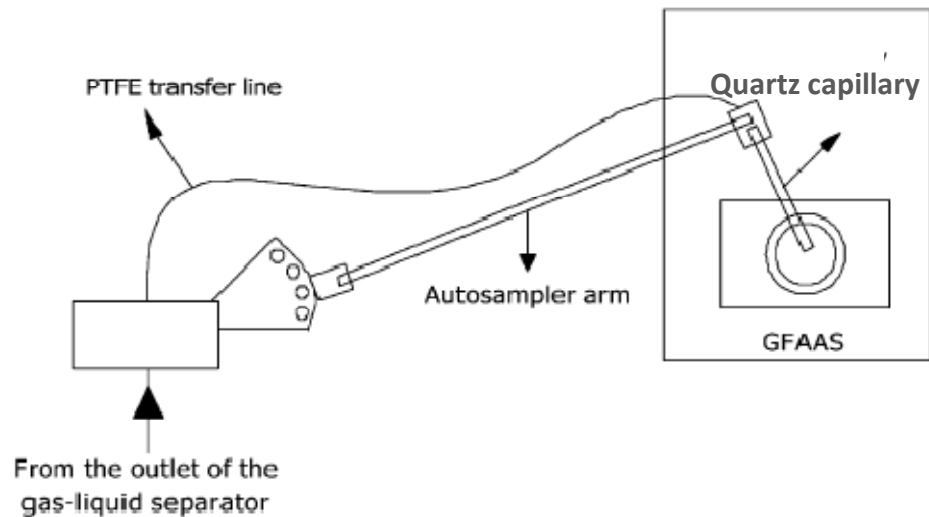


Figure 8 Schematic representation of graphite furnace atom trapping system.

2.5 Procedures

2.5.1 Electrothermal Atomic Absorption System

Electrothermal atomic absorption studies were performed by the Varian GTA 120 graphite tube atomizer unit. A 100 ng/mL Te stock solution in 0.5 mol/L HNO₃ was prepared and since no significant difference between automix and premix mode of the instrument was observed, the automix mode was used. Intermediate working solutions were prepared by the help of Varian PSD 120 programmable sample dispenser. As suggested by the producer 20.0 µL of sample solution and 5.0 µL of 1000 mg/L Pd were co injected to the graphite tube. Temperature program given in Table 6 was followed and a transient signal was obtained. Both peak area and peak height values were collected for all measurements.

Table 6 Temperature program used for the ETAAS system

| Step | Temperature, °C | Ramp time, s | Hold time, s | Ar flow, L/min |
|------|-----------------|--------------|--------------|----------------|
| 1 | 85 | 5.0 | 0 | 0.3 |
| 2 | 95 | 40.0 | 0 | 0.3 |
| 2 | 120 | 10.0 | 0 | 0.3 |
| 3 | Varied | 5.0 | 3.0 | 0.3 |
| 5* | Varied | 0.7 | 0.8 | 0 |
| 6 | 2500 | 0.5 | 2.0 | 0.3 |

*Read at this step

2.5.2 Continuous Flow Hydride Generation System

For the continuous flow hydride generation system pretreated sample solution was acidified with HCl to get a final solution in 4.0 mol/L HCl. Solution flow rate was optimized and used as 6.5 mL/min. Sample solution was merged with the reductant solution that was made up of 0.5 % (m/v) NaBH₄ in 0.5 % (m/v) NaOH solution. Reductant flow rate was set to 1.5 mL/min. Stripping Ar flow was set to 435 ml/min. An integrated signal was collected for 10 seconds. Each result was the mean of at least two replicate measurements.

2.5.3 Microwave Assisted Te(VI) Reduction System

For the reduction of Te(VI) species 5.0 mL sample solution and 5.0 mL concentrated HCl solution was placed in the PTFE digestion bombs of microwave digestion system (Ethos Plus, Milestone). Bomb was closed and the microwave program given in Table 7 was applied. Digested samples were transferred to volumetric flask by using a PTFE funnel. Solutions were diluted to appropriate volume by adding acid and water so that the final solution contains 4.0 mol/L HCl.

Table 7 Temperature program for the microwave assisted reduction of Te(VI)

| Step | Temperature, °C | Ramp Time, min | Hold Time, min | Power, W |
|-------------|------------------------|-----------------------|-----------------------|-----------------|
| 1 | 100 | 3.0 | 2.0 | 700 |
| 2 | 150 | 3.0 | 2.0 | 700 |

2.5.4 Graphite Trapping System

Outlet of the GLS was connected to autosampler arm as described in section 2.4.2. Sample and reductant flow rates were set to 1.5 and 0.75 mL/min, respectively. Stripping Ar flow was adjusted to 53 mL/min. Peristaltic pumps were turned on and the temperature program given in Table 8 was initiated. When the program reached to collection temperature, i.e. Step 3, autosampler arm was manually inserted into graphite tube and was kept inside during collection period. Arm was removed just before step 5.

Table 8 Temperature program applied for the *in-situ* trapping of H₂Te in pyrolytic coated and Ru modified graphite tubes

| Step | Temperature, °C | Ramp time, s | Hold time, s | Ar flow, L/min |
|------|-----------------|--------------|--------------|----------------|
| 1 | 95 | 5.0 | 5.0 | 0.30 |
| 2 | 120 | 5.0 | 5.0 | 0.30 |
| 3 | 300 | 5.0 | Varied | 0 |
| 5* | Varied | 0.5 | 1.0 | 0 |
| 6 | 2100 | 0.5 | 2.0 | 0.30 |

*Read at this step

For trapping of Te species in Pd modified graphite tube a slightly changed procedure was applied. 10 µL 1000 mg/L Pd modifier was placed into graphite tube by using a micropipette. Sample flow rate was adjusted to 3.2 mL/min and Ar flow was set to 133 mL/min. After the injection of modifier, peristaltic pumps were turned on and temperature program given in Table 9 was initiated. An initial drying step was added to the temperature program, step 2 in Table 9. When temperature was reached to collection temperature, step 3, autosampler arm was placed into graphite tube and kept there for an optimized collection period. Then the arm was removed just before step 5.

Table 9 Temperature program applied for the *in-situ* trapping of H₂Te in Pd modified graphite tube

| Step | Temperature, °C | Ramp time, s | Hold time, s | Ar flow, L/min |
|-----------|-----------------|--------------|--------------|----------------|
| 1 | 95 | 5.0 | 5.0 | 0.30 |
| 2 | 120 | 5.0 | 30 | 0.30 |
| 3 | 300 | 5.0 | Varied | 0 |
| 4 | 800 | 1.2 | 5.0 | 0.30 |
| 5* | 2300 | 0.5 | 1.0 | 0 |
| 6 | 2600 | 0.5 | 2.0 | 0.30 |

*Read at this step

2.5.5 Coating Procedure

Graphite surface was modified with Ru as permanent modifier. For the coating of the surface, 50 µL of 100 mg/L Ru solution was introduced into the graphite tube and the temperature program given in Table 10 was applied. This procedure was repeated 5 times to get a total of 25 µg of the modifier deposited on the surface. During this procedure of coating, since relatively large volumes of solutions were used with very high concentration, windows of the graphite furnace assembly were removed to prevent damaging of the lenses.

Due to its relative high volatility most of the Pd modifier was lost during atomization and cleanup stages. Hence, Pd was introduced into graphite furnace before each reading and an initial drying step was performed to remove solvent residue.

Table 10 Temperature program applied for the permanent coating of graphite tube

| Step | Temperature, °C | Ramp time, s | Hold time, s | Ar flow, L/min |
|------|-----------------|--------------|--------------|----------------|
| 1 | 95 | 5 | 60 | 0.30 |
| 2 | 150 | 5 | 60 | 0.30 |
| 3 | 300 | 5 | 30 | 0.30 |
| 4 | 1800 | 1.1 | 2.0 | 0 |
| 5 | 2000 | 0.1 | 2.0 | 0.30 |

2.6 Accuracy Check

To check the accuracy of the system NIST 1643e “Trace Elements in Water” SRM was used. Since only the total Te amount was certified, reduction procedure given in section 2.5.3 was applied. Composition of the SRM is given in Table 11.

Table 11 Certified Values for NIST 1643e “Trace elements in Water” SRM

| Element | Mass Fraction ($\mu\text{g/kg}$) | | | Mass Concentration ($\mu\text{g/L}$) | | |
|------------|---------------------------------------|-------|-------|---|-------|-------|
| Aluminum | 138.33 | \pm | 8.4 | 141.8 | \pm | 8.6 |
| Antimony | 56.88 | \pm | 0.60 | 58.30 | \pm | 0.61 |
| Arsenic | 58.98 | \pm | 0.70 | 60.45 | \pm | 0.72 |
| Barium | 531.0 | \pm | 5.6 | 544.2 | \pm | 5.8 |
| Beryllium | 13.64 | \pm | 0.16 | 13.98 | \pm | 0.17 |
| Bismuth | 13.75 | \pm | 0.15 | 14.09 | \pm | 0.15 |
| Boron | 154.0 | \pm | 3.8 | 157.9 | \pm | 3.9 |
| Cadmium | 6.408 | \pm | 0.071 | 6.568 | \pm | 0.073 |
| Calcium | 31 500 | \pm | 1 100 | 32 300 | \pm | 1 100 |
| Chromium | 19.90 | \pm | 0.23 | 20.40 | \pm | 0.24 |
| Cobalt | 26.40 | \pm | 0.32 | 27.06 | \pm | 0.32 |
| Copper | 22.20 | \pm | 0.31 | 22.76 | \pm | 0.31 |
| Iron | 95.7 | \pm | 1.4 | 98.1 | \pm | 1.4 |
| Lead | 19.15 | \pm | 0.20 | 19.63 | \pm | 0.21 |
| Lithium | 17.0 | \pm | 1.7 | 17.4 | \pm | 1.7 |
| Magnesium | 7 841 | \pm | 96 | 8 037 | \pm | 98 |
| Manganese | 38.02 | \pm | 0.44 | 38.97 | \pm | 0.45 |
| Molybdenum | 118.5 | \pm | 1.3 | 121.4 | \pm | 1.3 |
| Nickel | 60.89 | \pm | 0.67 | 62.41 | \pm | 0.69 |
| Potassium | 1 984 | \pm | 29 | 2 034 | \pm | 29 |
| Rubidium | 13.80 | \pm | 0.17 | 14.14 | \pm | 0.18 |
| Selenium | 11.68 | \pm | 0.13 | 11.97 | \pm | 0.14 |
| Silver | 1.036 | \pm | 0.073 | 1.062 | \pm | 0.075 |
| Sodium | 20 230 | \pm | 250 | 20 740 | \pm | 260 |
| Strontium | 315.2 | \pm | 3.5 | 323.1 | \pm | 3.6 |
| Tellurium | 1.07 | \pm | 0.11 | 1.09 | \pm | 0.11 |
| Thallium | 7.263 | \pm | 0.094 | 7.445 | \pm | 0.096 |
| Vanadium | 36.93 | \pm | 0.57 | 37.86 | \pm | 0.59 |
| Zinc | 76.5 | \pm | 2.1 | 78.5 | \pm | 2.2 |

CHAPTER 3

RESULTS AND DISCUSSION

This study involves development of analytical methods for the speciation of tellurium in different water samples.

First part includes the direct determination of total Te by ETAAS method. Pyrolytic coated, Pd modified and Ru modified graphite surfaces were used and the performance characteristics were compared. This method was mostly used as the reference method for the comparison of developed hydride generation and graphite tube trapping systems.

Second part involves quantitative determination and speciation of Te by continuous flow hydride generation AAS system. In this part hydride generation method and parameters that affect hydride generation efficiency were optimized. In addition, reduction conditions of Te(VI) species to Te(IV) were investigated since only Te(IV) forms volatile H₂Te upon reduction with NaBH₄.

Third part consists of trapping of H₂Te in a heated pyrolytic coated graphite tube. Parameters like trapping temperature, atomization temperature, trapping period and flow rates of sample, reducing agent and stripping Ar were optimized. Developed method was compared with the direct ETAAS determination and enhancement factors were calculated.

Fourth part involves trapping of H₂Te in a graphite tube, whose surface was previously modified with Pd modifier solution, was investigated. Analytical parameters that gave the best analytical signal output were optimized.

The last part involves the investigation of permanent surface modifiers for the *in-situ* trapping of H₂Te. At this step Ru modifier was used as the permanent coating material and analytical performances were evaluated.

3.1 Direct ETAAS Study

At this step acidified Te solutions were introduced into graphite surface directly and performance of Pd and Ru modifiers were investigated.

Preliminary studies showed that when sample solution was prepared in 0.5 mol/L HNO₃ signal intensity was two times higher than the signal intensity of same concentration prepared in 0.5 mol/L HCl. Reason of this behavior was not fully understood but it was suggested that Te species prepared in HCl was lost at the ashing stage possibly through formation of volatile chloride compounds. Use of lower ashing temperatures resulted in increase of background signal and lowered the reproducibility. These data showed that Te species were relatively unstable towards heating in the absence of a modifier solution. Many authors and manufacturers recommend use of either temporary or permanent modifiers for the determination of Te by ETAAS (**D'Ulivo, 1997**) (**Liao & Haug, 1997**).

Performance of pyrolytic graphite surface, pyrolytic graphite surface modified with Pd or Ru were investigated. Only peak height values were used for the construction of graphs for simplicity. At least two replicate measurements were taken for each data point.

3.1.1 Pyrolysis Temperature

The pyrolysis temperature curves for pyrolytic coated, Pd modified and Ru modified graphite tubes are shown in Figure 9. As can be seen from the figure, pyrolytic coated graphite tube could only be used up to pyrolysis temperature of 500 °C, after which loss of sample was observed. Ru modified graphite tube had a maximum pyrolysis temperature of 1000 °C. After this temperature decrease in analytical signal was observed. Pd modified graphite tube stabilize the Te species up to 1400 °C. It can be concluded that Pd and Ru could stabilize Te allowing application of higher pyrolysis temperatures. This behavior is particularly useful for samples with high organic content.

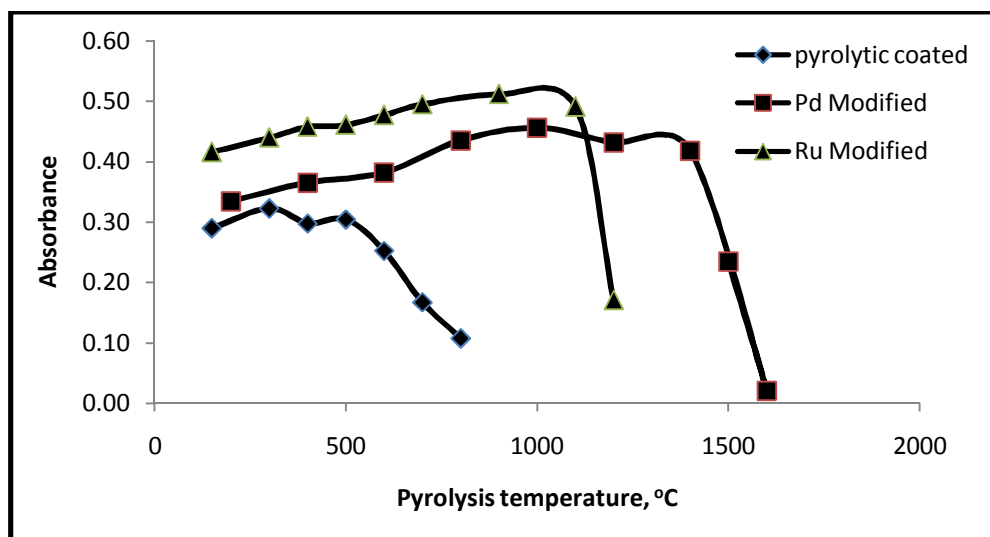


Figure 9 Effect of pyrolysis temperature on the analytical signal of 20 μL 50.0 ng/mL Te solution in 0.5 mol/L HNO₃. 2000 °C atomization temperature was used for pyrolytic coated and Ru modified graphite tubes. 2300 °C atomization temperature was used for Pd modified graphite tube. Each point represents mean value of three replicate measurements.

3.1.2 Atomization Temperature

Another important parameter was the atomization temperature. Atomization temperature curves of pyrolytic coated, Pd modified and Ru modified graphite tubes are given in Figure 10. For pyrolytic coated graphite, atomization was almost completed at 1300 °C. For Ru modified graphite tube analytical signal reached maximum at about 1800 °C and was the same up to 2100 °C. Atomization temperature was the highest one for Pd modified graphite tube; maximum signal was attained at 2300 °C.

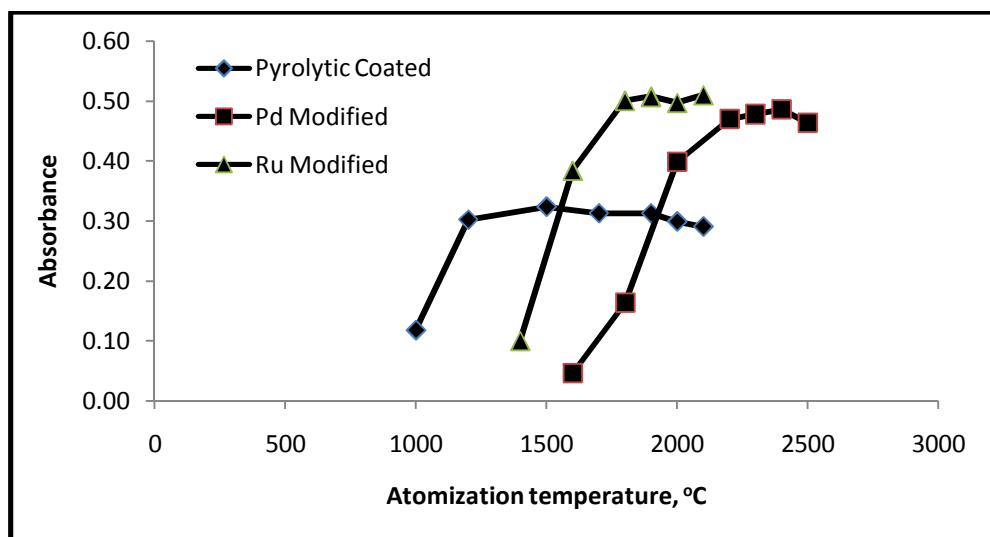


Figure 10 Effect of atomization temperature on analytical signal of 20 µL 50.0 ng/mL Te solution prepared in 0.5 mol/L HNO₃. 500 °C pyrolysis temperature was used for pyrolytic coated graphite tube and 1000 °C pyrolysis temperature was used for Pd modified and Ru modified graphite tubes. Each point represents mean value of three replicate measurements.

Considering the analytical signals it could be concluded that Pd and Ru coatings not only stabilize the Te species by allowing higher pyrolysis and atomization temperatures, but also enhances the analytical signal intensity.

3.1.3 Calibration Graphs and Analytical Signals

After the pyrolysis and atomization temperature optimizations, analytical signals of sample solutions ranging from 5.0 ng/mL to 200 ng/mL were measured to determine the linear dynamic range and calibration plot of three systems; the data are given in Figure 11. Data points are the average of three replicate measurements. Regarding the linear range Pd modified graphite tube gave the widest linear range from 5.0 to 80 ng/mL. Ru modified tube had the linear range between 5.0 and 60 ng/mL. Linear range was limited between 5.0 to 40.0 ng/mL for pyrolytic coated graphite tube.

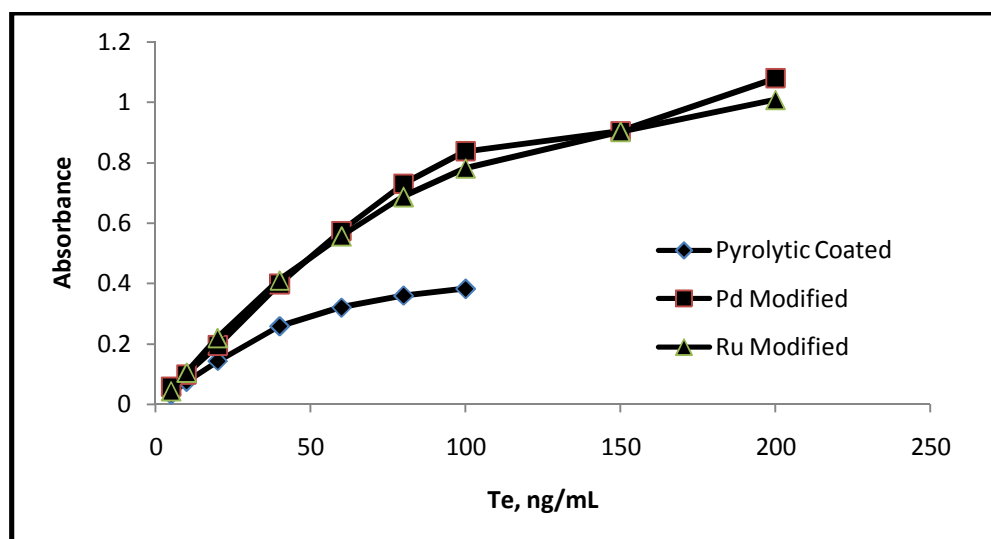


Figure 11 Calibration plot for 20 μL injection volumes for pyrolytic coated, Pd modified and Ru modified graphite tubes. 500 $^{\circ}\text{C}$ pyrolysis temperature and 2000 $^{\circ}\text{C}$

atomization temperatures were used for pyrolytic coated graphite. 1000 °C pyrolysis temperature and 2300 °C atomization temperatures were used for Pd modified graphite tube. 1000 °C pyrolysis temperature and 2000 °C atomization temperatures were used for Ru modified graphite tube.

Corresponding linear calibration plots and best line equations were given in Figure 12, Figure 13 and Figure 14.

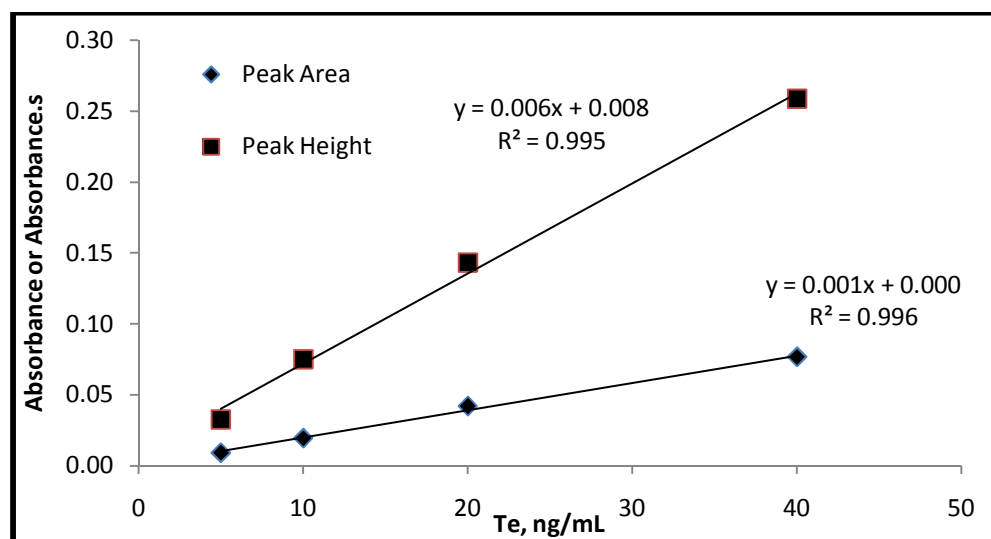


Figure 12 Linear portion of the calibration plot and best line equation for pyrolytic coated graphite tube. 500 °C pyrolysis temperature and 2000 °C were used.

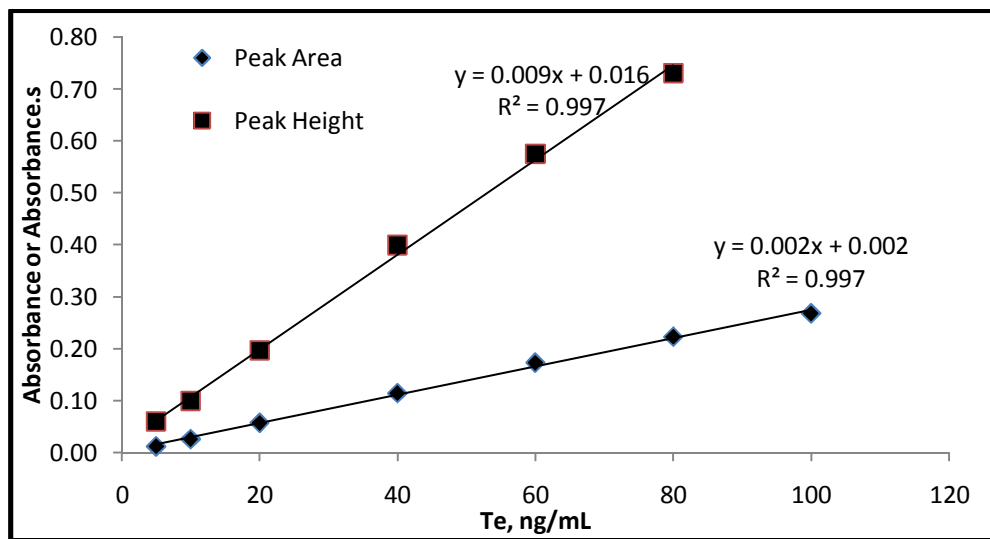


Figure 13 Linear portion of calibration plot and best line equation for Pd modified graphite tube. 1000 °C pyrolysis temperature and 2300 °C atomization temperature was used.

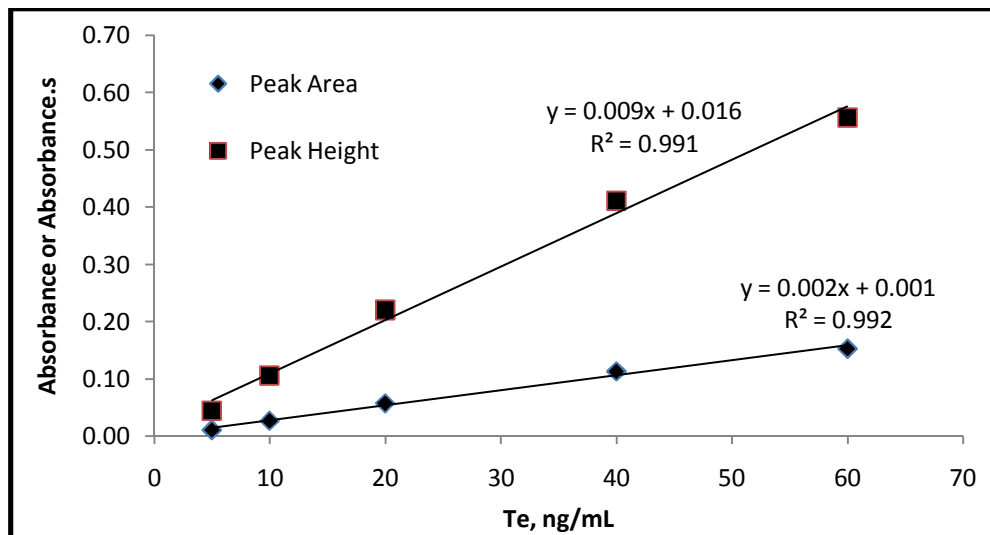
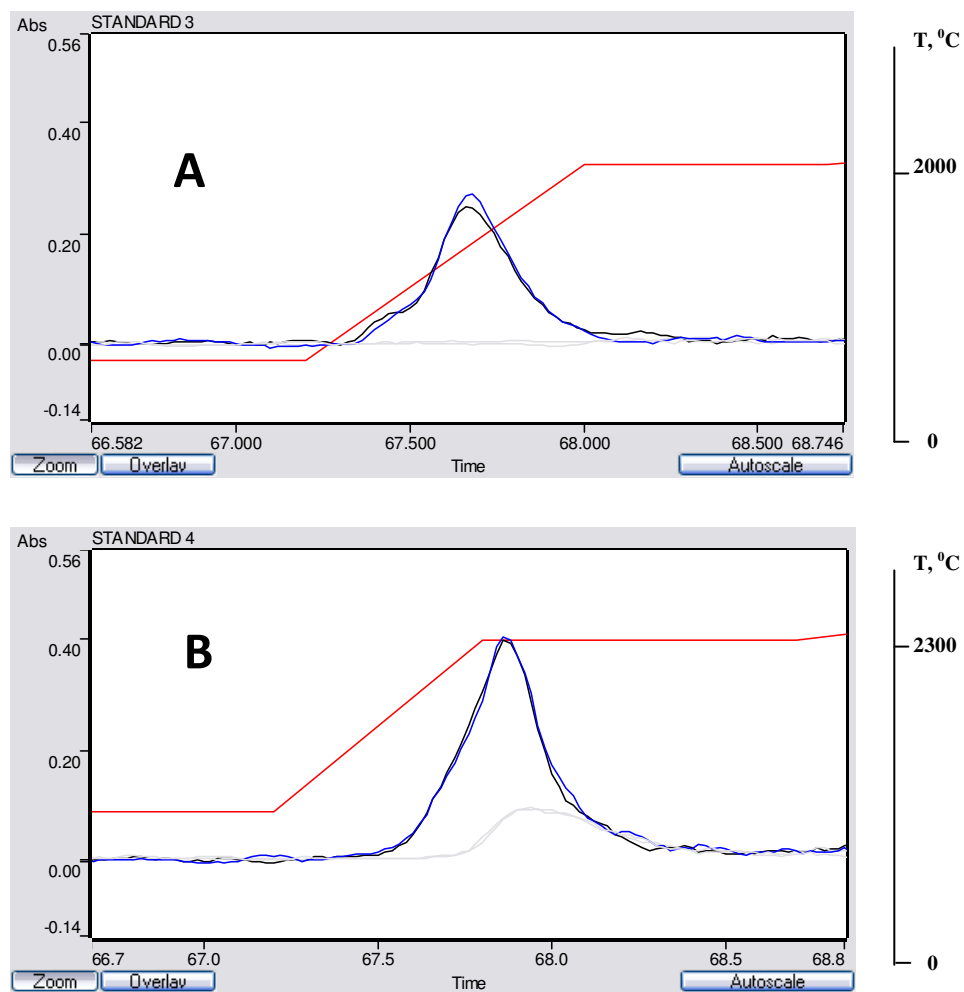


Figure 14 Linear portion of the calibration plot and best line equation for Ru modified graphite tube. 1000 °C pyrolysis temperature and 2000 °C atomization temperature were used.

It was observed that the linear ranges for Pd modified and Ru modified graphite tubes were higher than that of the pyrolytic coated graphite tube. It was also seen that calibration sensitivity, which is defined as the slope of the calibration plot, of Pd modified and Ru modified graphite tubes were very close to each other whereas calibration sensitivity of pyrolytic coated graphite tube was around 30 % lower.

Analytical signals for two replicate measurements of 40 ng/mL Te solutions for three graphite tubes were given in Figure 15.



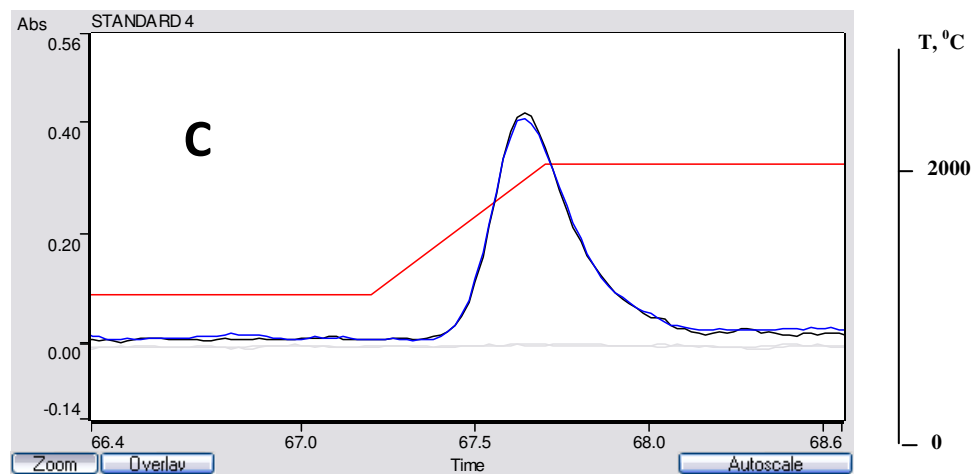


Figure 15 Analytical signals in duplicate for 20 μL of 40 ng/mL Te solutions for A- Pyrolytic coated graphite tube, B- Pd modified graphite tube, C- Ru modified graphite tube. Temperature changes are indicated by the straight lines.

Optimized values of temperature program for each surface are given in Table 12.

Table 12 Optimized parameters for pyrolytic coated, Pd modified and Ru modified graphite tubes.

| | Pyrolytic coated graphite tube | Pd modified graphite tube | Ru modified graphite tube |
|--|-----------------------------------|------------------------------|------------------------------|
| Pyrolysis temperature, °C | 500 | 1000 | 1000 |
| Atomization temperature, °C | 2000 | 2300 | 2000 |

3.1.4 Analytical Figures of Merit

Concentration and mass limits of detection (LOD), Concentration and mass limits of quantification (LOQ), characteristic concentration (C_0), characteristic mass for peak absorption (m_p) and characteristic mass for peak area (m_a) of three graphite tubes were calculated and given in Table 13.

LOD and LOQ values were calculated from the $3s/m$ and $10s/m$ formulas where s was the standard deviation of 7 replicate measurements of 5.0 ng/mL Te solution. For mass LOD and mass LOQ calculations, concentration LOD and LOQ values were multiplied by the volume of sample solution injected to the system. Lowest LOD values were obtained with Ru and Pd modified graphite tube as 0.17 ng/mL according to peak height measurements.

Enhancement factor (E) was calculated as the ratio of characteristic concentrations of two methods. Regarding the RSD and enhancement factors best analytical performance were attained with Ru and Pd modified graphite tubes.

Table 13 Analytical parameters of pyrolytic coated, Pd modified and Ru modified graphite tubes.

| | Pyrolytic coated Graphite tube | | Pd modified graphite tube | | Ru modified graphite tube | |
|---|-----------------------------------|------|------------------------------|------|------------------------------|------|
| | P.A. | P.H. | P.A. | P.H. | P.A. | P.H. |
| Concentration Limit of Detection, LOD, 3s/m (N=7), ng/mL | 1.66 | 0.49 | 0.57 | 0.17 | 0.59 | 0.17 |
| Mass Limit of Detection, LOD, 3s/m (N=7), pg | 33.2 | 9.9 | 11.5 | 3.4 | 12.0 | 3.4 |
| Concentration Limit of Quantification, LOQ, 10s/m (N=7), ng/mL | 5.53 | 1.64 | 1.91 | 0.57 | 1.99 | 0.56 |
| Mass Limit of Quantification, LOQ, 10s/m (N=7), pg | 111.2 | 32.8 | 38.4 | 11.4 | 39.8 | 11.3 |
| Characteristic Concentration, C₀, ng/mL | 2.10 | 0.61 | 1.53 | 0.44 | 1.56 | 0.43 |
| Characteristic mass for peak absorption, m_p, pg | - | 12.0 | - | 8.8 | - | 8.8 |
| Characteristic mass for peak area, m_a pg | 42.0 | - | 30.6 | - | 31.2 | - |
| Enhancement, with respect to pyrolytic coated graphite tube | 1.00 | 1.00 | 1.37 | 1.38 | 1.35 | 1.43 |
| RSD, 10 replicate of 5.0 ng/mL solution | 6.3 | 5.1 | 3.6 | 2.9 | 2.5 | 2.5 |

P.A.: Peak Area

P.H.: Peak Height

3.2 Continuous Flow Hydride Generation System

This part of the study deals with continuous flow hydride generation system and reduction parameters for Te(VI) species. AAS was used for detection.

3.2.1 NaBH₄ and HCl Concentrations

Rapid and efficient formation of volatile species strongly depends on the concentrations of reducing agent and acid. Small changes in concentrations may lead to significant increase or decrease of the analytical signal since pH of the resulting solution is changing accordingly. HCl concentration of sample solution was varied between 2.0 to 8.0 mol/L and NaBH₄ solutions ranging from 0.25 % (w/v) to 2.5 % (w/v) were prepared. All NaBH₄ solutions were stabilized in 0.5 % (w/v) NaOH. Sample solution flow rate and reductant flow rates were kept at 2.9 mL/min and 3.1 mL/min, respectively. Ar flow was set to 435ml/min and kept constant throughout the optimization. Change of analytical signal of 20.0 ng/mL Te(IV) solution with acidity and reductant concentration is given in Figure 16 as a surface plot. Signal deviated 20% from the mean value within the ranges studied. Analytical signal was increasing with decreasing reductant concentration and reaches a maximum at 0.5 % (w/v) reductant concentration. This behavior can be attributed to the dilution effect of H₂ gas produced as a result of the reaction between HCl and NaBH₄. Best signal was observed between 0.5-1.0 % (w/v) NaBH₄ and 3.0-6.0 mol/L HCl concentration ranges. Although 4.0 mol/L HCl and 0.5 % NaBH₄ concentrations were selected as the optimum working concentrations for this work it can be concluded from Figure 16 that H₂Te can be studied over a wide range of acid and reductant concentrations without any significant loss of sensitivity. This behavior is particularly useful for multielement analysis since same sample solution and same

parameters can be used for the analysis of more than one element.

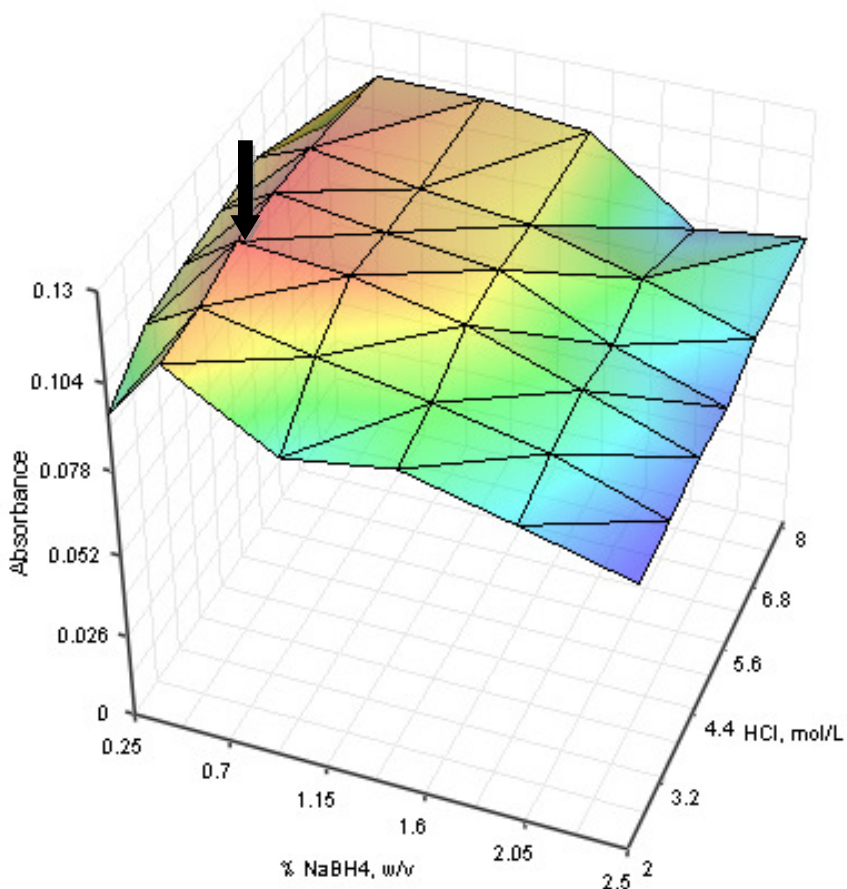


Figure 16 Variation of HGAAS signal with NaBH₄ and HCl concentration for 20 ng/mL Te(IV) sample solution. Sample and reductant flow rates were adjusted to 2.9 and 3.1 mL/min, respectively.

3.2.2 Sample Solution and NaBH₄ Flow Rates

Sample and reductant solutions were merged with different flow rates ranging from 1.5 mL/min to 6.5 mL/min to determine the optimum flow rates. A surface plot was constructed and is given in Figure 17. Signal intensity increased with increasing sample flow rate and decreasing reductant flow rate. This result implies that

analytical signal largely depends on sample flow rate. This is an expected result since increasing sample flow rate means increasing analyte atom concentration in the reaction medium. To keep the sample consumption at reasonable levels, 6.5 mL/min sample flow rate was selected as the optimum value. It was also observed from the plot that increasing reductant flow rate decreased the analytical signal probably due to the dilution effect of excess H₂ formed. This plot also showed that hydride formation efficiency was not changing significantly at different flow rates.

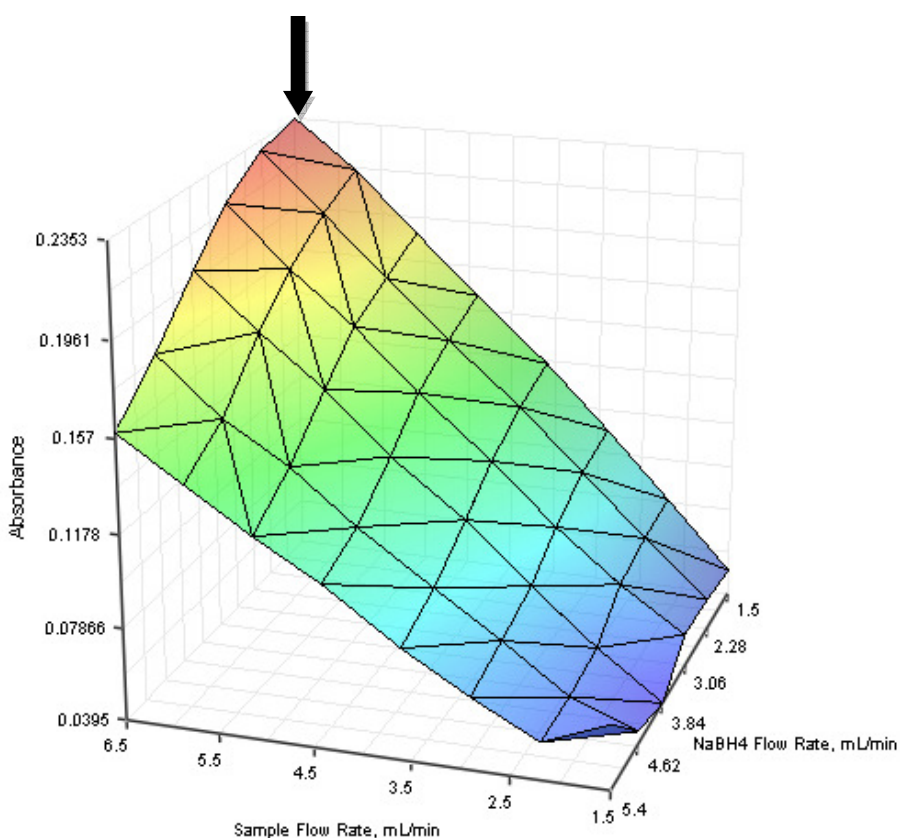


Figure 17 Effect of sample and NaBH₄ flow rates on the HGAAS signal of 20 ng/mL Te(IV) solution. Sample solution was prepared in 4.0 mol/L HCl and 0.5% (w/v) NaBH₄ solutions were used.

3.2.3 Length of Reaction Coil

After merging sample solution and NaBH₄ a PTFE reaction coil (0.056 mm id) was placed into the reaction pathway. The length of reaction coil should be optimized to complete the reaction and minimize the transport losses. The length was varied between 5.0 cm, corresponding to 12 µL internal volume, and 100 cm, 246 µL internal volume. Results given in Figure 18 implied that there was no significant change in the absorbance signal of the analyte atoms within the investigated conditions. After 20 cm, signal reached a plateau. 30 cm was chosen as the optimum reaction coil length value for easy operation.

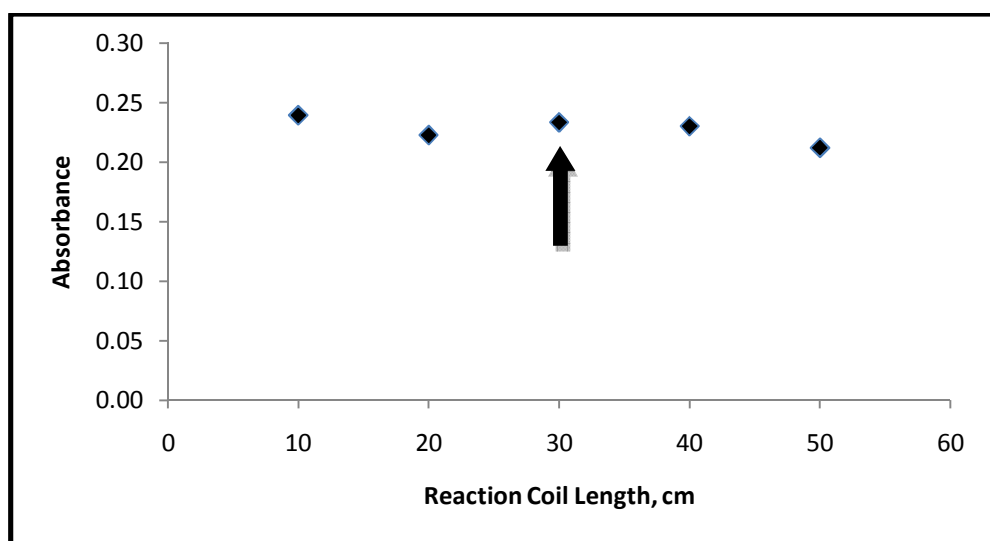


Figure 18 Effect of reaction coil length on the HGAAS signal of 20 ng/mL Te(IV) solution. Sample solution was prepared in 4.0 mol/L HCl solution and pumped at 6.5 mL/min flow rate. 0.5% (w/v) NaBH₄ was used at a flow rate of 1.5 mL/min.

3.2.4 Length of Stripping Coil

Formed volatile species were purged from the liquid mixture by the help of stripping coil. To determine the optimum value, PTFE tubings (0.056 mm id) with different lengths were studied. As can be seen from Figure 19 absorbance value was not changing significantly with the stripping coil length. These results imply that formation reaction of H₂Te is rather fast and formed species are stable enough to travel through the system.

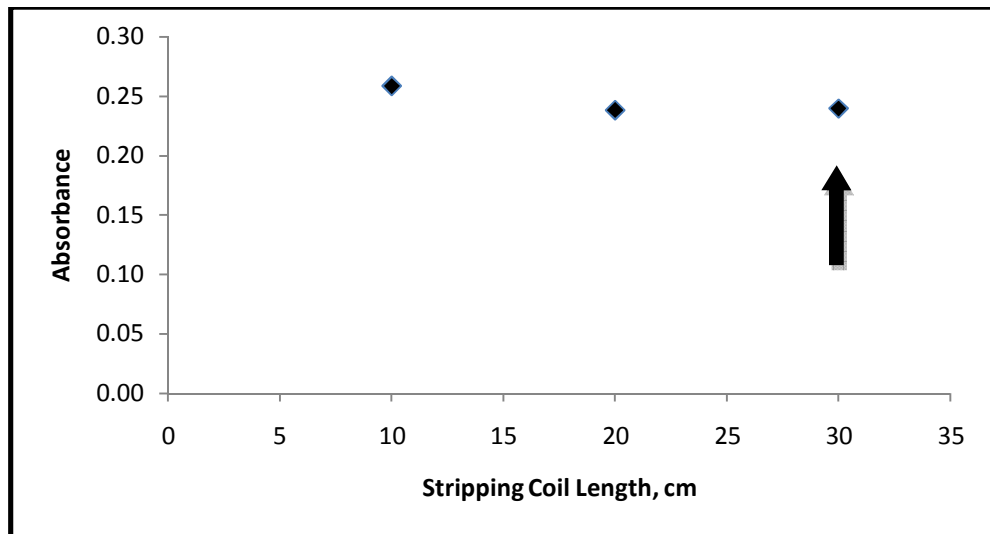


Figure 19 Effect of stripping coil length on the HGAAS signal of 20 ng/mL Te(IV) solution. Sample solution was prepared in 4.0 mol/L HCl solution and pumped at 6.5 mL/min flow rate. 0.5% (w/v) NaBH₄ was used at a flow rate of 1.5 mL/min.

3.2.5 NaOH Concentration

NaOH is usually added to NaBH_4 solution to decrease the rate of hydrolysis of NaBH_4 . It was shown that NaOH concentration can affect the AAS analytical signal significantly for certain cases since the reaction rate strongly depends on the equilibrium pH value of the reaction mixture (**Cankur O., 2004**). To see the effect of NaOH concentration on the analytical signal a set of reductant solutions were prepared with different NaOH content. As can be seen from Figure 20, NaOH concentration did not have a significant effect on the analytical signal in the studied range. This can be attributed to the relatively high acid concentration. To increase the stability of reductant solution 0.5 % (w/v) NaOH concentration was selected as the optimum value. With this NaOH content reductant solution was stable more than 24 hours at room temperature. With lower NaOH concentrations, lifetime of reductant solution decreases down to few hours at room temperature.

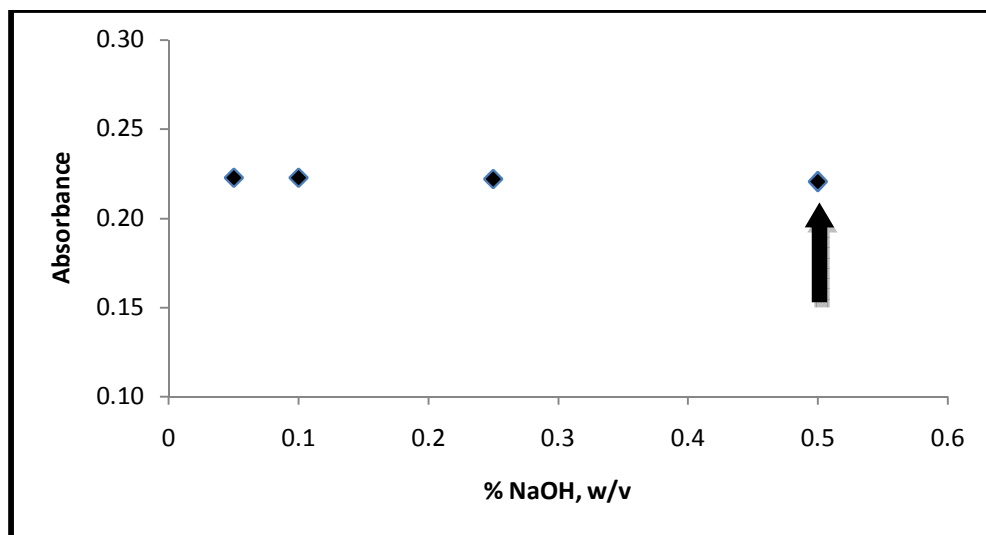


Figure 20 Effect of NaOH concentration in 0.5% (w/v) NaBH_4 solution on HGAAS signal for 20 ng/mL Te(IV) solution.

3.2.6 Stripping Ar Flow Rate

Stripping Ar flow rate is one of the critical factors that affect the performance of the system. As can be seen from Figure 21, lower Ar flows resulted in high absorbance values with RSD values below 3%. However, this behavior was misleading; since signals were integrated over 10 seconds period of time and average values were displayed. Analytical signals for 133 and 435 mL/min Ar flow rates are given in Figure 22. As can be seen from the figure, even though the average value of 133 mL/min Ar flow was higher, shape of the signal was not constant and could not be used for lower integration times.

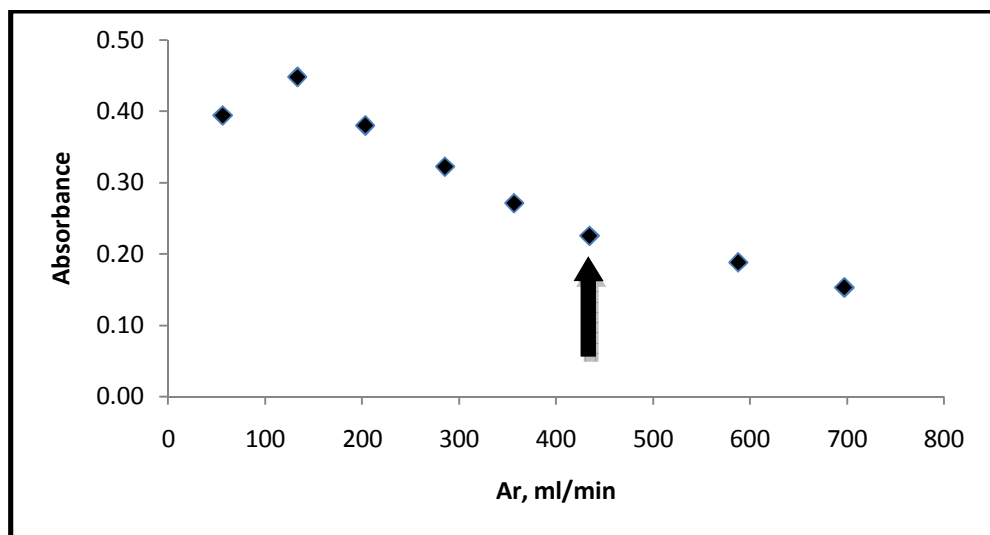


Figure 21 Effect of stripping Ar flow rate on HGAAS signal of 20 ng/mL Te(IV) solution. Sample solution was prepared in 4.0 mol/L HCl solution and pumped at 6.5 mL/min flow rate. 0.5% (w/v) NaBH₄ was used at a flow rate of 1.5 mL/min.

As the optimum Ar flow 435 mL/min was selected since this value gave the most stable signal with highest signal to noise ratio.

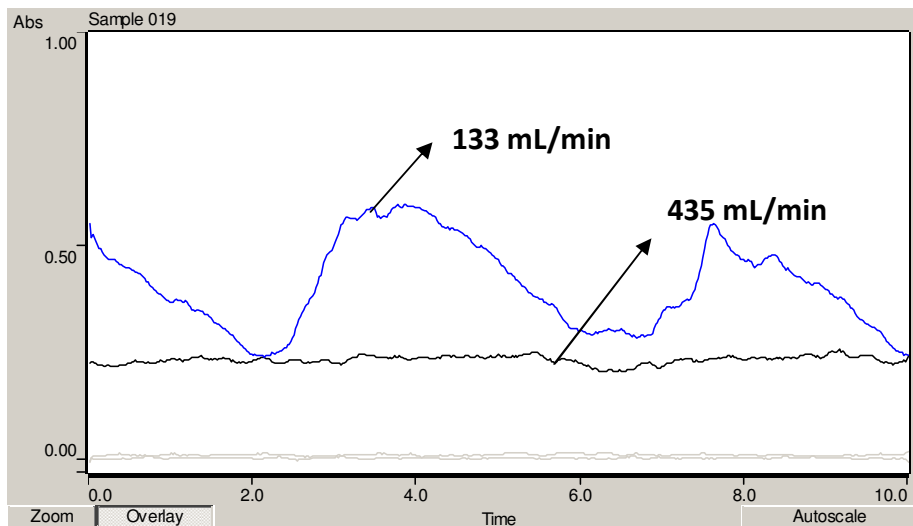


Figure 22 Effect of stripping Ar flow rate on shape of HGAAS signal of 20.0 ng/mL Te(IV) solution pumped at 6.5 mL/min flow rate.

3.2.7 Linear Range and Calibration Plot for Te(IV)

After all optimization studies a set of solutions were prepared to see the analytical working range and linear calibration plot of Te(IV) (Figure 23) using HGAAS. Each data point is the mean of three replicate measurements. It was observed that the plot was linear between 1.0 ng/mL to 40.0 ng/mL Te(IV). After this point, deviation from linearity was observed. Constructed calibration plot (Figure 24) had the linear equation and correlation coefficient as $y=0.105C + 0.0058$ and $R^2=0.9987$, respectively.

Developed method had LOD and LOQ values of 0.19 and 0.64 ng/mL, respectively. LOD and LOQ values were calculated from the standard deviation of 7 replicate measurements of the smallest standard, i.e. 1.0 ng/mL. Characteristic concentration was found as 0.38 ng/mL. For the calculation of characteristic concentration

absorbance value of 10 ng/mL standard was used. Analytical figures of merit of continuous flow HGAAS is given in Table 14.

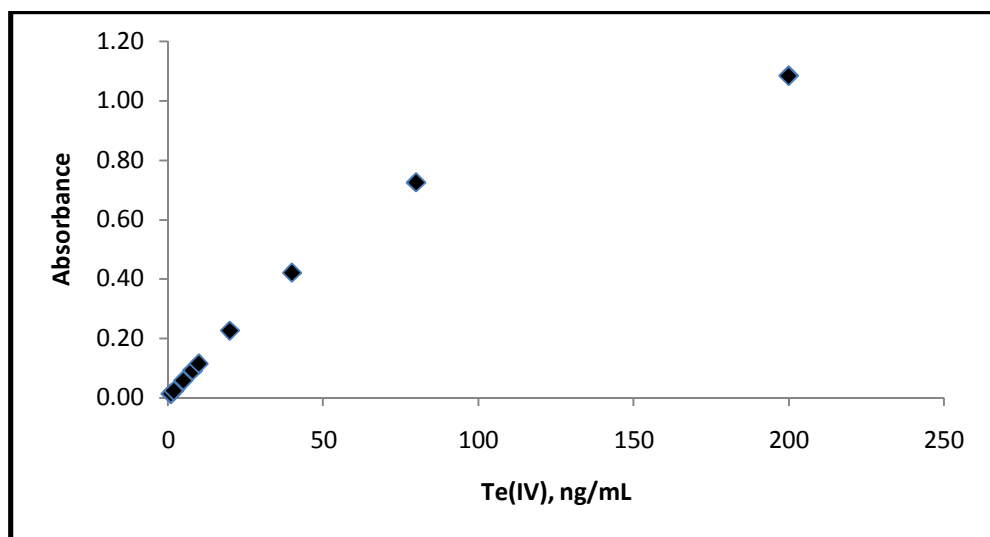


Figure 23 Calibration plot for continuous flow HGAAS system for Te(IV) solution. Sample solution was prepared in 4.0 mol/L HCl solution and pumped at 6.5 mL/min flow rate. 0.5% (w/v) NaBH₄ was used at a flow rate of 1.5 mL/min.

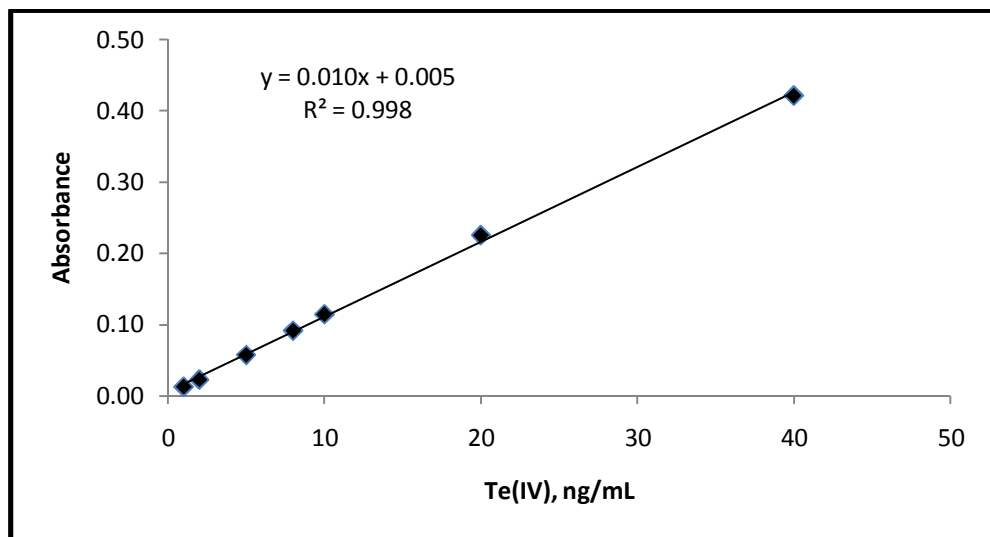


Figure 24 Linear portion of calibration plot for Te(IV) continuous flow HGAAS system.

Table 14 Analytical figures of merit for continuous flow HGAAS system.

| | |
|---|------|
| Limit of Detection, LOD, 3s/m (N=7) ng/mL | 0.19 |
| Limit of Quantification, LOQ, 10s/m (N=7) ng/mL | 0.64 |
| Characteristic Concentration, C_0 ng/mL | 0.38 |

Optimized parameters of the continuous flow HGAAS system were summarized in Table 15.

Table 15 Optimized parameters for continuous flow hydride generation system

| Parameter | Optimum value |
|---------------------------------|---------------|
| Acidity | 4.0 mol/L HCl |
| NaBH ₄ concentration | 0.5 % (w/v) |
| Ar flow rate | 435 mL/min |
| Sample flow rate | 6.5 mL/min |
| NaBH ₄ flow rate | 1.5 mL/min |
| NaOH concentration | 0.5 % (w/v) |
| Stripping coil length | 30 cm |
| Reaction coil length | 30 cm |

3.2.8 Speciation Strategy

For the quantitative speciation of an organic or inorganic target element, chromatographic and nonchromatographic methods are present (**Kumar & Riyazuddin, 2007**). It is well known from the literature that only tetravalent form of Te is forming volatile H₂Te upon reaction with NaBH₄. This principle was used for the speciation of inorganic Te. For the determination of Te(IV), samples were acidified and analyzed directly without applying a reduction procedure. For the total Te determination a reduction procedure was applied. The difference between the total Te and Te(IV) gave the concentration of Te(VI) species in the sample since Te(IV) and Te(VI) forms are known to be present as the dominant inorganic Te species in the nature (**D'Ulivo, Determination of Selenium and Tellurium in Environmental Samples, 1997**).

3.2.9 Reduction Studies

For the reduction of Te(VI) to Te(IV) several procedures were proposed in the literature (**Dedina & Tsalev, 1995**). Most frequently applied method is the heating of the sample solution in HCl solution. To see the effect of HCl concentration on reduction, a series of solutions were prepared with HCl concentration ranging from 1.0 to 8.0 mol/L and kept at ambient conditions for about 2.5 hours. No significant reduction was observed up to 6.0 mol/L HCl solution and only 20% of the Te(VI) was reduced to Te(IV) in 8 mol/L HCl solution (Figure 25).

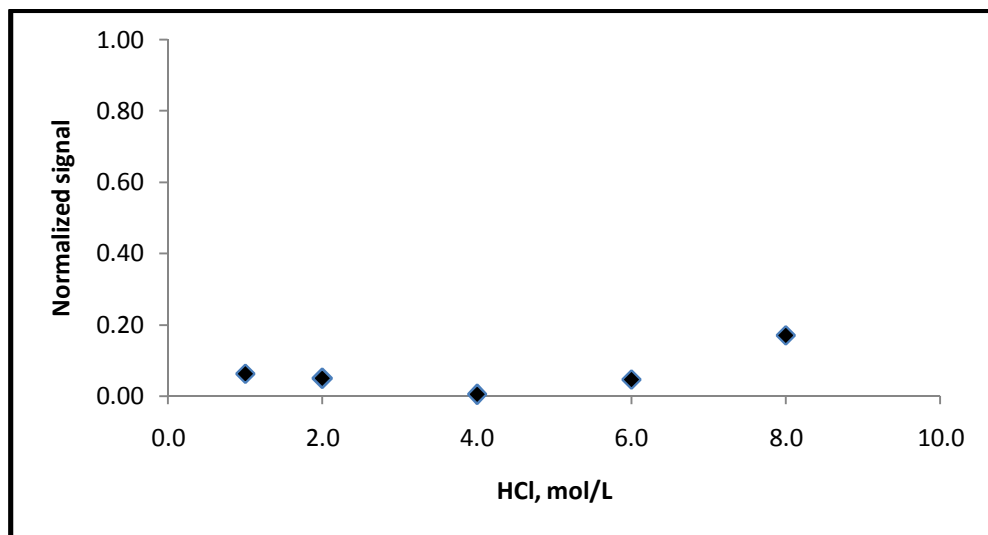


Figure 25 Effect of HCl concentration on the reduction of 20 ng/mL Te(VI) species upon waiting for 2.5 hours at ambient conditions.

It was obvious that rate of reduction is limited at room conditions. To see the effect of heating, solutions were heated to 90 °C on a conventional laboratory hot plate and measurements were taken every 15 minutes. It was observed that heating in 6.0 mol/L HCl for 15 minutes was enough for the quantitative reduction of Te(VI) species to Te(IV). Disadvantage of the method was the sample and HCl loss during the heating step which made the adjustment of acidity difficult.

To overcome the disadvantages of open vessel reduction a comparative study was performed. Sample solutions were taken into digestion bombs of a microwave digestion system. Heating program given in Table 7 was applied. After cooling, sample solutions were diluted to 50 mL and acidity was adjusted to 4.0 mol/L HCl. As can be seen from Figure 26 heating with 5.0 mol/L HCl was enough to quantitatively reduce all Te(VI) species with the given temperature program. Considering the real samples that had high oxidizing character, reduction in 6.0 mol/L HCl was chosen as the optimum condition.

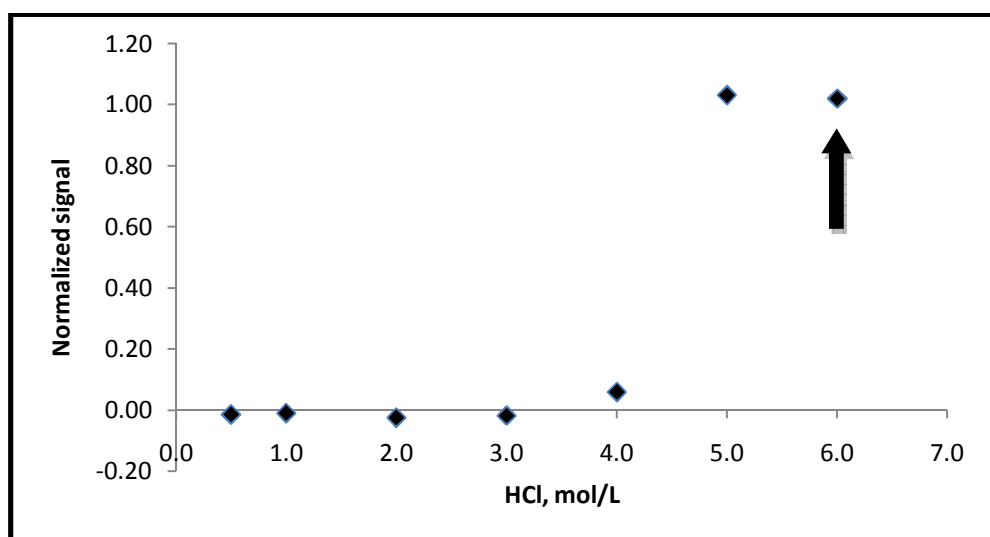


Figure 26 Effect of HCl concentration on the reduction of 20 ng/mL Te(VI) to Te(IV) by using microwave assisted reduction system.

After deciding about the reduction procedure, a set of solutions were prepared with different Te(IV) and Te(VI) contents as given in Table 16. Total Te content was kept constant as 20 ng/mL in the final solution. 6.0 mol/L HCl and the conditions in Table 7 were used.

Table 16 Final Te(IV) and Te(VI) concentrations in mixtures prepared for the reduction system.

| Te(IV), ng/mL | Te(VI), ng/mL | Total Te, ng/mL |
|---------------|---------------|-----------------|
| 0 | 20.0 | 20.0 |
| 4.0 | 16.0 | 20.0 |
| 8.0 | 12.0 | 20.0 |
| 10.0 | 10.0 | 20.0 |
| 12.0 | 8.0 | 20.0 |
| 16.0 | 4.0 | 20.0 |
| 20.0 | 0 | 20.0 |

Absorbance values of these solutions without a prereduction step were given in Figure 27.

From the plot it was clear that all the analytical signal was originated from Te(IV) species. If a calibration curve was constructed with this system (Figure 27) slope of this plot perfectly fits with the one given in Figure 24 which was constructed by using Te(IV) species only.

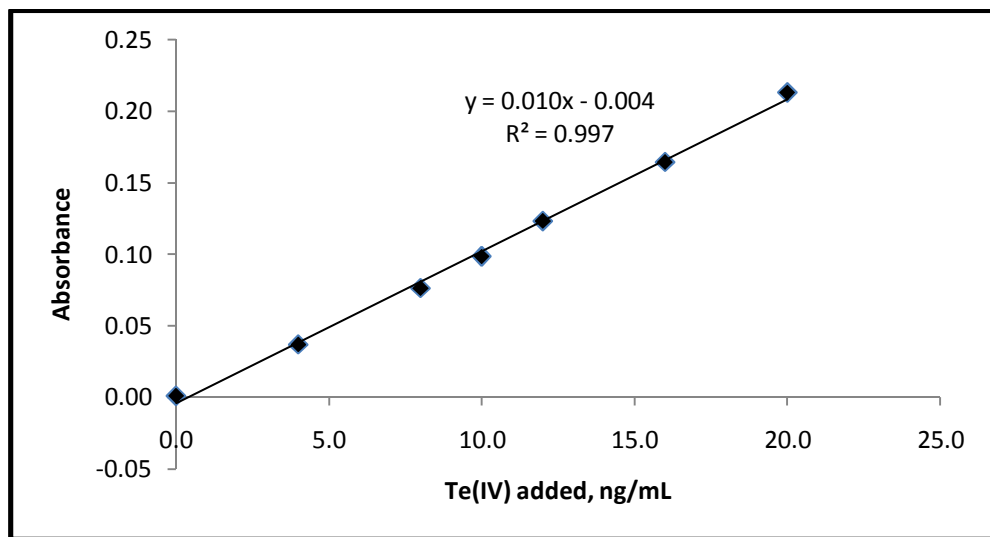


Figure 27 Calibration plot obtained without a prereduction step using HGAAS.

As the next step, mix solutions were prerduced with the microwave assisted reduction system as described in Section 2.5.3 and the plot given in Figure 28 was obtained.

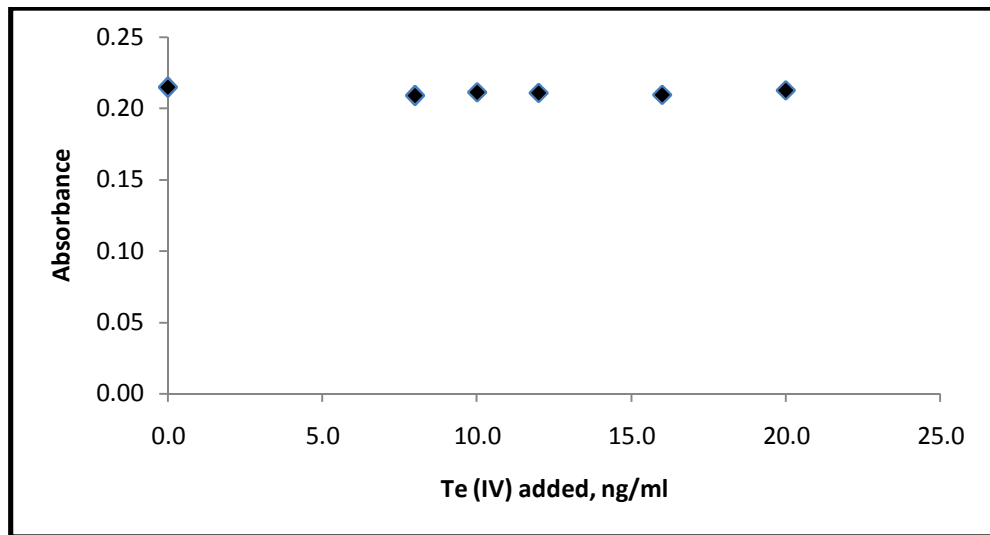


Figure 28 Absorbance values of mixtures after applying prereduction using HGAAS.

This plot showed that all Te(VI) species were reduced to Te(IV) by the reduction system applied.

After the subtraction of the values given in **Figure 27** from values given in Figure 28 the following plot was obtained. This plot represents the amount of Te(VI) species in the mixtures. Again the slope of Figure 29 perfectly matched with the slope of Figure 24, except that it has a negative sign.

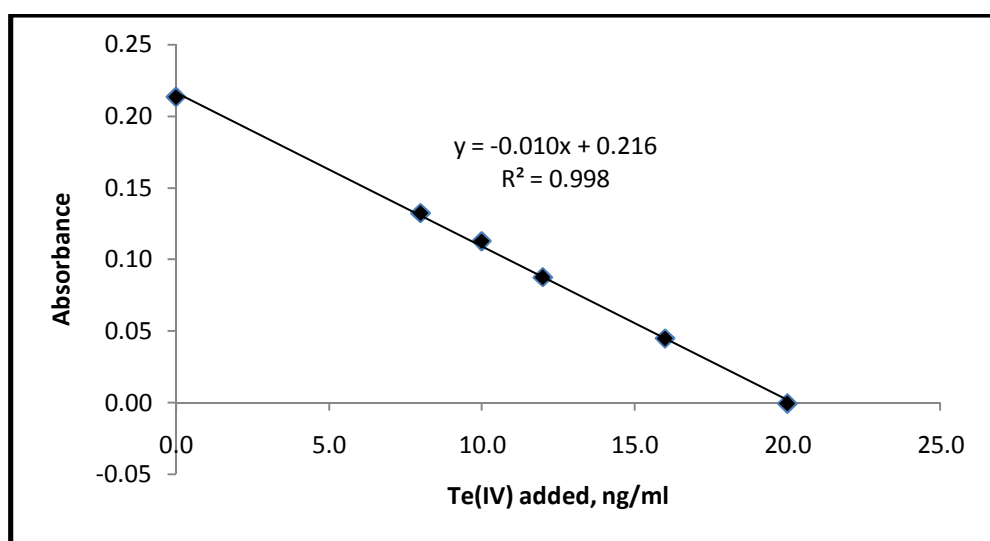


Figure 29 Calibration plot of reduced Te(VI) using HGAAS.

After validating the reduction procedure, a series of Te(VI) solutions were prepared and the reduction procedure was applied to each sample. Linear range and calibration plot were obtained. Results are presented in Figure 30.

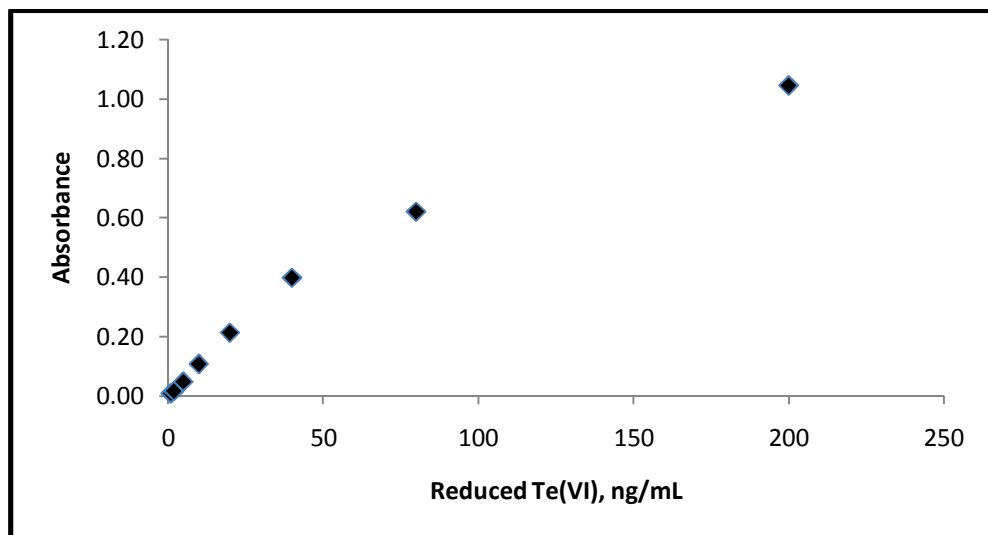


Figure 30 Calibration plot for reduced Te(VI) using HGAAS. Sample solution was prepared in 4.0 mol/L HCl solution and pumped at 6.5 mL/min flow rate. 0.5% (w/v) NaBH₄ was used at a flow rate of 1.5 mL/min.

Plot showed very similar behavior as the one given in Figure 23. Resultant calibration plot was given in Figure 31. As it is clear from the slope of this plot and the previous graphs reduction was achieved with very high yield.

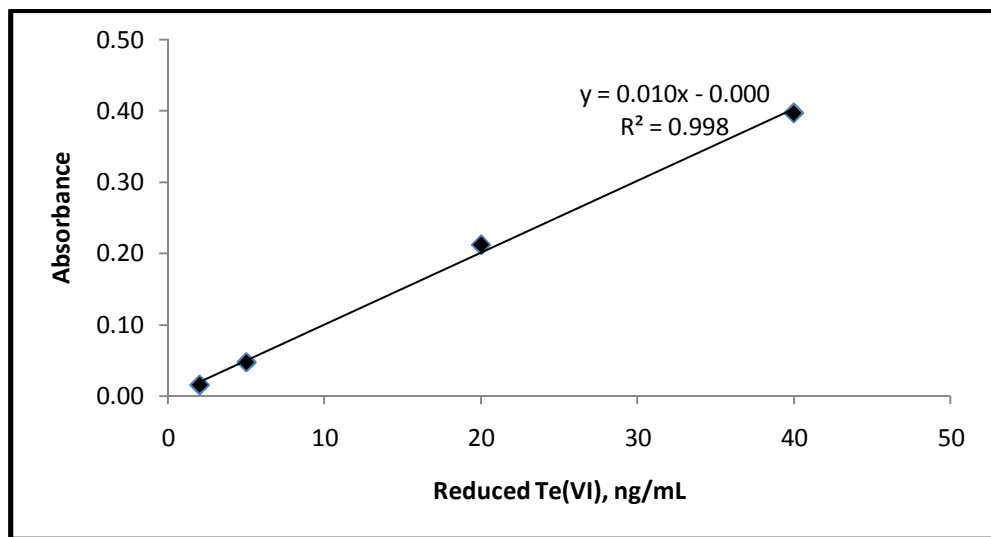


Figure 31 Linear portion of the calibration plot and best line equation for reduced Te(VI) using HGAAS.

Analytical parameters for reduced Te(VI) species are given in Table 17. LOD, LOQ and C_0 values were very similar to those given for Te(IV), which is another indication of the completeness of the reduction.

Table 17 Analytical figures of merit for reduced Te(VI) species using HGAAS.

| | |
|--|------|
| Limit of Detection, LOD, $3s/m$ ($N=10$) ng/mL | 0.18 |
| Limit of Quantification, LOQ, $10s/m$ ($N=10$) ng/mL | 0.60 |
| Characteristic Concentration, C_0 ng/mL | 0.41 |

3.3 Trapping of H_2Te on Pyrolytic Coated Graphite Tube

Continuous flow hydride generation system is an easy and fast method for the trace determination of Te. However, the Te content of environmental and biological

samples are often even lower than the LOD of the developed method. Sensitivity of the method can further be enhanced by application of a trapping system as described in Section 1.4. This approach will then be called as hydride generation-electrothermal atomic absorption spectrometry (HG-ETAAS).

General strategy for the trapping system was sending the formed hydride to a graphite tube, either pretreated or untreated, heated to an optimized trapping temperature and collecting the hydrides on the surface of the graphite tube for an optimized period of time. This step is usually called as *collection*. After collection step, temperature was increased rapidly to the *atomization* temperature and a transient signal was obtained. Both peak area and peak height values of the signals were collected and reported.

In this stage, a pyrolytic coated graphite tube was used directly without a pretreatment step. Tubes were conditioned by using a 10 ng/mL Te solution at optimized conditions before analytical measurements. This procedure was repeated for several cycles until the system gave a constant response over three consecutive measurements. Generally, about 4 cycles were sufficient. Optimized parameters for HCl and NaBH₄ concentrations were used directly whereas the flow rates of the solutions and Ar were optimized for each case.

Several analytical parameters were optimized as given in the following sections. Experiments were performed in the order given below and when a parameter was optimized it was used for the subsequent experiments.

3.3.1 Stripping Ar Flow Rate

It is a known fact that trapping is closely related with the Ar flow rate. Here, the two parameters, namely residence time and transport efficiency, compete with each other. As Ar flow decrease, residence time increases, hence trapping efficiency should increase since atoms spend more time at the trapping area. On the other hand low Ar flow rates resulted in uneven transport of formed hydrides as shown in Section 3.2.6. Stripping Ar flow should be as low as possible to increase the residence time but it should be high enough to efficiently strip and transport formed species to trapping medium. As seen in Figure 32, HG-ETAAS signal decreased with increasing Ar flow even though transport efficiency was lower below 133 mL/min (Figure 21). This result indicated that residence time dominates the trapping process, which means that trapping efficiency of pyrolytic coated surface was relatively poor.

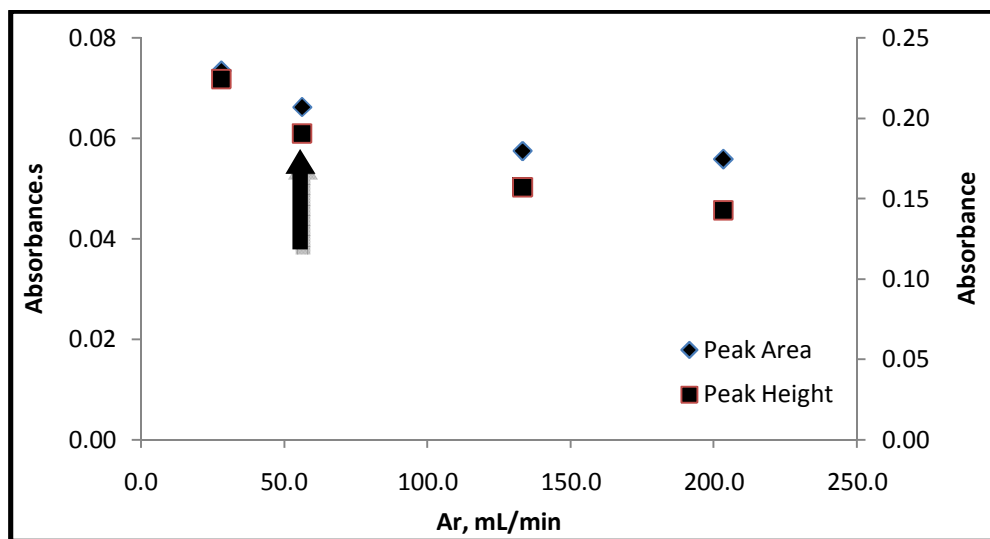


Figure 32 Effect of Ar flow rate on HG-ETAAS signal of 2.0 ng/mL Te(IV) solution trapped over 60 seconds. Sample flow rate was adjusted to 1.6 mL/min. Trapping temperature was 300 °C and atomization temperature was 1900 °C.

53 ml/min Ar flow rate was selected as the optimum value since at lower flow rates reproducibility of the signal decreased.

Another conclusion was that even though low Ar flow could not be used for the continuous flow hydride generation study (Section 3.2.6) application of the graphite trap made it possible working with low Ar flows. Here trap behaves as an online integrator for the signal. In other words, at low flow rates although the HGAAS signals are irregular and unacceptable, once the trapping is used, the integration effect renders the system analytically useful since the reproducibility is improved.

3.3.2 Sample Flow Rate

Preliminary studies showed that trapping efficiency was changing with changing sample flow rate. To find the optimum value two experiments were performed. First one used a constant sample volume, 800 µL, and flow rates of sample and NaBH₄ were varied whereas ratio of sample to NaBH₄ flow rate was kept constant as 2.2. Results were given in Figure 33.

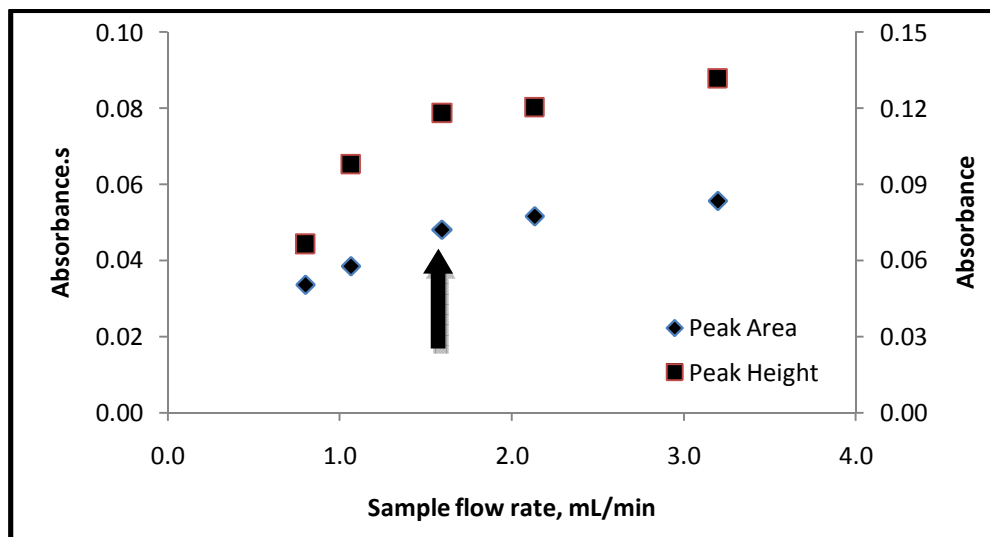


Figure 33 Effect of sample flow rate on HG-ETAAS signal of 800 μL 2.0 ng/mL Te solutions. Trapping temperature was 300 $^{\circ}\text{C}$ and atomization temperature was 1900 $^{\circ}\text{C}$. The ratio of sample to NaBH₄ flow rate was kept constant as 2.2

As it is seen from Figure 33, at flow rates lower than 1.6 mL/min trapping efficiency decreased significantly. A similar experiment was performed with constant collection period. Results were shown in Figure 34.

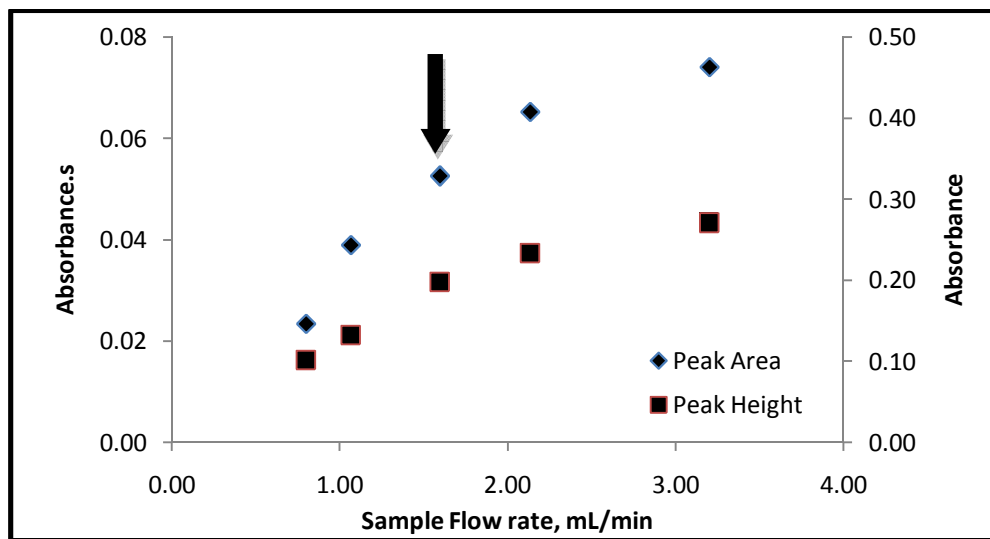


Figure 34 Effect of sample flow rate on HG-ETAAS signal of 2.0 ng/mL Te solution at 60 seconds trapping time. Trapping temperature was 300 °C and atomization temperature was 1900 °C. The ratio of sample to NaBH₄ flow rate was kept constant as 2.2.

As it is seen from the figure, trapping efficiency decreases above 1.6 mL/min flow rate. Above experiments showed that trapping efficiency of the surface was maximum at a restricted sample flow rate.

3.3.3 Trapping Temperature

Trapping temperatures between 100 and 800 °C were studied and atomization temperature was kept constant at 1900 °C. Sample and NaBH₄ flow rates were set to 1.6 and 0.71 mL/min, respectively. Results were shown in Figure 35.

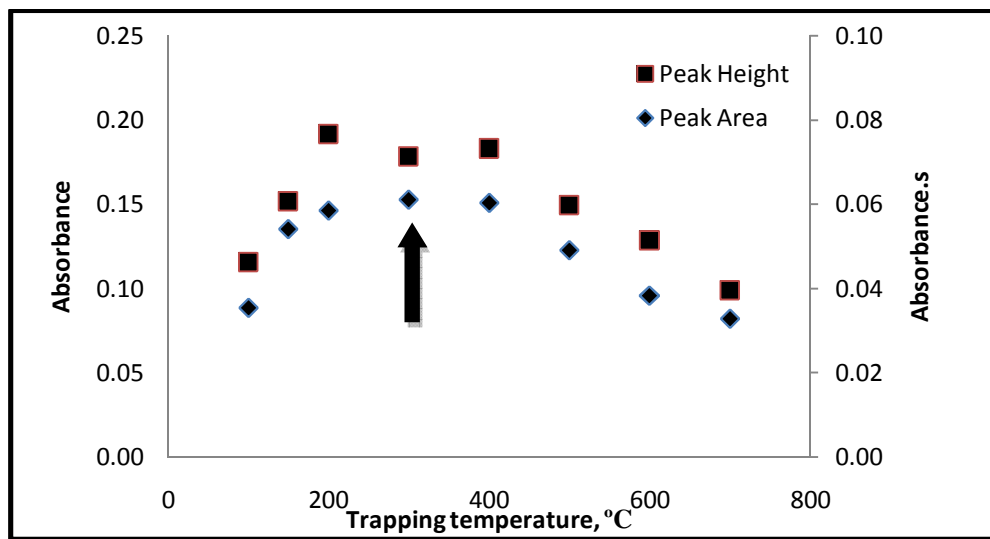


Figure 35 Effect of trapping temperature on HG-ETAAS signal of 2.0 ng/mL Te(IV) solution trapped over 60 second time period. Atomization temperature was kept at 1900 °C.

As can be seen from the figure, analytical signal reaches a maximum between 200 and 400 °C. At this temperature range it could be assumed that decomposition rate of H₂Te was maximum. At temperatures higher than 500 °C signal intensity and signal reproducibility decreased. At high temperatures defects were observed on the quartz capillary due to excessive heating. In addition, lifetime of the graphite tube decreased with increasing trapping temperature since the tube was held at trapping temperature for a relatively long period.

Position of capillary inside the graphite tube was varied and no significant change was observed as far as the tip of the quartz capillary was placed inside the graphite tube.

Observing the behavior shown in Figure 35, 300 °C was selected as the optimum temperature value and used for the rest of the HG-ETAAS studies.

3.3.4 Atomization Temperature

Atomization temperature was varied between 1000 and 2200 $^{\circ}\text{C}$ for the HG-ETAAS studies; the results are given in **Figure 36**. It was observed that at temperatures below 1900 $^{\circ}\text{C}$ peaks were tailed and distorted peaks were observed. Although the best signals, for both peak height and peak area, were observed at 1200 $^{\circ}\text{C}$, this value was not chosen since it might cause interference for the analysis of real samples. Gradual increase in signal peak area between 1900 to 2200 $^{\circ}\text{C}$ was not because of the signal increase but mostly due to increase of noise at high temperatures.

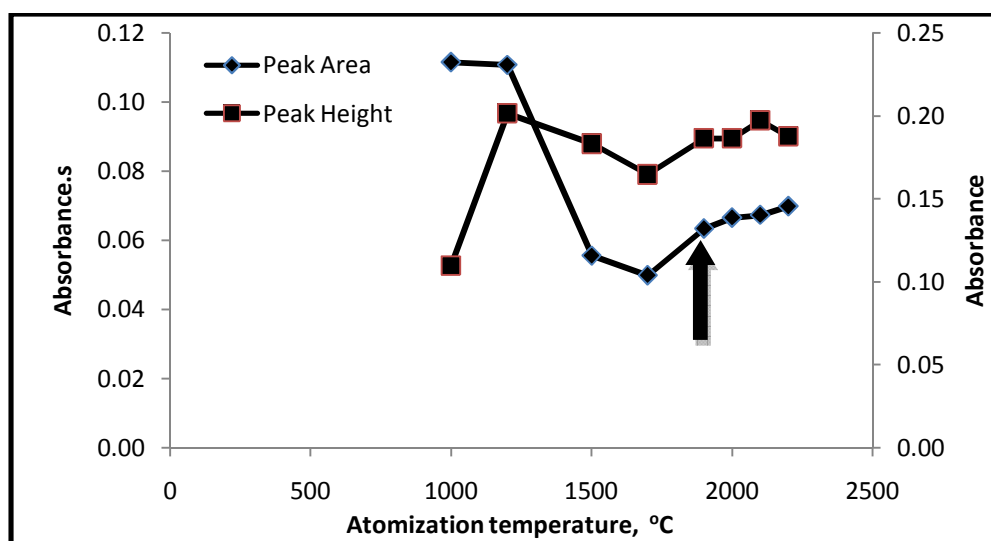


Figure 36 Effect of atomization temperature on HG-ETAAS signal of 2.0 ng/mL Te solution trapped over 60 seconds time period. Trapping temperature was kept at 300 $^{\circ}\text{C}$.

1900 $^{\circ}\text{C}$ was selected as the optimum atomization temperature. A cleaning step at 2100 $^{\circ}\text{C}$ was added to the temperature program.

3.3.5 Collection Period

Trapping period was varied between 30 to 150 seconds. Results are given in Figure 37. As can be seen from the figure, signal increases with increasing trapping period within the range studied. In order to shorten the analysis time and lower the sample consumption, 60 seconds trapping time was selected as the optimum value. At lower trapping periods, reproducibility decreased since the operation was controlled manually and it was affected by the operator's timing skills.

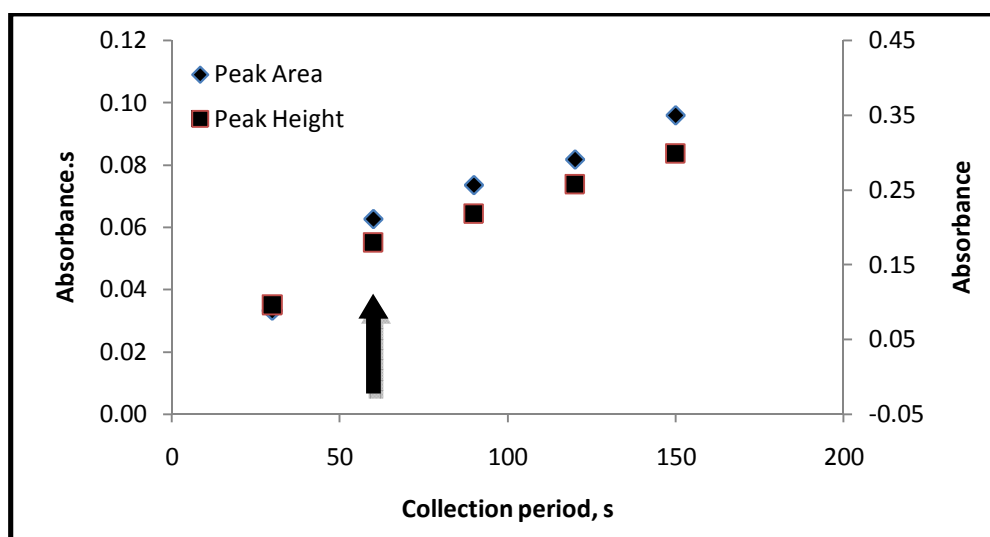


Figure 37 Effect of trapping period on analytical signal of 2.0 ng/mL Te solution. Trapping temperature and atomization temperature was 300 °C and 1900 °C, respectively.

3.3.6 Calibration Plot and Linear Range

A set of solutions ranging from 0.3 to 10 ng/mL Te was prepared and the peak area and peak height values were recorded for 60 seconds trapping period. Sample and

NaBH_4 flow rates were set to 1.60 and 0.76, respectively. Results are given in Figure 38.

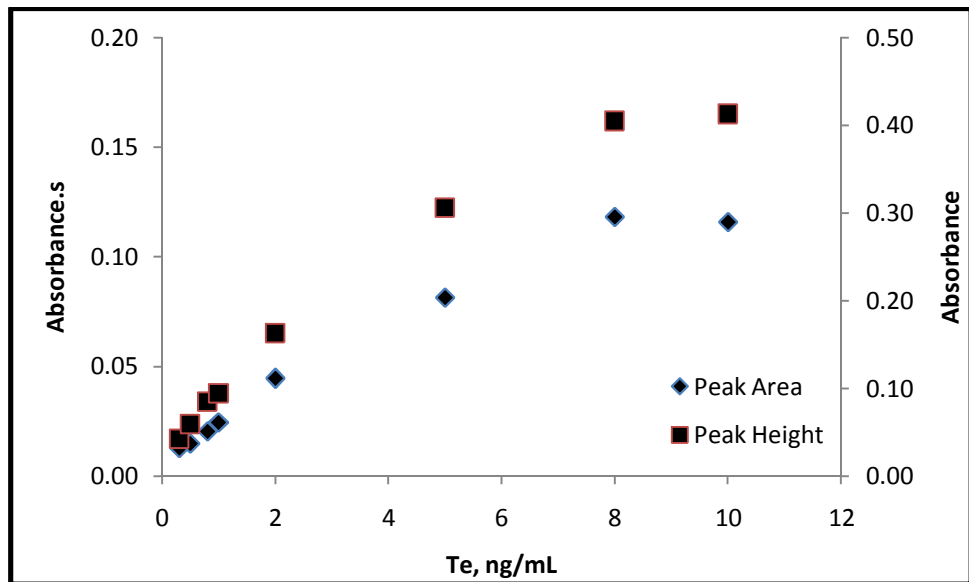


Figure 38 Calibration plot for trapping of H_2Te on pyrolytic coated graphite tube using HG-ETAAS. Trapping temperature and atomization temperatures were set to 300 and 1900 $^{\circ}\text{C}$, respectively. Sample flow rate was adjusted to 1.6 mL/min.

It was seen that analytical signal was linear for both peak area and peak height values up to 2.0 ng/mL. After this point deviation from linearity was observed. Thus, linear range was determined as 0.3 to 2.0 ng/mL, which is roughly one order of magnitude better than continuous flow HGAAS system.

A calibration plot and corresponding best line equation for HG-ETAAS is given in Figure 39.

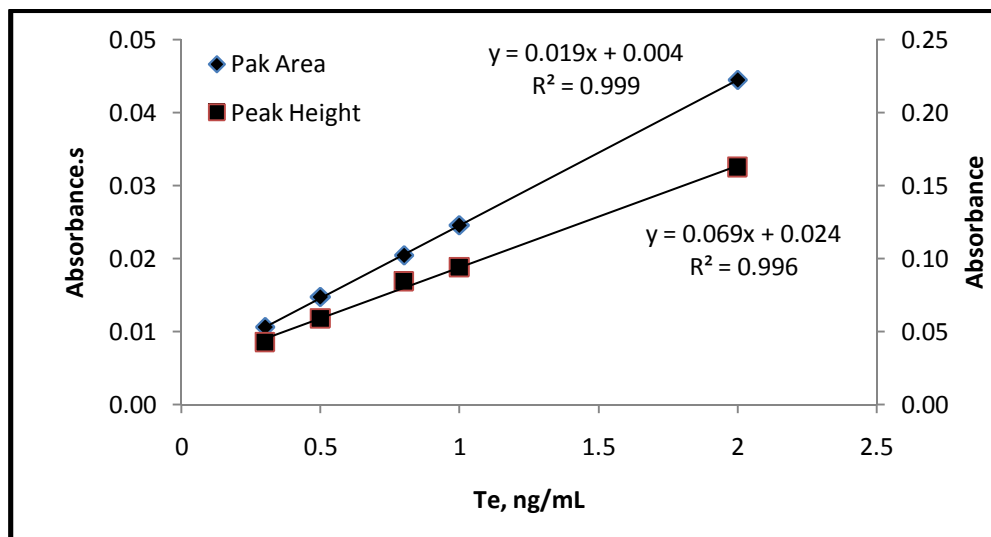


Figure 39 Linear portion of the calibration plot and best line equation for Te determination by HG-ETAAS using pyrolytic coated graphite tube.

3.3.7 Analytical Figures of Merit

LOD, LOQ, characteristic concentration (C_o), characteristic mass for peak absorption (m_p) and characteristic mass for peak area (m_a) values were calculated and given in Table 18. 60 seconds trapping time and 1.60 and 0.75 mL/min sample and NaBH₄ flow rates were used, respectively. Enhancement factors (E) for HG-ETAAS with respect to continuous flow HGAAS and direct ETAAS were calculated as the ratio of characteristic concentrations. Trapping efficiency was calculated as the ratio of the characteristic masses of direct ETAAS analysis and trapping system using peak area signals. Under the optimized conditions, RSD value for 1.0 ng/mL solution was calculated as 8% (N=7). With 60 seconds trapping time, 30 samples could be analyzed in one hour.

Table 18 Analytical figures of merit for Te determination by HG-ETAAS using pyrolytic coated graphite tube.

| | 60 seconds trapping time | |
|---|--------------------------|----------------|
| | By Peak Area | By Peak Height |
| Concentration Limit of Detection, LOD, 3s/m (N=7), pg/mL | 274 | 86 |
| Mass Limit of Detection, LOD, 3s/m (N=7), pg | 438 | 138 |
| Concentration Limit of Quantification, LOQ, 10s/m (N=7), pg/mL | 915 | 287 |
| Mass Limit of Quantification, LOQ, 10s/m (N=7), pg | 1463 | 460 |
| Characteristic concentration, C₀, pg/mL | 179 | 45 |
| Characteristic mass for peak absorption, m_p, pg | - | 72 |
| Characteristic concentration for peak area, m_a, pg | 286 | - |
| Enhancement factor with respect to direct ETAAS with pyrolytic coating | 11.7 | 13.4 |
| Enhancement factor with respect to continuous flow HGAAS | - | 8.3 |
| Efficiency with respect to direct ETAAS | 14.6% | 16.7% |
| RSD, 10 replicates of 0.3 ng/mL solution | 8.2 | 7.5 |

3.4 Trapping of H₂Te on Pd Modified Graphite Tube

It was seen from the previous section that pyrolytic coated graphite surface has a limited efficiency to trap H₂Te species. Modification of the surface may increase the trapping efficiency of the surface. Some transition metals were studied as temporary surface modifiers and it was observed that Pd, Ag and Au increase the activity of the surface. Among the metals, Pd was selected as a surface modifier since volatility of Pd is relatively lower as compared to Au and Ag. This will decrease the loss of modifier during collection stage and allow the use of a higher ashing temperature.

Even though Pd is relatively less volatile, most of it was lost during the atomization and clean-up stages. Due to this reason an optimized amount of Pd was introduced into the graphite surface before each reading. An initial drying step was added to the temperature program applied.

Several analytical parameters affecting the analytical signal were optimized.

3.4.1 Stripping Ar Flow Rate

For pyrolytic coated graphite surface, analytical signal was decreasing with increasing the Ar flow rate due to the lowered trapping efficiency of the surface as discussed in the previous sections. A reversed case was observed for the Pd modified graphite surface. Analytical signal was increasing up to 133 mL/min Ar flow. After this point signal reached to a constant value as shown in Figure 40. This behavior may be attributed to the increased trapping efficiency of the surface. At

low Ar flow rates formed hydrides could not be efficiently transported to the trapping zone and decrease in HG-ETAAS signal was observed. After 133 mL/min, transportation efficiency reached the maximum value and the signal stayed same for the higher flow rates. Here, the trap eliminates the dilution effect of Ar gas by collecting and separating the formed species from the excess gasses. It could be concluded that analytical signal was dominated by transport efficiency rather than residence time. Another conclusion was that trapping efficiency was high even at high gas flow rates corresponding to lower residence time. 133 mL/min Ar flow was selected as the optimum value since higher flow rates created a high back pressure inside the GLS and leaking was observed at the connection points of capillaries.

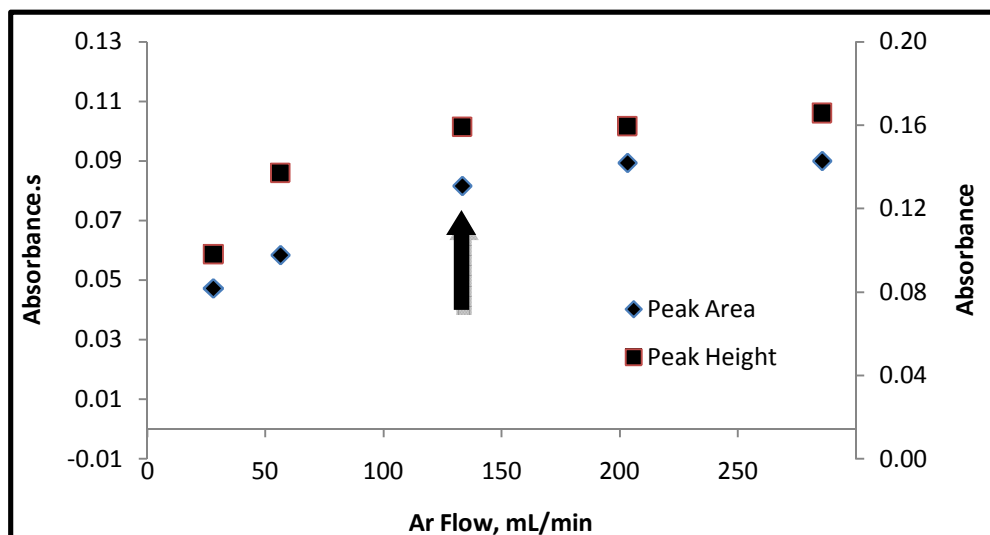


Figure 40 Effect of Ar flow rate on the HG-ETAAS signal of 0.5 ng/mL Te(IV) solution trapped over 60 seconds time period. Trapping temperature and atomization temperature were adjusted to 300 °C and 2300 °C, respectively. 10 µL 1000 mg/L Pd modifier was injected into the graphite tube before each measurement.

3.4.2 Flow Rates of Sample and Reductant Solutions

Another critical parameter affecting the HG-ETAAS signal intensity is the sample flow rate. Sample flow rates ranging from 0.8 to 4.8 mL/min were studied while ratio of sample flow rate to reductant flow rate was kept constant as 2.2. Results are given in Figure 41 showing that unlike the pyrolytic coated graphite tube, trapping was linear with respect to flow rate when Pd modifier was used. This was another indication of the increase in the trapping efficiency of the modified surface. 3.2 mL/min sample flow rate was selected as the optimum value to keep the sample consumption at a reasonable level.

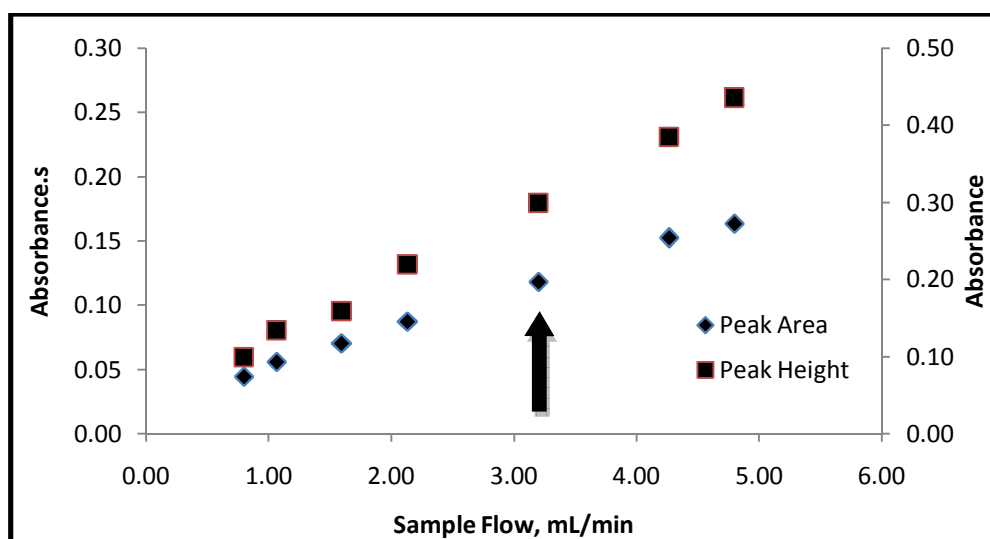


Figure 41 Sample flow rate on HG-ETAAS signal of 0.5 ng/mL Te(IV) solution trapped over 60 seconds time period. Trapping temperature and atomization temperature were adjusted to 300 °C and 2300 °C, respectively. 10 µL 1000 mg/L Pd modifier was injected into the graphite tube before each measurement.

3.4.3 Trapping Temperature

Trapping temperature was varied between 100 to 1000 °C. Atomization temperature was kept constant at 2300 °C and the sample flow rate was 3.2 mL/min. Change of HG-ETAAS signal with trapping temperature is given in Figure 42 for Pd modified graphite surface. Trapping efficiency was nearly constant over the range studied. This indicates that catalytic effect of Pd for the decomposition of H₂Te was nearly constant over a range of temperatures. 300 °C was selected as the optimum trapping time to make the data comparable with other surfaces.

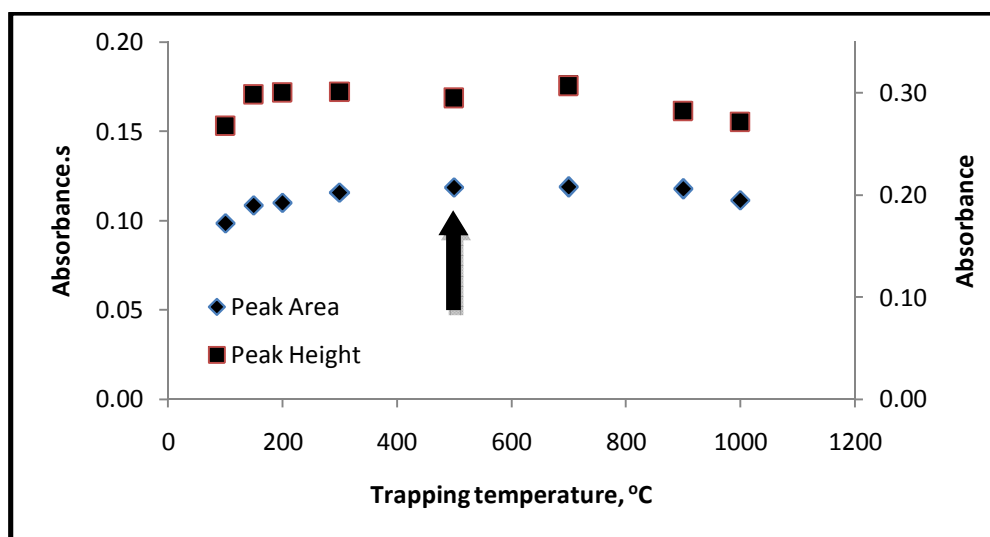


Figure 42 Effect of trapping temperature on HG-ETAAS signal intensity for 60 seconds trapping of 0.5 ng/mL Te(IV) solution. Atomization temperature was 2300 °C. 10 µL 1000 mg/L Pd modifier was injected into the graphite tube before each measurement.

3.4.4 Atomization Temperature

Atomization temperature was varied between 1000 to 2500 °C; the results are given in Figure 43. Stabilizing effect of Pd was higher than the bare graphite surface and a relatively high atomization temperature was needed. At low atomization temperatures defected and tailed peaks were observed due to incomplete vaporization. 2300 °C was selected as the optimum atomization temperature since at higher atomization temperatures noise level increased. Following the atomization stage, a cleanup step at 2500 °C was added to the temperature program to completely remove any residual modifier from the surface. Atomization temperature was varied between 1000 to 2500 °C and results were given in Figure 43. Stabilizing effect of Pd was higher and a relatively high atomization temperature was needed. At low atomization temperatures defected and tailed peaks were observed due to incomplete vaporization. 2300 °C was selected as the optimum atomization temperature since at higher atomization temperatures noise level increased. Following the atomization stage a cleanup step at 2500 °C was added to the temperature program to completely remove any residual modifier from the surface (Table 9).

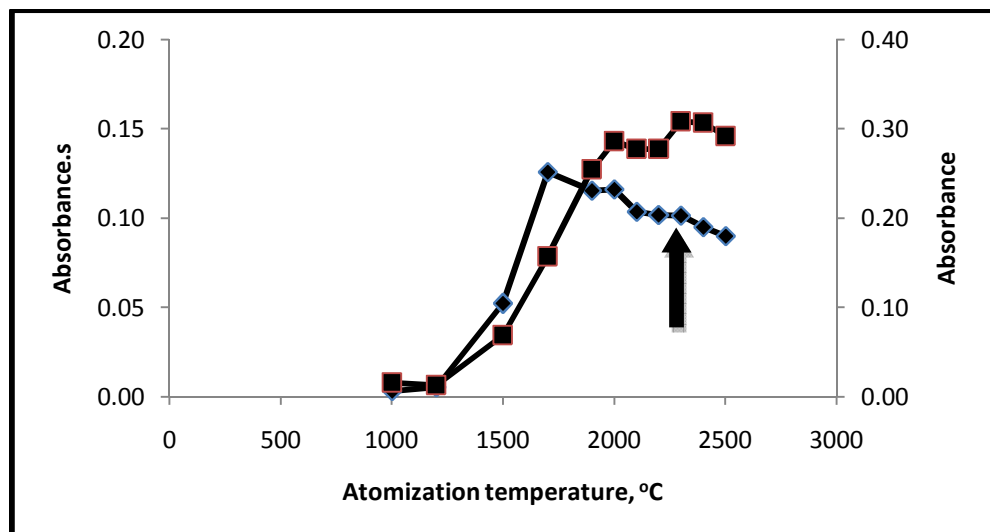


Figure 43 Effect of atomization temperature on HG-ETAAS signal of 0.5 ng/mL Te(IV) solution trapped over 60 seconds time period. Trapping temperature was 300 °C. 10 µL 1000 mg/L Pd modifier was injected into the graphite tube before each measurement.

3.4.5 Pyrolysis Temperature

An intermediate pyrolysis step was added to the temperature program since liquid modifier was introduced to the system. Temperatures between 300 and 1200 °C were studied and the results are given in Figure 44. At pyrolysis temperatures lower than 800 °C, increase in background signal at atomization step was observed. After 800 °C, decrease in HG-ETAAS signal due to sample loss was observed. This behavior was different than direct ETAAS analysis, for which case the signal decrease was observed after 1400 °C. This observation indicated that Te was deposited in different forms on the pyrolytic coated and Pd modified graphite surfaces. 800 °C was selected as the optimum pyrolysis temperature.

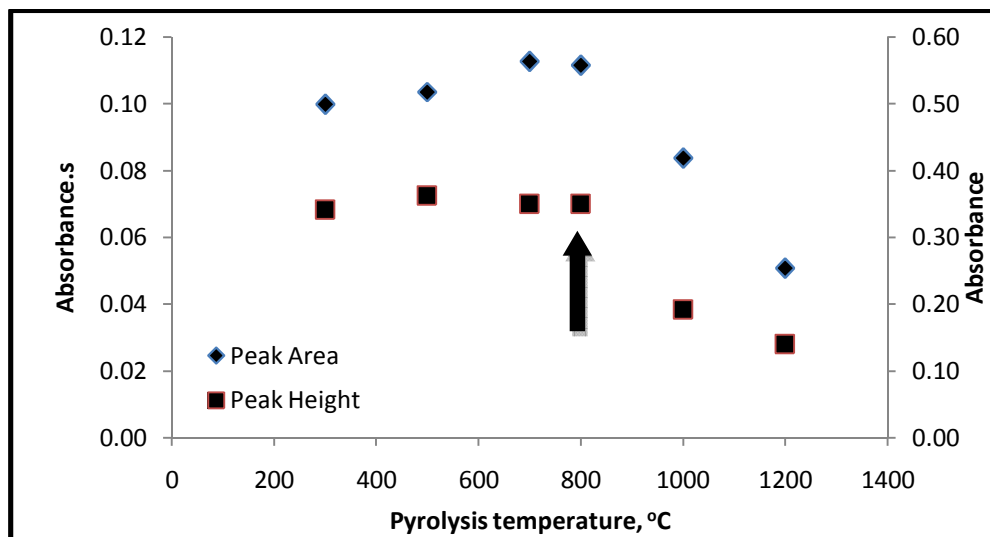


Figure 44 Effect of pyrolysis temperature on HG-ETAAS signal of 0.5 ng/mL Te(IV) solution trapped over 60 seconds time period. Trapping temperature and atomization temperature was 300 °C and 2300 °C, respectively. 10 µL 1000 mg/L Pd modifier was injected into the graphite tube before each measurement.

3.4.6 Amount of Pd Modifier

Efficient trapping of the graphite surface is closely related with the amount of Pd injected before each reading. To find the optimum Pd amount, concentration of injected Pd solution was varied while keeping the injection volume constant as 10 µL (**Figure 45**). Results showed that the peak height stayed relatively same whereas increase in the peak area with increasing Pd amount was observed. This behavior resulted in decrease of peak width at half height. Also shifting of the position of peaks, indicating decrease of atomization temperature, was observed. This behavior is given in **Figure 46**.

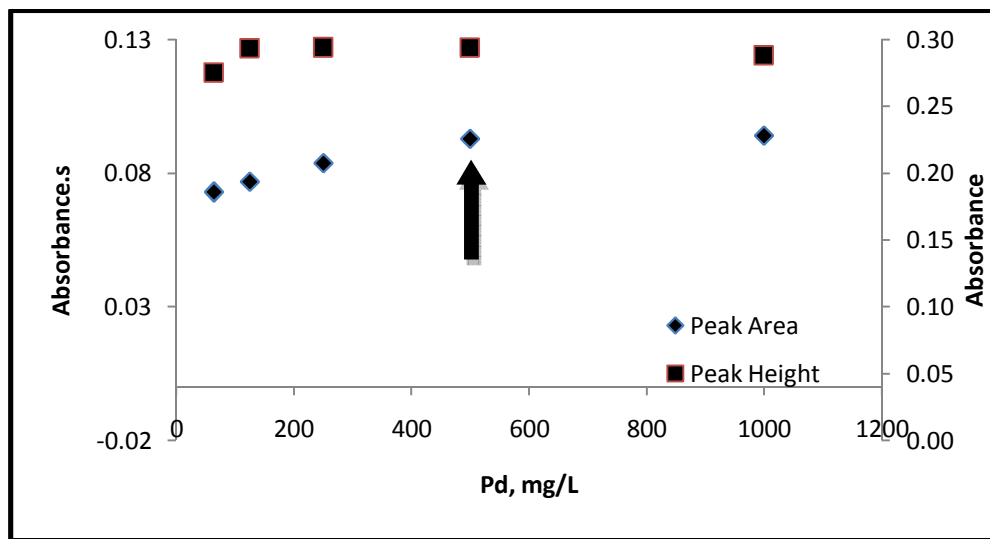


Figure 45 Effect of Pd amount injected on HG-ETAAS signal of 0.5 ng/mL Te(IV) solution trapped over 60 seconds. Trapping temperature and atomization temperature was 300 °C and 2300 °C, respectively. Pyrolysis temperature was adjusted to 800 °C. 10 µL Pd modifier was injected into the graphite tube before each measurement.

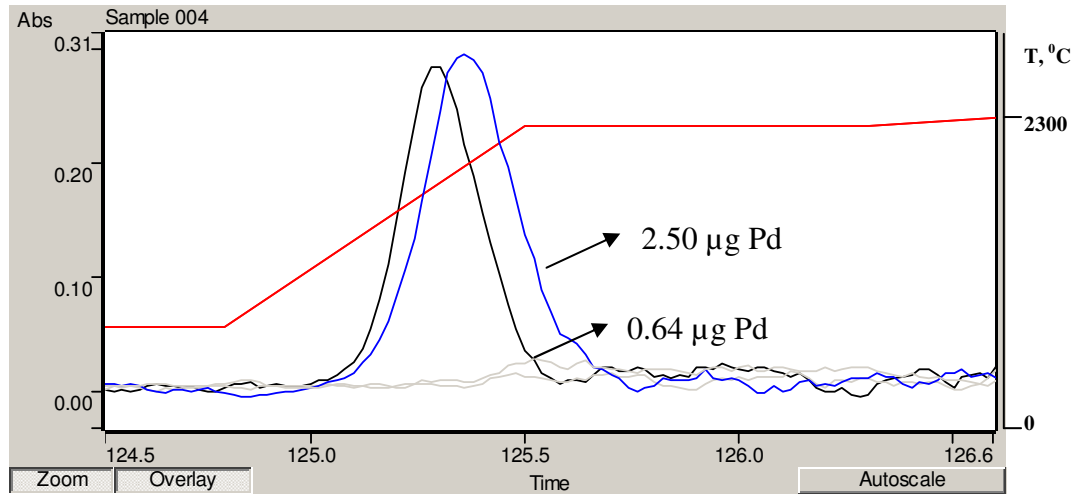


Figure 46 Shapes and positions of analytical signal with changing Pd amount. Shapes and positions of HG-ETAAS signal with varying Pd amount. 0.5 ng/mL Te(IV) solution was trapped over 60 seconds. Trapping temperature and atomization temperature

was 300°C and 2300°C , respectively. Pyrolysis temperature was adjusted to 800°C . $10\ \mu\text{L}$ Pd modifier was injected into the graphite tube before each measurement.

3.4.7 Collection Period

Collection period was varied from 30 seconds to 180 seconds. Analytical signal for HG-ETAAS was found to be increasing linearly within the range studied as shown in Figure 47. Here, the two points, for 60 seconds and 180 seconds, were selected and calibration plots were constructed for both points.

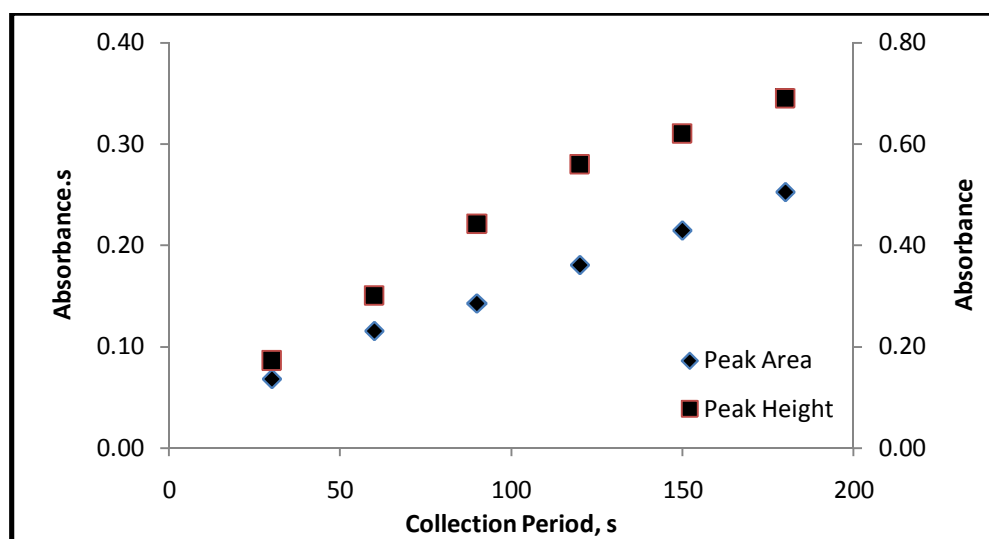


Figure 47 Effect of collection period on HG-ETAAS signal of $0.5\ \text{ng/mL}$ Te(IV) solution. Trapping temperature and atomization temperature was 300°C and 2300°C , respectively. Pyrolysis temperature was adjusted to 800°C . $10\ \mu\text{L}$ $1000\ \text{mg/L}$ Pd modifier was injected into the graphite tube before each measurement.

3.4.8 Calibration Plot and Linear Range

A set of solutions ranging from 0.05 to 5.00 ng/mL was prepared to determine the analytical working range for 60 seconds and 180 seconds trapping periods and results were given in Figure 48. 300 °C for trapping temperature, 800 °C for pyrolysis temperature and 2300 °C for atomization temperature were used. It was seen that for 60 seconds, HG-ETAAS signal was changing linearly up to 1.00 ng/mL. After this point signal deviated from linearity. Constructed calibration graph had the best line equation, $y = 0.5092x + 0.011$, with a correlation coefficient of 0.9914 according to peak height values (Figure 49).

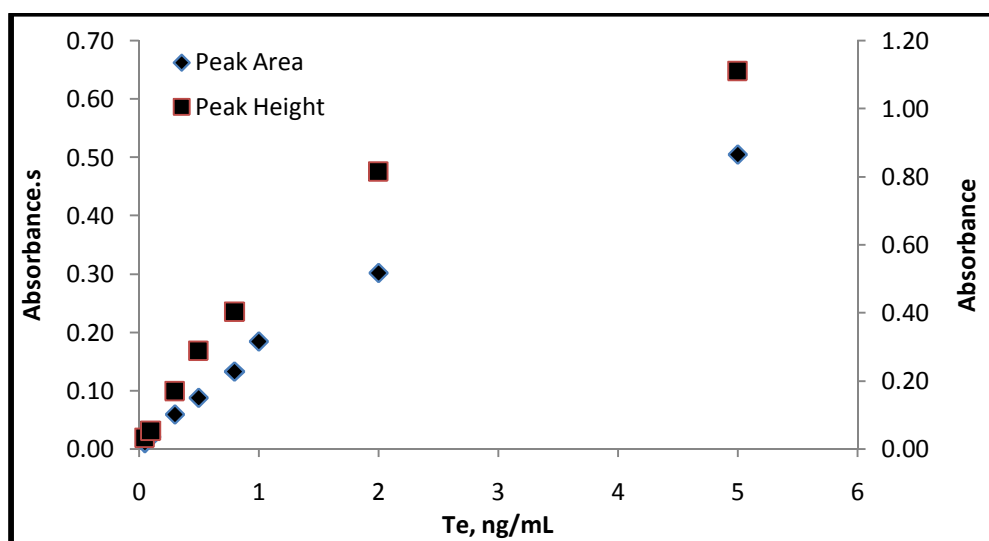


Figure 48 Calibration plot for Te using HG-ETAAS using Pd modified graphite tube over 60 seconds time period. Trapping temperature and atomization temperatures were set to 300 and 2300 °C, respectively. Pyrolysis temperature was adjusted to 800 °C. 10 µL 1000 mg/L Pd modifier was injected into the graphite tube before each measurement. Sample flow rate was adjusted to 3.2 mL/min.

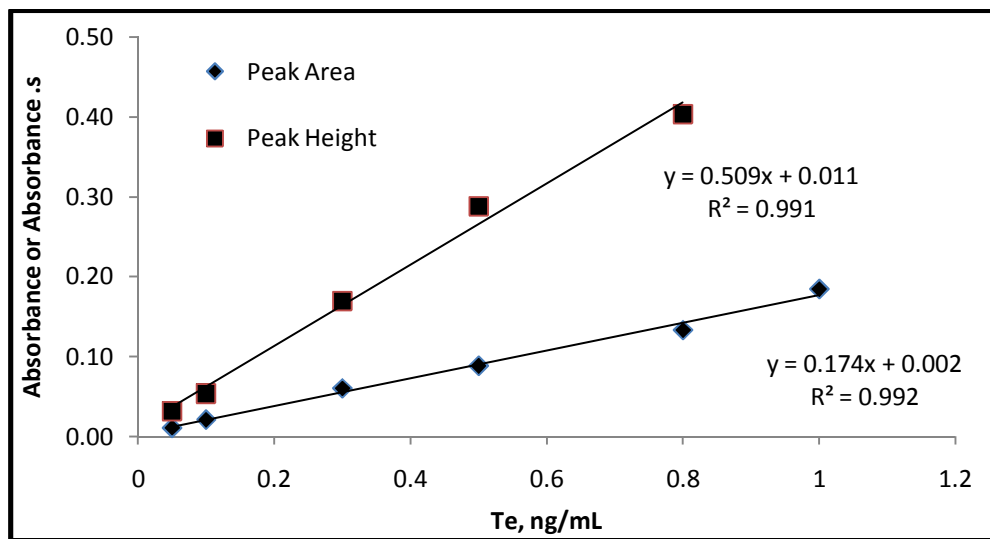


Figure 49 Linear portion of the HG-ETAAS calibration plot and best line equation for Te using Pd modified graphite tube and trapping for 60 seconds time period. Trapping temperature and atomization temperatures were set to 300 and 2300 °C, respectively. Pyrolysis temperature was adjusted to 800 °C. 10 µL 1000 mg/L Pd modifier was injected into the graphite tube before each measurement. Sample flow rate was adjusted to 3.2 mL/min.

For 180 seconds trapping, constructed calibration graph was linear up to 0.50 ng/mL (**Figure 50**). Constructed calibration plot for HG-ETAAS had the best line equation of $y = 1.2406x + 0.0437$ with a correlation coefficient of 0.9999 according to peak height values (**Figure 51**).

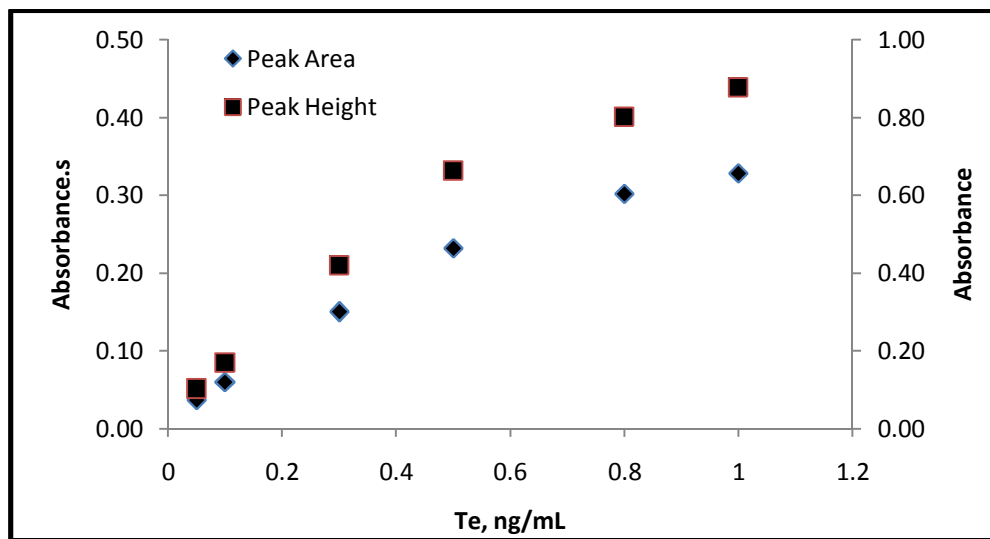


Figure 50 Calibration plot for Te using HG-ETAAS and Pd modified graphite tube over 180 seconds time period. Trapping temperature and atomization temperatures were set to 300 and 2300 °C, respectively. Pyrolysis temperature was adjusted to 800 °C. 10 µL 1000 mg/L Pd modifier was injected into the graphite tube before each measurement. Sample flow rate was adjusted to 3.2 mL/min.

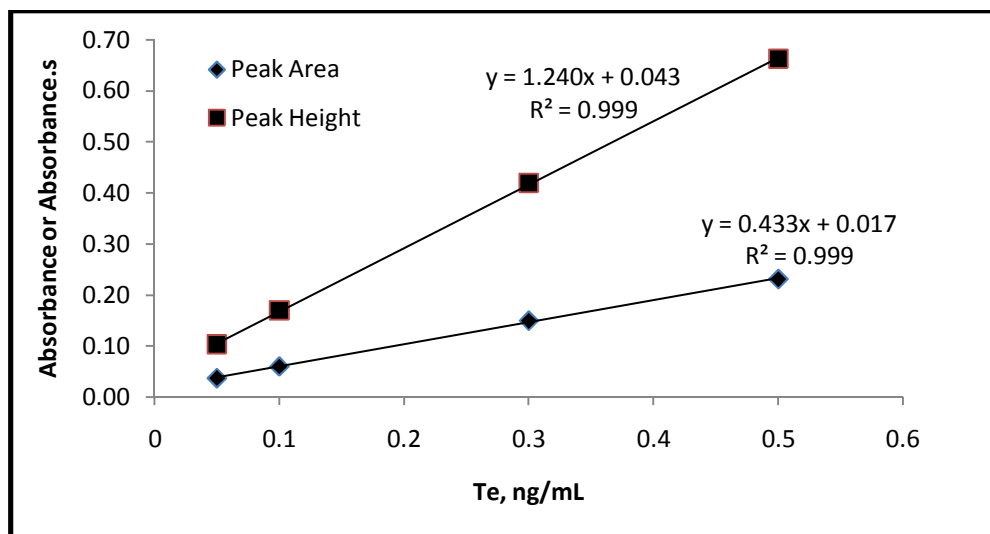


Figure 51 Linear portion of the calibration plot and best line equation for Te using HG-ETAAS and Pd modified graphite tube over 180 seconds time period. Trapping temperature and atomization temperatures were set to 300 and 2300 °C, respectively. Pyrolysis temperature was adjusted to 800 °C. 10 µL 1000 mg/L Pd

modifier was injected into the graphite tube before each measurement. Sample flow rate was adjusted to 3.2 mL/min.

3.4.9 Analytical Figures of Merit and Method Validation

LOD, LOQ, characteristic concentration (C_o) characteristic mass for peak absorption (m_p) and characteristic mass for peak area (m_a) values were calculated and given in Table 19. 60 seconds and 180 seconds trapping time and 3.20 and 1.10 mL/min sample and NaBH₄ flow rates were used, respectively. Enhancement factor (E) with respect to continuous flow HGAAS and direct ETAAS were calculated as the ratio of characteristic concentrations. Trapping efficiency was calculated as the ratio of the characteristic masses of direct ETAAS analysis and trapping system using peak area signals. Under the optimized conditions, RSD value for 1.0 ng/mL solution was calculated below 4% (N=7) for all cases.

Table 19 Analytical figures of merit for trapping of H₂Te in Pd modified graphite tube.

| | 60 seconds trapping time | | 180 seconds trapping time | |
|---|--------------------------|-------------|---------------------------|-------------|
| | Peak Area | Peak Height | Peak Area | Peak Height |
| Concentration Limit of Detection, LOD, 3s/m (N=) pg/mL | 34.3 | 15.8 | 13.8 | 6.4 |
| Mass limit of Detection, LOD, 3s/m (N=7) pg | 109.7 | 50.7 | 132.5 | 61.4 |
| Concentration Limit of Quantification, LOQ, 10s/m (N=7) pg/mL | 114.4 | 52.3 | 46.0 | 21.6 |
| Mass Limit of Quantification, LOQ, 10s/m (N=7) pg | 366.1 | 167.4 | 441.6 | 207.4 |
| Characteristic Concentration, C₀ pg/mL | 22.1 | 7.8 | 8.8 | 3.1 |
| Characteristic mass for peak absorption, m_p, pg | - | 25.7 | - | 30.2 |
| Characteristic mass for peak area, m_a, pg | 70.5 | - | 84.4 | - |
| Enhancement factor with respect to direct ETAAS with Pd modifier | 69 | 56 | 174 | 140 |
| Enhancement factor with respect to continuous flow HGAAS | - | 48 | - | 120 |
| Efficiency with respect to direct ETAAS | 59.5% | 46.7% | 49.7% | 39.7% |
| RSD, 10 replicate of 0.3 ng/mL solution | 4.3 | 3.3 | 3.7 | 2.5 |

Accuracy of the method was tested by NIST 1643e “Trace elements in water” SRM. Before the analysis, reduction procedure given in Section 2.5.3 was applied. Direct calibration method was used with three parallel samples. Results are shown in Table 20. Student t-test at 95% confidence level shows no significant difference between the values.

Table 20 Results of accuracy check for trapping of H₂Te on Pd modified graphite tube using NIST 1643e “Trace elements in water” SRM.

| | Certified Value | Found Value |
|------------------------|-----------------|-------------|
| Total Te, ng/mL | 1.09 ± 0.11 | 1.30 ± 0.13 |

3.5 Trapping of H₂Te on Ru Modified Graphite Tube

Application of Pd modifier enhanced the sensitivity of Te analysis by HG-ETAAS; but the system had some drawbacks. First of all, Pd was lost during atomization and cleanup stages and should be introduced to the system before each measurement. This not only increases the analysis time but also causes a higher cost of analysis since Pd is an expensive reagent and continuous consumption of the modifier increases the operating cost. Another disadvantage was that during atomization and cleanup stages high temperatures were applied. This decreases the lifetime of the tube. Additionally, background signal increases due to introduction of liquid modifier.

To overcome these disadvantages a Ru permanent modifier was tested and it was observed that Ru modifier efficiently traps and releases Te species. An optimization

was performed to find the best analytical working conditions using a Ru modified graphite tube in HG-ETAAS.

Graphite tubes were coated according to the procedure given in Section 2.5.5. A total of 25 µg of Ru were introduced to the graphite surface.

3.5.1 Stripping Ar Flow Rate

Ar flow was varied between 28 and 203 mL/min. Results showed that signal was increasing up to 56 mL/min Ar flow and decreasing after 133 mL/min Ar flow as shown in Figure 52. This behavior was the result of the competition between transport efficiency and residence time. At low Ar flows transport efficiency dominated the system and increase of analytical signal with increasing Ar flow was observed. At Ar flows above 133 mL/min residence time started dominating the system and decrease of analytical signal was observed.

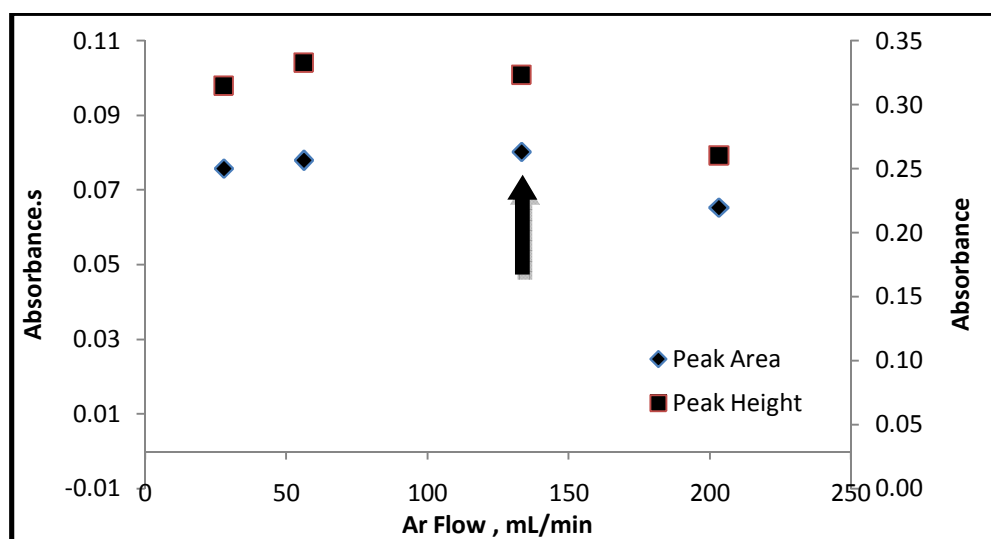


Figure 52 Effect of stripping Ar flow rate on HG-ETAAS signal of 0.5 ng/mL Te(IV) solution trapped over 60 seconds time period. Sample solution was pumped at 3.2 mL/min. Trapping temperature and atomization temperatures were adjusted to 300 °C and 2000 °C, respectively.

3.5.2 Sample Flow Rate

Sample flow rate was varied from 0.8 to 3.7 mL/min while keeping the ratio of sample flow rate to reductant flow rate constant as 2.2. Results given in **Figure 53** indicated that HG-ETAAS signal was increasing linearly with increasing sample flow rate. To keep the sample consumption at a reasonable level and render the data comparable with the previous methods, sample flow rate of 3.2 mL/min was selected.

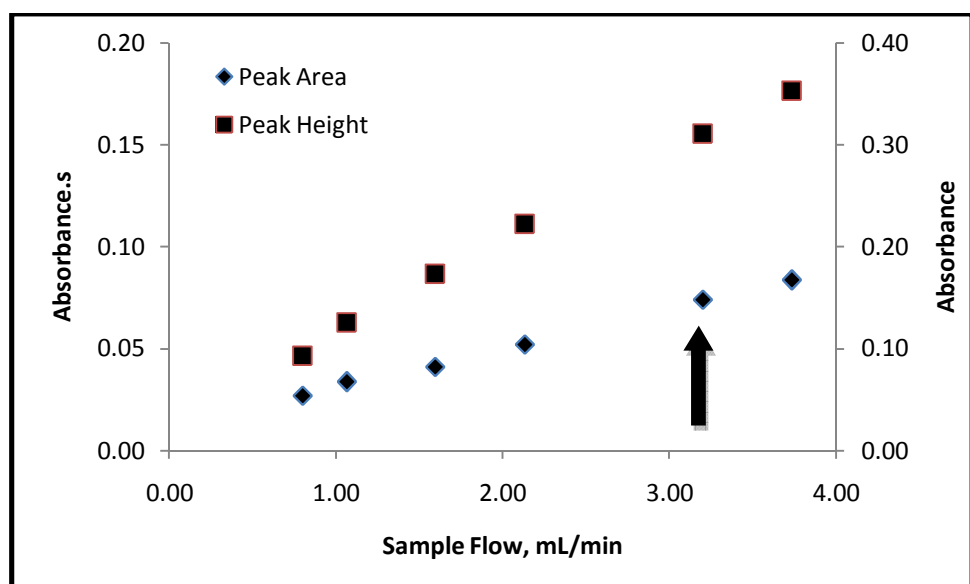


Figure 53 Effect of sample flow rate on HG-ETAAS signal of 0.5 ng/mL Te(IV) solution trapped over 60 seconds on Ru modified graphite tube. Ar flow rate was set to 133 mL/min, trapping temperature and atomization temperatures were adjusted to 300 and 2000 °C, respectively.

3.5.3 Trapping Temperature

Trapping temperature was varied between 150 to 800 °C and the results were given in Figure 54 for HG-ETAAS. A small increase between 100 and 300 °C was observed.

Unlike the previous cases, i.e. pyrolytic coated graphite tube and Pd modified graphite tube, a distinctive increase in the analytical signal was seen after 600 °C. Blank studies revealed that this increase was not due to an increase of the trapping efficiency but it was rather originating from a carryover effect. Most probable explanation of this behavior was that at high furnace temperatures quartz capillary, which was used for the introduction of the hydrides, was heated and started to function as a trap. Therefore, the trapped species were carried to the next measurements. This behavior was facilitated in the presence of Ru since no carryover effect was observed for pyrolytic coated and Pd modified surfaces. A similar effect was observed by Liao and Haug (**Liao & Haug, 1997**) for Ir coated graphite surface. 300 °C was selected as the optimum value to make the data comparable with the other methods.

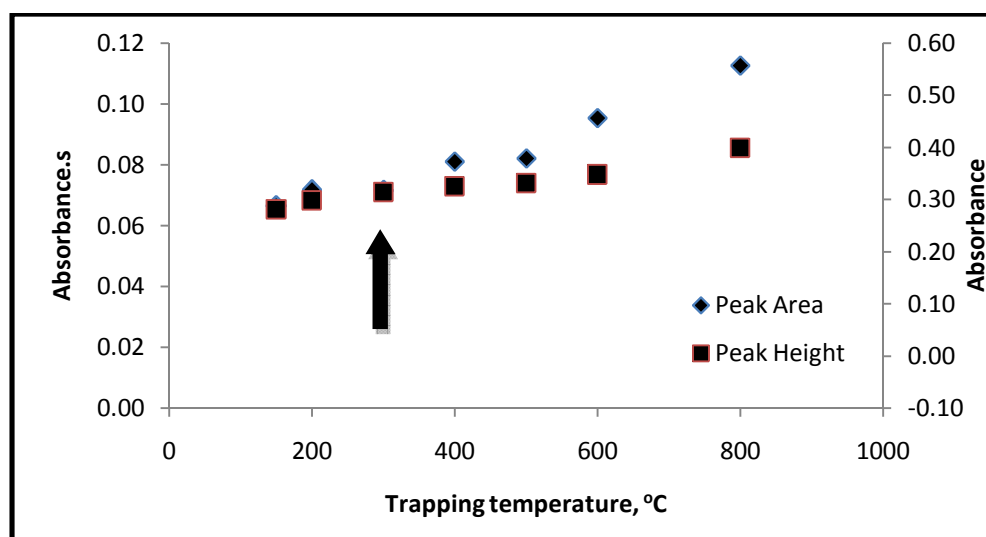


Figure 54 Effect of trapping temperature on HG-ETAAS signal of 0.5 ng/mL Te(IV) solution trapped over 60 seconds. Atomization temperature was set to 2000 °C and sample flow rate was 3.2 mL/min.

3.5.4 Atomization Temperature

Atomization temperature was varied from 1000°C to 2100°C ; the data are shown in Figure 55 for HG-ETAAS. A sharp and reproducible signal was obtained after 1600°C but 2000°C was determined as the optimum value considering the real life samples with volatile interferences. Atomization temperature of 2100°C was not exceeded to increase the lifetime of permanent Ru coating.

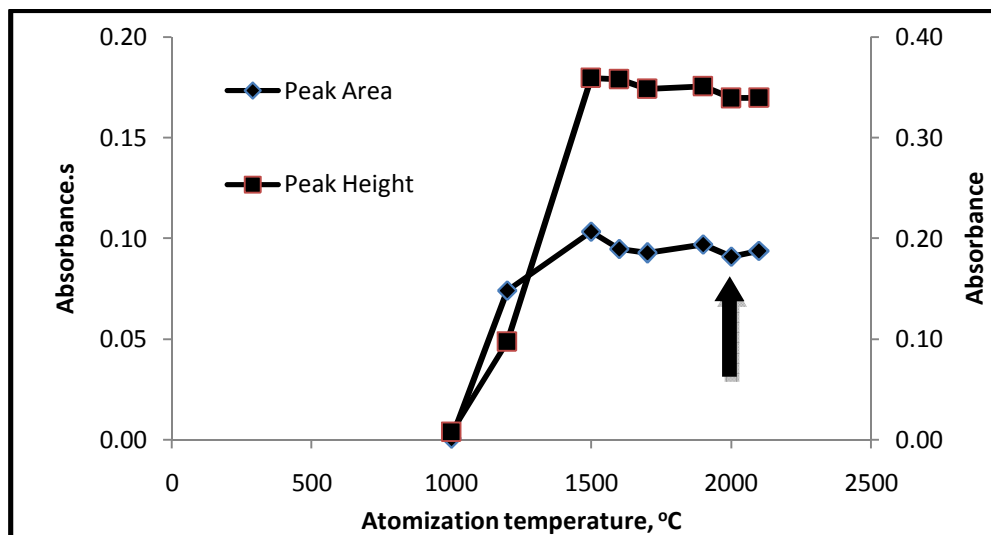


Figure 55 Effect of atomization temperature on the HG-ETAAS signal of 0.5 ng/mL Te solution trapped over 60 seconds. 300°C trapping temperature was used and sample flow rate was adjusted to 3.2 mL/min .

3.5.5 Collection Period

Collection period was varied from 30 seconds to 180 seconds and the results are given in Figure 56. A linear relation between collection period and signal intensity was observed over the range studied for HG-ETAAS. 60 seconds and 180 seconds collection periods were selected as optimum values and calibration plots were constructed for both cases.

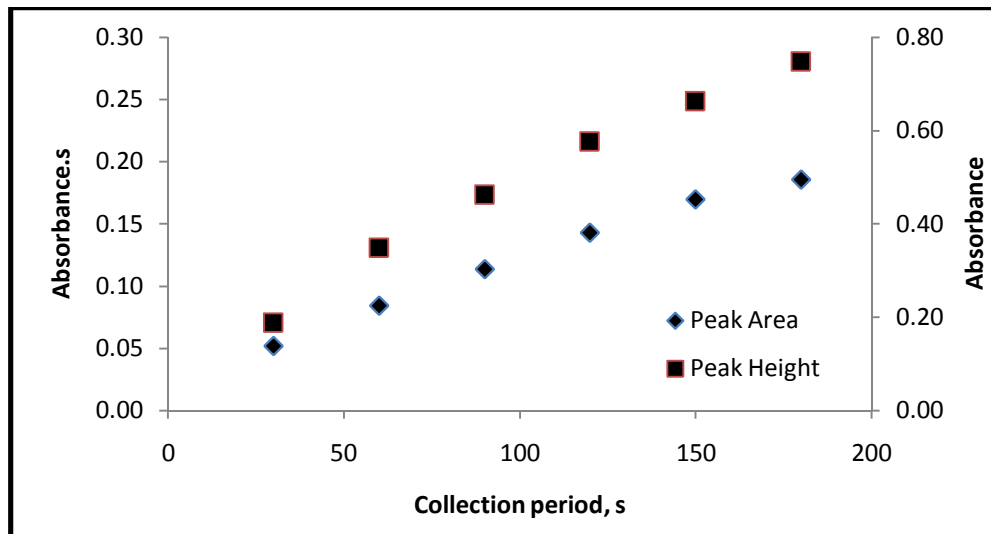


Figure 56 Effect of collection period on HG-ETAAS signal of 0.5 ng/mL Te solution pumped at 3.2 mL/min flow rate. Collection and atomization temperatures were adjusted to 300 °C and 2000 °C, respectively.

3.5.6 Calibration Plot and Linear Range

A set of solutions ranging from 0.010 to 5.00 ng/mL was prepared to determine the linear dynamic range of 60 seconds trapping and 180 seconds trapping in HG-ETAAS. Results are given in Figure 57 and Figure 58.

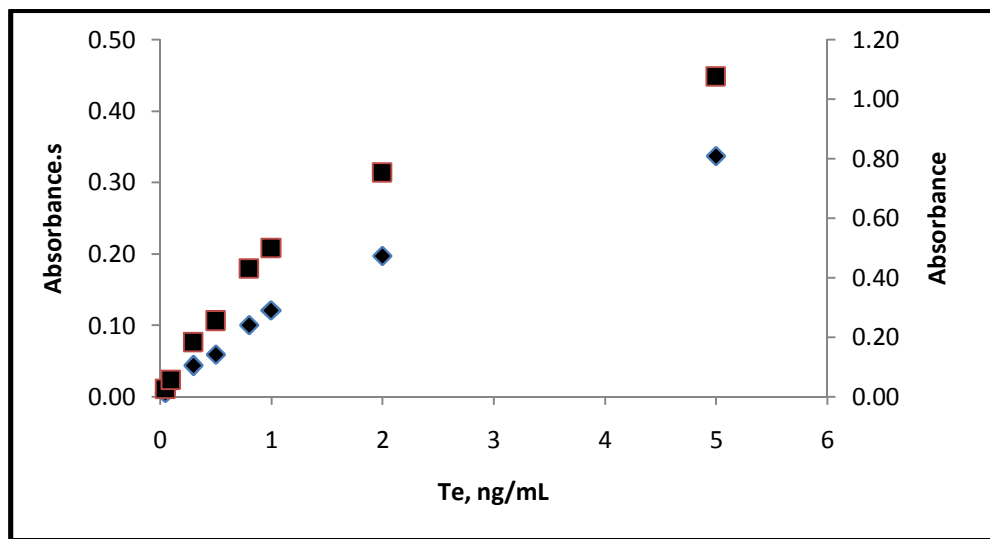


Figure 57 Calibration plot for trapping of H_2Te on Ru modified graphite tube over 60 seconds using HG-ETAAS. Sample flow rate was adjusted to 3.2 mL/min. $300\text{ }^\circ\text{C}$ and $2000\text{ }^\circ\text{C}$ were selected as trapping temperature and atomization temperature, respectively.

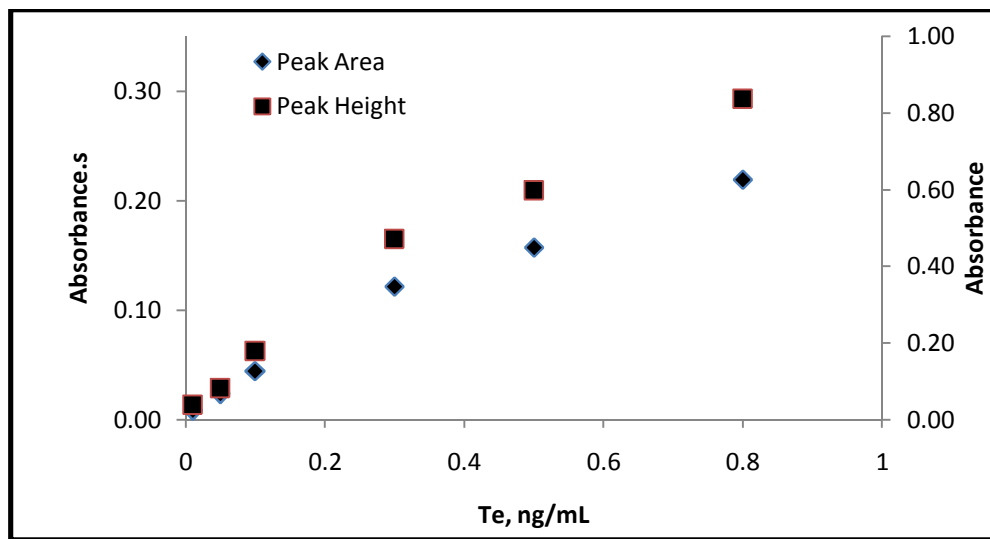


Figure 58 Calibration plot for trapping of H_2Te on Ru modified graphite tube trapped over 180 seconds using HG-ETAAS. Sample flow rate was adjusted to 3.2 mL/min. $300\text{ }^\circ\text{C}$ and $2000\text{ }^\circ\text{C}$ were used as trapping temperature and atomization temperature, respectively.

Linear ranges were determined as 0.05-1.00 ng/mL for 60 seconds trapping and 0.01-0.30 ng/mL for 180 seconds trapping periods. Corresponding linear calibration plots are given in Figure 59 and Figure 60.

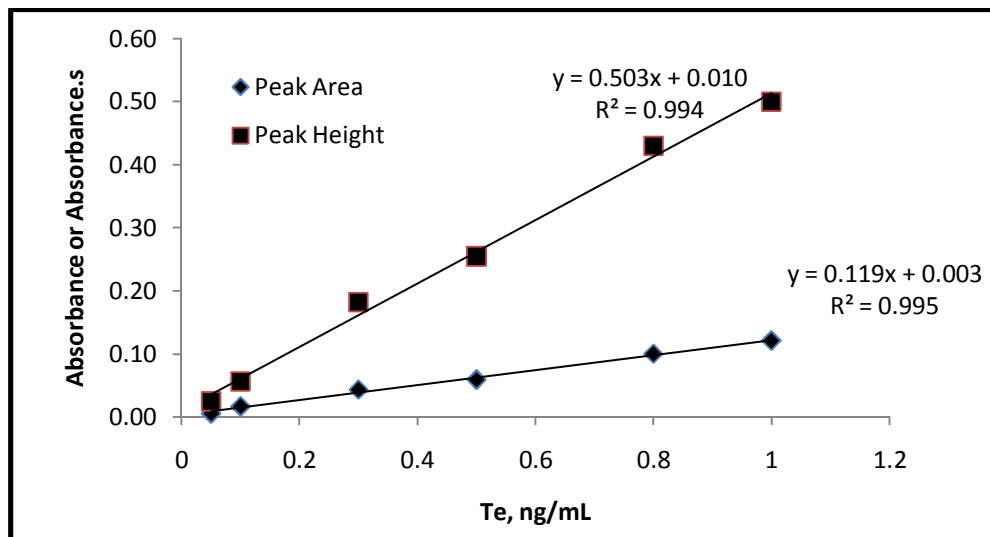


Figure 59 Linear portion of the calibration plot and best line equations for 60 seconds trapping time using HG-ETAAS. Sample flow rate was adjusted to 3.2 mL/min. 300 °C and 2000 °C were used as trapping temperature and atomization temperature, respectively.

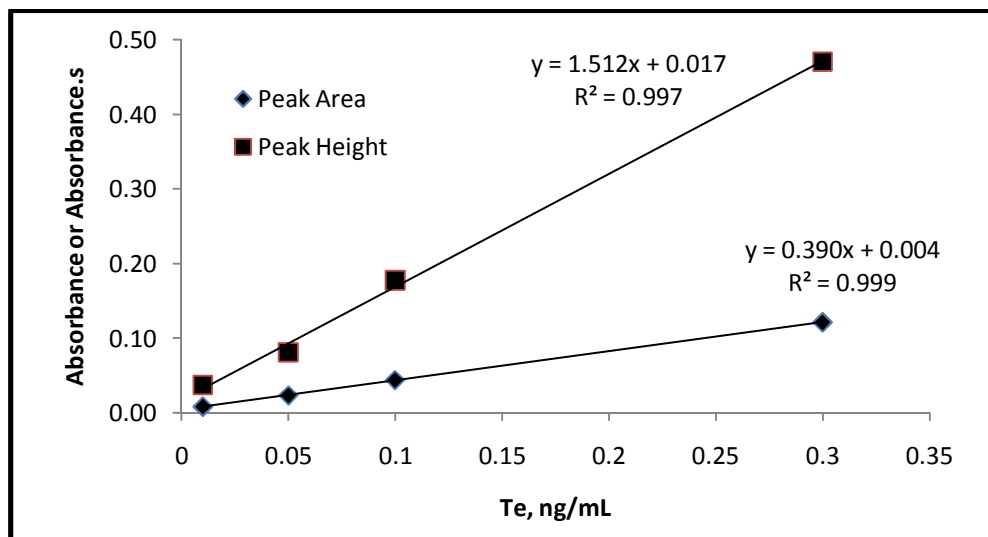


Figure 60 Linear portion of the calibration plot and best line equations for 180 seconds trapping time using HG-ETAAS. Sample flow rate was adjusted to 3.2 mL/min. 300 °C and 2000 °C were used as trapping temperature and atomization temperature, respectively.

3.5.7 Analytical Figures of Merit and Method Validation

Several analytical parameters of HG-ETAAS method using Ru-modified tube were calculated and given in Table 21.

Table 21 Analytical figures of merit for trapping of H₂Te on Ru modified graphite tube.

| | 60 seconds trapping time | | 180 seconds trapping time | |
|---|--------------------------|-------------|---------------------------|-------------|
| | Peak Area | Peak Height | Peak Area | Peak Height |
| Concentration Limit of | | | | |
| Detection, LOD, 3s/m (N=7) pg/mL | 24.5 | 6.8 | 7.4 | 2.2 |
| Mass Limit of Detection, 3s/m (N=7) pg | 78.4 | 21.8 | 71.0 | 21.2 |
| Concentration Limit of | | | | |
| Quantification, LOQ, 10s/m (N=7) pg/mL | 81.8 | 22.7 | 24.9 | 7.5 |
| Mass Limit of | | | | |
| Quantification, LOQ, 10s/m (N=7) pg | 261.8 | 72.6 | 239.0 | 72 |
| Characteristic Concentration, C₀ pg/mL | 37.3 | 8.6 | 1.0 | 2.5 |
| Characteristic mass for peak absorption, m_p, pg | - | 27.6 | - | 23.8 |
| Characteristic mass for peak area, m_a, pg | 119 | - | 96 | - |
| Enhancement with respect to direct ETAAS with Ru modifier | 41.8 | 50.0 | 156 | 173 |

| | | | | |
|--|-----|-----|-----|-----|
| Enhancement with respect to continuous flow HGAAS | - | 44 | - | 156 |
| Efficiency with respect to direct ETAAS | 26% | 32% | 33% | 37% |
| RSD, 10 replicate of 0.3 ng/mL solution | 2.5 | 1.5 | 3.2 | 1.8 |

Accuracy of the method was tested by NIST 1643e “Trace elements in water” SRM. Before the analysis reduction procedure given in Section 2.5.3 was applied. Direct calibration method and 180 seconds trapping was used with three parallel samples. Results were given in Table 22. Student t-test at 95% confidence level shows no significant difference between the values.

Table 22 Results of accuracy check for trapping of H₂Te on Ru modified graphite tube using HG-ETAAS and NIST 1643e “Trace elements in water” SRM.

| | Certified Value | Found Value |
|------------------------|------------------------|--------------------|
| Total Te, ng/mL | 1.09 ± 0.11 | 1.17 ± 0.10 |

3.6 Evaluation of System Performance

Developed methods were compared in terms of sensitivity enhancement. Enhancement was calculated as the ratio of characteristic concentrations of two methods but sometimes enhancement factor became insufficient for the

comparison of two methods since sample consumption and/or time of integration changes significantly from one method to other. Ataman (2008) suggested two new terms that normalize the enhancement with respect to time and volume. E_t was defined as enhancement factor for unit time and E_v is defined as enhancement factor in unit volume; these terms have the units of s^{-1} and mL^{-1} , respectively. The relevant results are given in Table 23.

Table 23 Comparison of the performance of developed methods.

| | E with respect to ETAAS | E with respect to HGAAS | E_t with respect to ETAAS | E_v with respect to ETAAS |
|---|---------------------------------|---------------------------------|-----------------------------------|-----------------------------------|
| Direct ETAAS | - | 0.6 | - | - |
| Continuous flow HGAAS | 1.6 | - | - | - |
| Pyrolytic coated graphite HG- ETAAS, 60 seconds trapping | 14 | 8.4 | 14 | 14 |
| Pd modified graphite HG- ETAAS, 60 seconds trapping | 56 | 48 | 56 | 18 |
| Pd modified graphite HG- ETAAS 180 seconds trapping | 142 | 122 | 47 | 15 |
| Ru modified graphite HG- ETAAS, 60 seconds trapping | 50 | 44 | 50 | 16 |
| Ru modified graphite HG- ETAAS, 180 seconds trapping | 172 | 152 | 57 | 18 |

3.7 Interference Study

After the optimizations, an interference study was performed both for direct ETAAS and HG-ETAAS method using *in-situ* trapping of H₂Te on Ru modified graphite tube. 50 ng/mL Te solution in 0.5 mol/L HNO₃ was used for direct ETAAS analysis and 1.0 ng/mL Te(IV) solution was used for graphite trapping system. Interfering elements were grouped into four as hydride forming elements, cold vapor forming elements, transition metals and earth metals. For most of the cases, peak area results were very close to each other whereas for certain cases peak height values were decreased significantly and defects on peak shapes were observed. Graphics given below were calculated using peak height values and unusual behaviors were noted in the text.

To see the effect of hydride forming elements Te solutions were prepared in 1 to 1, 1 to 5, 1 to 50 and 1 to 500 mass ratios of analyte/interferent for As(III), Sb(III), Pb(II), Se(IV) and Sn(IV) ions. 1.0 ng/mL Te was used for HG-ETAAS system and 50 ng/mL Te was used for direct ETAAS system. Results for direct ETAAS analysis and hydride generation *in-situ* trapping AAS are given in Figure 61 and Figure 62, respectively.

It was observed that As deteriorated the Te signal by around 20% at 500 fold excess for both ETAAS and HG-ETAAS cases. Se was reducing the Te signal only for HG-ETAAS case which implies liquid phase interference rather than gas phase interference. Another observation was that Sb decreased the peak height signal 20 % for direct ETAAS case and about 30 % for hydride trapping case. However, peak area values were not affected. This result was indicating atomization interference since splitting of the peaks were recorded. Most probably Sb forms an alloy with Te on the graphite surface and thus the atomization profile was altered.

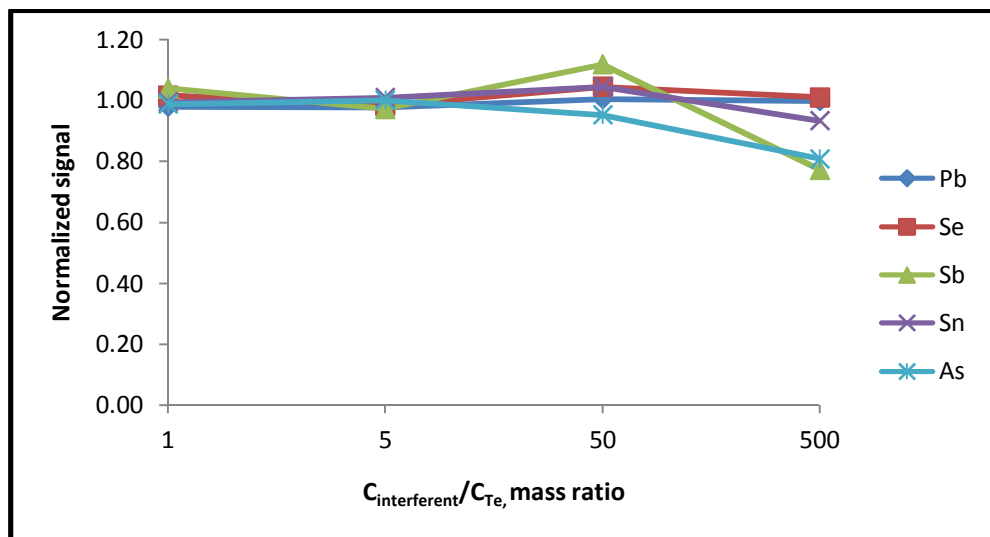


Figure 61 Effect of hydride forming elements on the analytical signal of 50.0 ng/mL Te solution by direct ETAAS analysis.

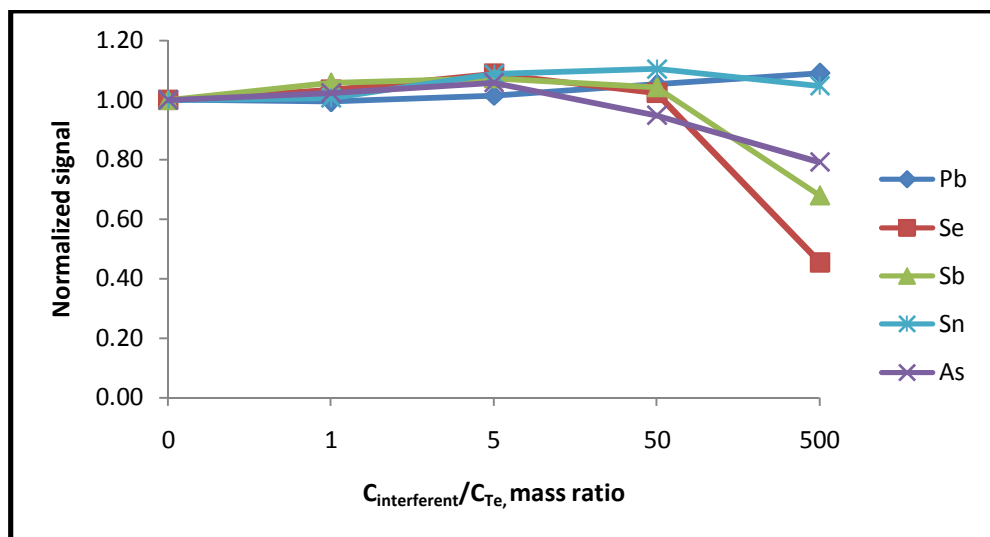


Figure 62 Effect of hydride forming elements on the HG-ETAAS signal of 1.0 ng/mL Te(IV) solution trapped over 60 seconds.

To see the effect of some transition metals, a set of solutions containing Te and interfering element in 1, 5, 50 and 500 fold excess were prepared. Fe, Mn and Cr were selected as the indicator elements while Cu, Co and Ni were omitted since they were known to cause interference and damage the graphite tubes irreversibly (**D'Ulivo, Determination of Selenium and Tellurium in Environmental Samples, 1997**). No significant interference was observed for both direct ETAAS analysis and hydride trapping cases (Figure 63 and Figure 64).

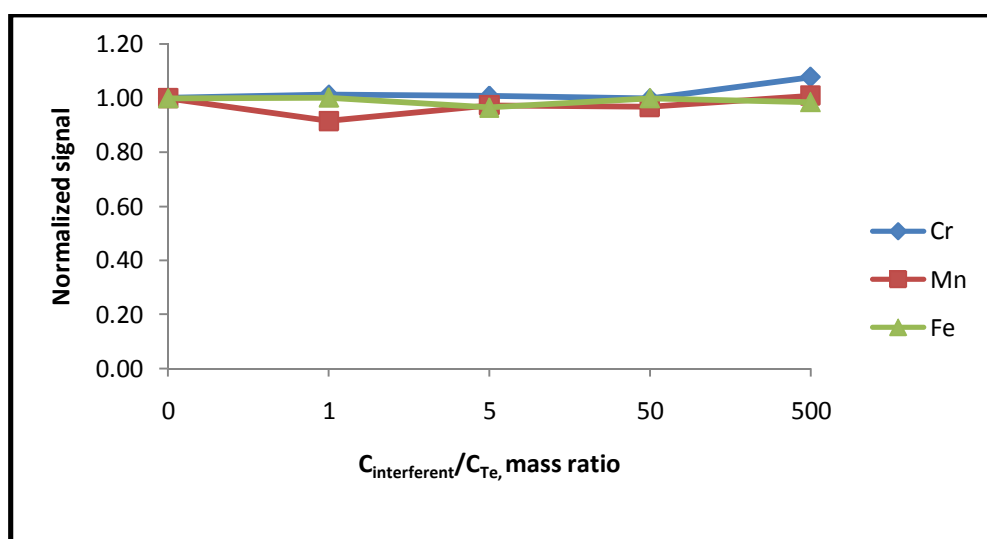


Figure 63 Effect of some transition metals on the analytical signal of 50.0 ng/mL Te solution by direct ETAAS analysis.

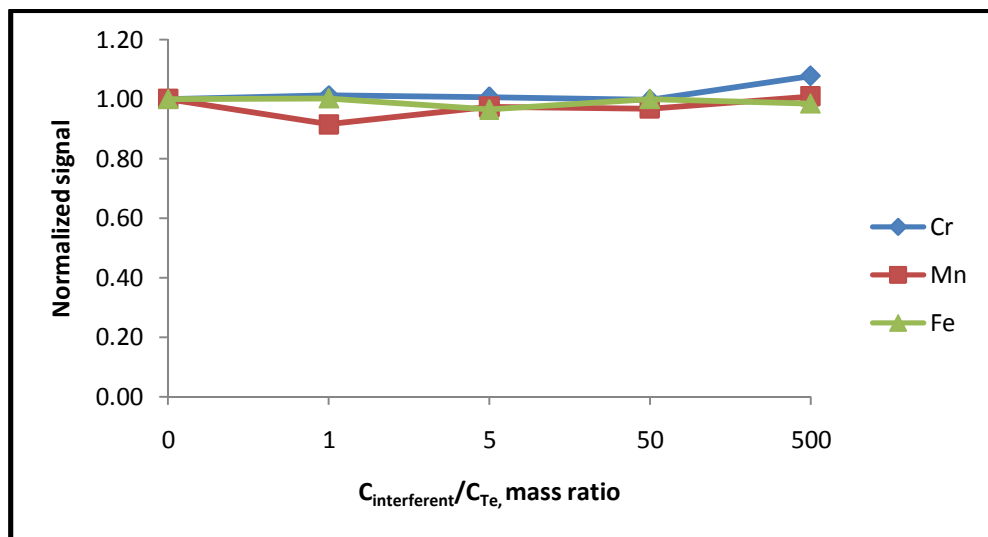


Figure 64 Effect of some transition metals on the HG-ETAAS signal of 1.0 ng/mL Te(IV) solution trapped over 60 seconds.

Hg and Cd were known to form cold vapor upon reduction with NaBH₄. Effects of these elements on Te were studied. No significant interference was observed within the range studied; the results are given in Figure 65 and Figure 66. This result may attribute to the relative high volatility of these interfering elements.

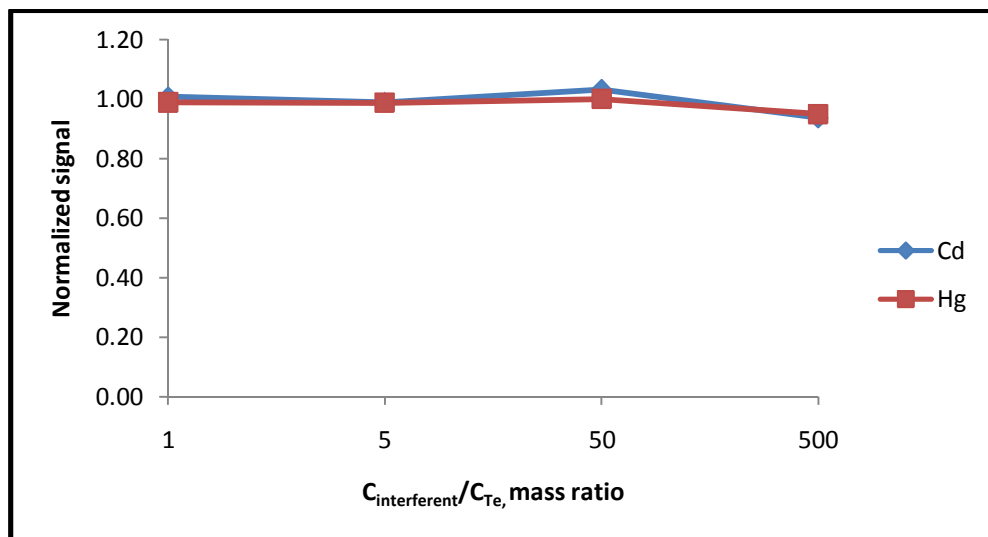


Figure 65 Effect of cold vapor forming element on the analytical signal of 50.0 ng/ml Te solution by direct ETAAS analysis.

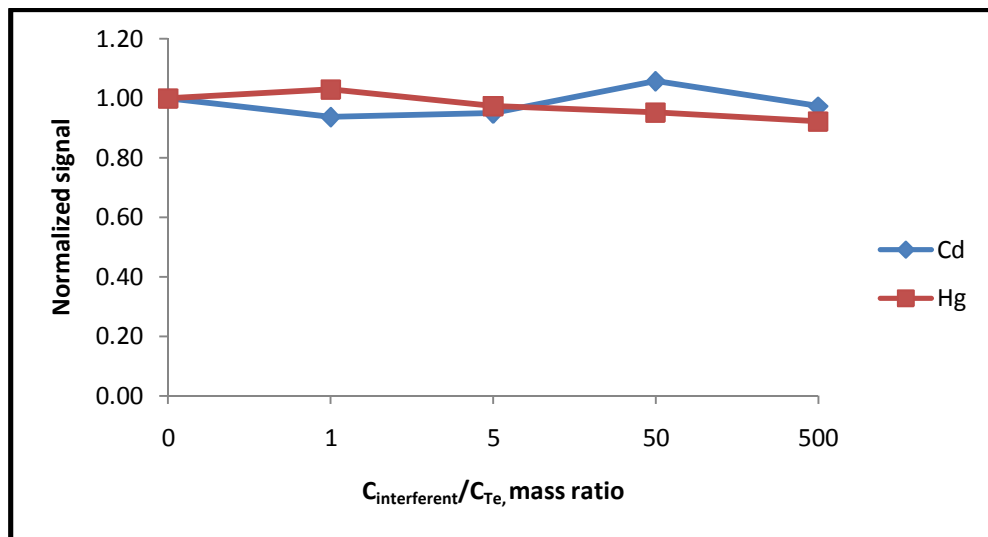


Figure 66 Effect of cold vapor forming elements on the HG-ETAAS signal of 1.0 ng/mL Te(IV) solution trapped over 60 seconds.

Finally the effect of earth metals was studied. Al and Ca were selected as the representative elements for the study. No significant interference was observed for

hydride trapping case; the data are given in Figure 67 and Figure 68. For direct ETAAS analysis a tailed peak, given in Figure 69, was observed for 500 fold excess Al.

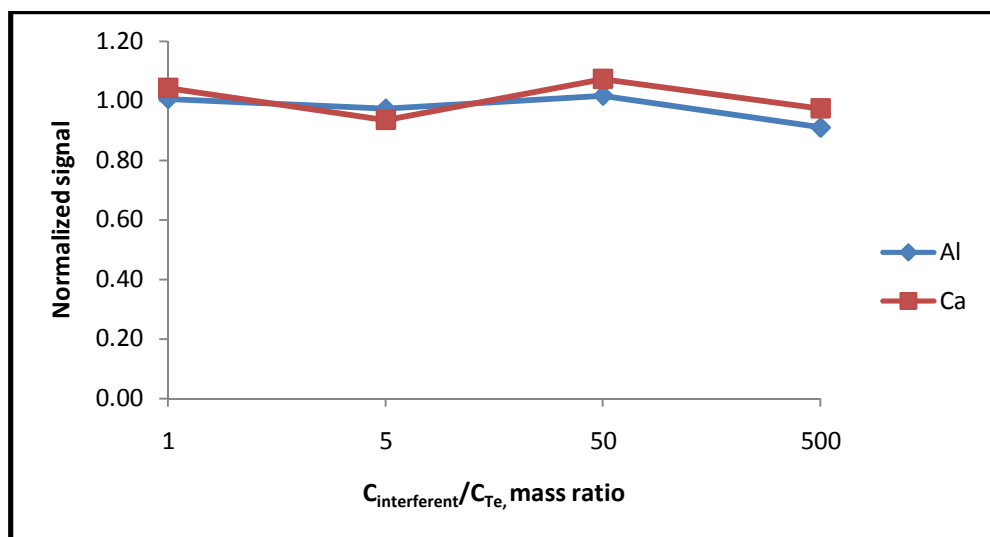


Figure 67 Effect of some soil based elements on the analytical signal of 50.0 ng/mL Te solution by direct ETAAS analysis.

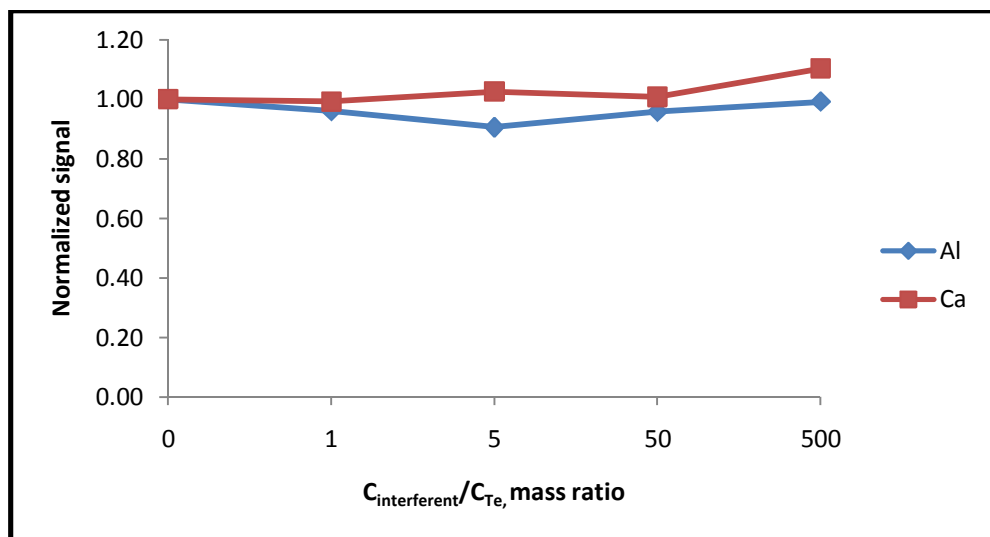


Figure 68 Effect of some soil based elements the HG-ETAAS signal of 1.0 ng/mL Te(IV) solution trapped over 60 seconds.

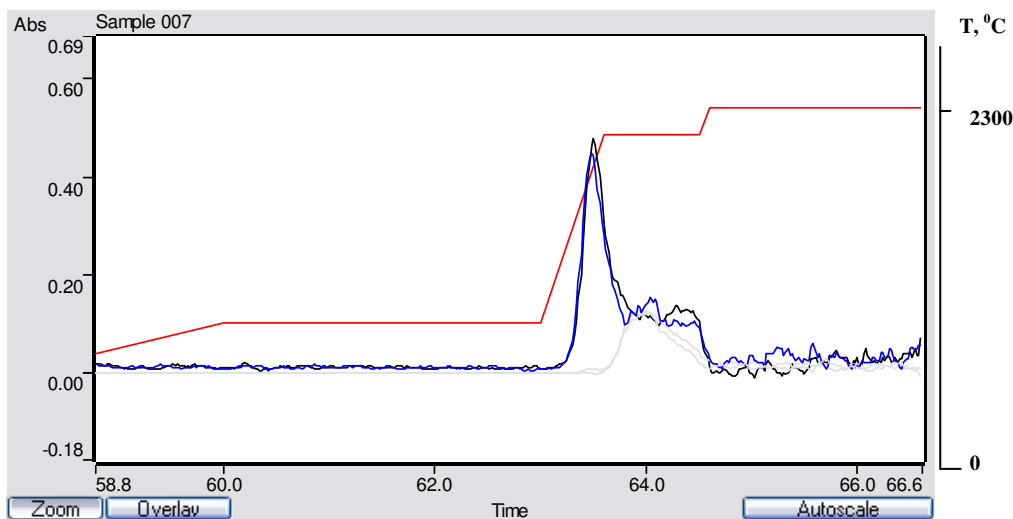


Figure 69 Effect of Al on the shape of analytical signal on 50.0 ng/mL Te solution.
The straight line denotes the furnace temperature.

3.8 Analysis of Samples and Recovery Studies

Among the methods developed Ru modified graphite tube was selected as the easiest method and sea water, natural water, tap water and mineral water samples were analyzed by this method. Among the samples analyzed neither Te(IV) nor Te(VI) was detected. To show the applicability of the method series of spike recovery test were performed. Results were given in Table 24. Te(IV) amounts were determined by direct analysis of samples without applying a prereduction step. Total Te was determined after application of a prereduction step. Te(VI) was determined as the difference between total Te and Te(IV). Three parallel samples were analyzed.

Table 24 Results of spike recovery test for some water samples (N=3).

| | Spiked values, ng/mL | | Found Values, ng/mL | | |
|--------------------|-------------------------|--------|---------------------|---------------|---------------|
| | Te(IV) | Te(VI) | Te(IV) | Te(VI) | Te, total |
| Natural water | 0.100 | 0.100 | 0.098 ± 0,005 | 0.095 ± 0,012 | 0,193 ± 0,011 |
| Tap water | 0.100 | 0.100 | 0.109 ± 0.005 | 0.081 ± 0.016 | 0.190 ± 0.015 |
| Sea water | 0.100 | 0.100 | 0.097 ± 0,007 | 0.107 ± 0.014 | 0.204 ± 0.012 |
| Mineral water 1 | 0.100 | 0.100 | 0.100 ± 0.011 | 0.091± 0.019 | 0.191 ± 0.015 |
| Mineral water 2 | 0.100 | 0.100 | 0.95 ± 0.009 | 0.100 ± 0.014 | 0.195 ± 0.010 |

CHAPTER 4

CONCLUSIONS

The main purpose of this study was development of a simple method for ultratrace speciation of Te in environmental samples.

First part of the study involves development of direct ETAAS analysis. Performance characteristics of pyrolytic coated graphite surface, Pd modified graphite surface and Ru modified graphite surfaces were compared. It was observed that volatility of Te was high in the presence of HCl solutions even at moderate temperatures probably through formation of volatile chloride complexes. HNO₃ stabilize Te better than HCl. Even in the presence of HNO₃ maximum pyrolysis temperature was 500 °C in pyrolytic coated graphite surface. Presence of Pd and Ru modifiers stabilize the Te species and allow use of relatively high pyrolysis temperatures. Maximum pyrolysis temperature was determined as 1400 °C for Pd modifier and 1000 °C for Ru modifier. Use of modifiers not only stabilize Te species by allowing high temperatures but also enhances the analytical signal.

Second part of the study involves development of continuous flow HGAAS system. Te was proved to form volatile H₂Te in variety of conditions without significant loss of sensitivity. Sample solutions were prepared in 4.0 mol/HCl and 0.5% (w/v) NaBH₄ these values were selected as the optimum working conditions for the rest of the study. Main factor that determines the quantity of the analytical signal was the sample flow rate.

Third part deals with the trapping of H₂Te on pyrolytic coated graphite tube. Here one of the critical experimental parameter was the stripping Ar flow rate. Low Ar flows increase the residence time of the atoms at the trapping zone but suffers from low transport efficiency. Optimum Ar flow rate was determined by the competition between residence time and transport efficiency. If residence time dominates the system, analytical signal should decrease with increasing Ar flow rate. This is the case observed for pyrolytic coated graphite surface. This is an indication of trapping efficiency of the surface towards H₂Te. Another observation was that efficient trapping of volatile species was limited to a small temperature and sample flow rate interval. 1.6 mL/min sample flow rate and 300 °C trapping temperatures were selected as the optimum working conditions. Trapping efficiency of the surface was calculated as 16.7% according to characteristic masses.

In the fourth part of the study performance characteristics of Pd modified graphite surface were evaluated. It was seen that trapping efficiency of Pd modified surface is better compared to pyrolytic coated surface. This result was attributed to the stabilizing effect of Pd on Te. Unlike the pyrolytic coated surface, Pd modified graphite tube exhibits better resistance to Ar flow regarding trapping efficiency. Analytical signal reached a maximum value after 133 mL/min Ar flow. After this point the signal does not change. This behavior was the indication of normalizing effect of trapping system. Trapping systems were not affected much from dilution of sample solution by stripping gas since they only respond for the mass of analyte rather than concentration. This made it possible to work with low Ar flows which could not be used for continuous HGAAS system due to low signal stability. With this method a relative LOD of 6.4 pg/mL and 39.7% trapping efficiency were achieved over 180 seconds trapping.

Fifth part of the study was the search for a permanent surface modifier for trapping of H₂Te. Ru was found to be an efficient permanent surface modifier for the determination of Te species. Deposition of 25 µg Ru was used over 300 cycles with

only 20% loss of sensitivity. Recoating of the surface regenerates the sensitivity. With this method 2.2 pg/mL LOD value was obtained with trapping of 9.6 mL sample solution. A carryover effect was observed at high trapping temperatures so the limiting collection temperature, namely 600 °C, should not be exceeded during analysis.

An interference study was also performed. It was seen that interfering elements mostly affect the peak height values while peak area measurements stay relatively stable. Distortion of the peaks was observed at high interfering element concentrations. Among hydride forming elements As and Sb were causing interference effect for both direct ETAAS analysis and HG-ETAAS analysis while Se only cause interference for HG-ETAAS. Application of HG-ETAAS eliminates the interference coming from Al efficiently.

Developed methods were applied for the speciation of Te in several water matrices. No Te was detected in the samples studied. A recovery study was performed and good recovery values were obtained for sea water, natural water, tap water and mineral water samples.

As a summary, HG-ETAAS in-situ trapping of H₂Te in pyrolytic coated, Pd modified and Ru modified surfaces was proven to be efficient for the determination of ultratrace amounts of Te in water samples.

REFERENCES

- Andreae, M. O. (1984). Determination of Inorganic Tellurium Species in Natural Waters. *Analytical Chemistry*, 56, 2064-2066.
- Ataman, O. Y. (2008). Vapor generation and atom traps: Atomic absorption spectrometry at the ng/L level. *Spectrochimica Acta Part B*, 63, 825–834.
- Barbosa, F. J., Souza, S. S., & Krug, F. J. (2002). In situ trapping of selenium hydride in rhodium-coated tungsten coil electrothermal atomic absorption spectrometry. *Journal of Analytical Atomic Spectrometry*, 17, 382–388.
- Bolotnikov, A., Camarda, G., Carini, G., Cui, Y., Li, L., & James, R. (2007). Cumulative effects of Te precipitates in CdZnTe radiation detectors. *Nuclear Instruments and Methods in Physics Research Section A*, 571, 687-698.
- Braman, R. S., Justen, L. L., & Foreback, C. C. (1972). Direct Volatilization-Spectral Emission Type Detection System for Nanogram Amounts of Arsenic and Antimony. *Analytical Chemistry*, 44, 2195–2199.
- Cankur, O. (2004). On-line preconcentration of vapor forming elements on resistively heated w-coil prior to their determination by atomic absorption spectrometry. *PhD Thesis*.
- Cankur, O., Ertas, N., & Ataman, O. Y. (2002). Determination of bismuth using on-line preconcentration by trapping. *Journal of Analytical Atomic Spectrometry*, 17, 603–609.
- Cava-Montesinos, P., Guardia, A. d., Teutsch, C., Cervera, M. L., & Guardia, M. d. (2004). Speciation of selenium and tellurium in milk by hydride generation atomic fluorescence spectrometry. *Journal of Analytical Atomic Spectrometry*, 19, 696 –699.
- Chau, Y. K., Wrong, P. T., & Bengert, G. A. (1982). Determination of methyltin (IV) and tin (IV) species in water by gas chromatography/atomic absorption spectrometry. *Analytical Chemistry* (54), 246-249.
- Chen, Y.-L., & Jiang, S.-J. (2000). Determination of tellurium in a nickel-based alloy by flow injection vapor generation inductively coupled plasma mass spectrometry. *Journal of Analytical Atomic Spectrometry*, 15, 1578-1582.

- Cohen, L. B. (1984). Anomalous behavior of tellurium abundances. *Geochimica et Cosmochimica Acta*, 48, 203–205.
- Dedina, J. (2007). Atomization of volatile compounds for atomic absorption and atomic fluorescence spectrometry: On the way towards the ideal atomizer. *Spectrochimica Acta Part B*, 62, 846–872.
- Dedina, J., & Matousek, T. (2000). Multiple microflame—a new approach to hydride atomization for atomic absorption spectrometry. *Journal of Analytical Atomic Spectrometry*, 15, 301 - 304.
- Dedina, J., & Rubeska, I. (1980). Hydride atomization in a cool hydrogen–oxygen flame burning in a quartz tube atomizer. *Spectrochimica Acta Part B*., 35, 119–128.
- Dedina, J., & Tsalev, D. L. (1995). *Hydride Generation Atomic Absorption Spectrometry*. Chichester: John Wiley and Sons Ltd.
- Denkhaus, E., Gollock, A., Guo, X. M., & Huang, B. (2001). Electrolytic Hydride Generation (EC-HG)-A Sample Introduction System with Some Special Features. *Journal of Analytical Atomic Spectrometry*, 16, 870.
- Ding, W., & Sturgeon, R. (1997). Minimization of transition metal interferences with hydride generation techniques. *Analytical Chemistry*, 69, 527–531.
- Drasch, G., Meyer, L. V., & Kauert, G. (1980). Application of the furnace AA method for the detection of As in biological samples by means of hydride technique. *Fresenius Journal of analytical Chemistry*, 304, 141-142.
- Droessler, M. S., & Holcombe, J. A. (1986). Molecular oxygen absorption in the determination of selenium by graphite furnace atomic absorption. *Canadian Journal of Spectroscopy*, 31, 6-10.
- D'Ulivo, A. (1997). Determination of Selenium and Tellurium in Environmental Samples. *Analyst*, 122, 117R–144R.
- D'Ulivo, A., Mester, Z., & Sturgeon, R. (2005). The mechanism of formation of volatile hydrides by tetrahydroborate(III) derivatization: a mass spectrometric study performed with deuterium labelled reagents. *Spectrochimica Acta Part B*, 60, 423–438.
- D'Ulivo, A., Mester, Z., Meija, J., & Sturgeon, R. E. (2006). Gas chromatography–mass spectrometry study of hydrogen–deuterium exchange reactions of volatile hydrides of As, Sb, Bi, Ge and Sn in aqueous media. *Spectrochimica Acta Part B*, 61, 778-787.
- Feng, Y.-L., Sturgeon, R. E., & Lam, J. W. (2003). Chemical vapor generation characteristics of transition and noble metals reacting with tetrahydroborate(III). *Journal of Analytical Atomic Spectrometry*, 18, 1435–1442.

Frech, W., & Baxter, D. (1995). Spatial distributions of non-atomic species in graphite furnaces. *Spectrochimica Acta Part B*, 51, 961-972.

Fuller, C. W. (1977). *Electrothermal atomization for atomic absorption spectrometry*. London: Chemical Society.

Furdíková, Z., & Dočekal, B. (2009). Trapping interference effects of arsenic, antimony and bismuth hydrides in collection of selenium hydride within iridium-modified transversally-heated graphite tube atomizer. *Spectrochimica Acta Part B*, 64 , 323–328.

George, M. W. (2003). *SELENIUM AND TELLURIUM*. U.S. GEOLOGICAL SURVEY MINERALS YEARBOOK.

Gonzálvez, A., Llorens, A., Cervera, M., Armenta, S., & Guardia, M. d. (2009). Non-chromatographic speciation of inorganic arsenic in mushrooms by hydride generation atomic fluorescence spectrometry. *Food Chemistry* (115), 360-364.

Gregorie, D. C. (1990). Sample introduction techniques for the determination of osmium isotope ratios by inductively coupled plasma mass spectrometry. *Analytical Chemistry* (62), 141-146.

Holak, W. (1969). Gas-sampling technique for arsenic determination by atomic absorption spectrophotometry. *Analytical Chemistry* , 41, 1712-1713.

Hollins, J. G. (1969). The metabolism of tellurium in rats. *Health Physics* , 17, 495-505.

Howard, A. G., & Salou, C. (1998). Arsenic speciation by cryogenic trap hydride generation atomic absorption spectroscopy: performance enhancement by pre-derivatization. *Journal of Analytical Atomic Spectrometry* , 13, 683-686.

Johansson, M., Snell, J., Frech, W., & Hansson, R. (1998). Determination of nickel using electrochemical reduction and carbonyl generation with in situ trapping electrothermal atomic absorption spectrometry. *Analyst* (123), 1223 - 1228.

Karlson, U., & Frankenberger, W. T. (1993). *Metal ions in biological systems*. New York: Marcel Dekker.

Korkmaz, D. K., Ertaş, N., & Ataman, O. Y. (2002). A novel silica trap for lead determination by hydride generation atomic absorption spectrometry. *Spectrochimica Acta Part B* (57), 571-580.

Körez, A., Eroğlu, A. E., Volkan, M., & Ataman, O. Y. (2000). Speciation and preconcentration of inorganic tellurium from waters using a mercaptosilica microcolumn and determination by hydride generation atomic absorption spectrometry. *Journal of Analytical Atomic Spectrometry* , 15, 1599-1605.

Kratzer, J., & Dedina, J. (2008). Stibine and bismuthine trapping in quartz tube atomizers for atomic absorption spectrometry — Method optimization and analytical applications. *Spectrochimica Acta Part B*, 63, 843-849.

Krivan, V., & Petrick, K. (1990). HGAAS performed at 1800-2300 °C atomization temperature using a GT. *Fresenius Journal of Analytical Chemistry*, 336, 480-483.

Kula, İ., Arslan, Y., Bakırdere, S., & Ataman, O. (2008). A novel analytical system involving hydride generation and gold-coated W-coil trapping atomic absorption spectrometry for selenium determination at ng l⁻¹ level. *Spectrochimica Acta Part B*, 63, 856–860.

Kumar, A. R., & Riyazuddin, P. (2007). Non-chromatographic hydride generation atomic spectrometric techniques for the speciation analysis of arsenic, antimony, selenium, and tellurium in water samples—a review. *International Journal of Environmental Analytical Chemistry*, 87, 469–500.

Laborda, F., Medrano, J., Cortés, J. I., Mir, J. M., & Castillo, J. R. (1999). Comparison of palladium and zirconium treated graphite tubes for in-atomizer trapping of hydrogen selenide in hydride generation electrothermal atomization atomic absorption spectrometry. *Spectrochimica Acta Part B*, 54, 343-353.

Lee, D. S. (1982). Determination of Bi in environmental samples by flameless AAS with HG. *Analytical Chemistry*, 54, 69-73.

Leskela, M., Niinistö, L., Nykanen, E., Soininen, P., & Titta, M. (1991). Thermoanalytical and mass spectrometric studies on volatile β-diketone chelates. *Thermochimica Acta* (175), 91-98.

Liao, Y.-p., & Haug, H. O. (1997). Investigation of Stable Coatings for in Situ Trapping of Se and Te in Flow-Injection Hydride Generation and Graphite Furnace Atomic Absorption Spectrometry for Automated Determination. *Microchemical Journal*, 56, 247–258.

Liva, M., Munoz-Olivas, R., & Camara, C. (2000). Determination of Cd in Sonicate Slurries and Leachates of Biological and Environmental Materials by FI-CV-AAS. *Talanta*, 51, 381-387.

L'vov, B. V. (2005). Fifty Years of Atomic Absorption Spectrometry. *Journal of Analytical Chemistry*, 60, 382–392.

Madsen, R. E. (1971). AA determination of As subsequent to arsine reaction with 0.01M silver nitrate. *Atomic Absorption Newsletter*, 10, 57-58.

Matusiewicz, H., & Krawczyk, M. (2008). Determination of total antimony and inorganic antimony species by hydride generation situ trapping flame atomic absorption

spectrometry: a new way to (ultra)trace speciation. *Journal of Analytical Atomic Spectrometry*, 23, 43–53.

Matusiewicz, H., & Krawczyk, M. K. (2007). Determination of tellurium by hydride generation with in situ trapping flame atomic absorption spectrometry. *Spectrochimica Acta Part B*, 62, 309–316.

Menemenlioğlu, İ., Korkmaz, D., & Ataman, O. Y. (2007). Determination of antimony by using a quartz atom trap and electrochemical hydride generation atomic absorption spectrometry. *Spectrochimica Acta Part B*, 62, 40-47.

Merian, E., Anke, M., Ihnat, M., & Stoeppler, M. (2004). *Elements and their Compounds in the Environment* (2. ed.). Weinheim: WILEY-VCH Verlag GmbH&Co.

Nakahara, T. (1991). Hydride Generation Techniques and Their Applications in Inductively Coupled Plasma-Atomic Emission Spectrometry. *Spectrochimica Acta Part B* (14), 95-109.

Narasaki, H. (1988). Semi-automated Determination of Arsenic and Selenium in River Water by Hydride Generation Atomic Absorption Spectrometry Using a Gas Collection Device. *Journal of Analytical Atomic Spectrometry*, 3, 517-521.

Nishiuchi, K., Kitaura, H., Yamada, N., & Akahira, N. (1998). Dual-Layer Optical Disk with Te–O–Pd Phase-Change Film. *Japhanese Journal of Applied Physics*, 37, 2163.

Pedro, J., Stripekis, J., Bonivardi, A., & Tudino, M. (2008). Determination of tellurium at ultra-trace levels in drinking water by on-line solid phase extraction coupled to graphite furnace atomic absorption spectrometer. *Spectrochimica Acta Part B*, 63, 86-91.

Rademeyer, J. C. (1996). A new nebulizer to atomic spectrometry. *Fresenius' Journal of Analytical Chemistry*, 355, 581–584.

Rezacova, O., & Dedina, J. (2009). Modular L-design of hydride atomizers for atomic absorption spectrometry. *Spectrochimica Acta Part B*, 64, 717-720.

Rigin, V. L. (1978). Dispersionless AF Determination of As in Biological Materials. *Journal of Analytical Chemistry of the USSR*, 33, 1966.

Siemer, D. D., & Hageman, L. (1975). An improved HG AA apparatus for Se determination. *Analytical Letters*, 8, 323-337.

Sindeeva, N. (1964). *Mineralogy and types of deposits of selenium and tellurium*. New York: Interscience Publications.

Skogerboe, R. K., Dick, D. L., Pavlica, D. A., & Lichte, F. E. (1975). Injection of samples into flames and plasmas by production of volatile chlorides. *Analytical Chemistry* (47), 568-570.

Sturgeon, R. E., Guo, X., & Mester, Z. (2005). Chemical vapor generation: are further advances yet possible? *Analytical and Bioanalytical Chemistry*, 382, 881–883.

Sun, H.-W., & Suo, R. (2004). Enhancement reagents for simultaneous vapor generation of zinc and cadmium with intermittent flow system coupled to atomic fluorescence spectrometry. *Analytica Chimica Acta*, 509, 71-76.

Tellurium: geological information. (2009). Retrieved 06 2009, from WebElements: <http://www.webelements.com/tellurium/geology.html>

Thompson, K. C., & Thomerson. (1974). AA studies on the determination of sb, As, Bi, Ge, Pb, Se, Te and Sn by utilizing the generation of covalent hydrides. *Analyst*, 99, 595-601.

Tsalev, D. L. (2000). Vapor generation or electrothermal atomic absorption spectrometry? — Both! *Spectrochimica Acta Part B*, 55, 917-933.

Villanueva-Alonso, J., Peña-Vázquez, E., & Bermejo-Barrera, P. (2009). Use of high resolution continuum source atomic absorption spectrometry as a detector for chemically generated noble and transition metal vapors. *Spectrochimica Acta Part B*, Article in Press.

Walsh, A. (1955). The application of atomic absorption spectra to chemical analysis. *Spectrochimica Acta*, 7, 108-117.

Welz, B., & Sperling, M. (1999). *Atomic Absorption Spectrometry* (2. ed.). Weinheim: WILEY-VCH.

Wikipedia. (2009). *Wikipedia- Tellurium.* Retrieved 06 2009, from Wikipedia: <http://en.wikipedia.org/wiki/Tellurium#Compounds>

Willie, S. N., Sturgeon, R., & Berman, S. (1986). Hydride Generation Atomic-Absorption Determination Of Selenium In Marine-Sediments, Tissues, And Seawater with in-situ Concentration in a Graphite-Furnace. *Analytical Chemistry*, 58, 1140-1143.